IVW - Schriftenreihe Band 112
Institut für Verbundwerkstoffe GmbH - Kaiserslautern

Markus Brzeski

Experimental and Analytical Investigation of Deconsolidation for Fiber Reinforced Thermoplastic Composites

Bibliografische Information Der Deutschen Bibliothek

Die Deutsche Bibliothek verzeichnet diese Publikation in der Deutschen Nationalbibliografie; detaillierte bibliografische Daten sind im Internet über <http://dnb.ddb.de> abrufbar.

Bibliographic information published by Die Deutsche Bibliothek

Die Deutsche Bibliothek lists this publication in the Deutsche Nationalbibliografie; detailed bibliographic data is available in the Internet at <http://dnb.ddb.de>.

Herausgeber: Institut für Verbundwerkstoffe GmbH
Prof. Dr.-Ing. Ulf Breuer
Erwin-Schrödinger-Straße
TU Kaiserslautern, Gebäude 58
67663 Kaiserslautern
http://www.ivw.uni-kl.de

Verlag: Institut für Verbundwerkstoffe GmbH

Druck: Technische Universität Kaiserslautern
ZBT – Abteilung Foto-Repro-Druck

D 386

Als Manuskript gedruckt. Printed in Germany.
ISSN 1615-021X
ISBN 978-3-944440-08-8

Experimental and Analytical Investigation of Deconsolidation for Fiber Reinforced Thermoplastic Composites

Dem Fachbereich Maschinenbau und Verfahrenstechnik

der Technischen Universität Kaiserslautern

zur Erlangung des akademischen Grades

Doktor-Ingenieur (Dr.-Ing.)

genehmigte

Dissertation

von

Herrn

Dipl.-Ing. Markus Brzeski

aus Bremen

2014

Tag der mündlichen Prüfung:	21.08.2014
Dekan:	Prof. Dr.-Ing. Christian Schindler
Prüfungsvorsitzender:	Prof. Dr.-Ing. Eberhard Kerscher
1. Berichterstatter:	Prof. Dr.-Ing. Peter Mitschang
2. Berichterstatter:	Univ.-Prof. Dr.-Ing. Ralf Schledjewski
	D386

Table of Contents

Abstract

The demand of sustainability is continuously increasing. Therefore, thermoplastic composites became a focus of research due to their good weight to performance ratio. Nevertheless, the limiting factor of their usage for some processes is the loss of consolidation during re-melting (deconsolidation), which reduces the part quality. Several studies dealing with deconsolidation are available. These studies investigate a single material and process, which limit their usefulness in terms of general interpretations as well as their comparability to other studies. There are two main approaches. The first approach identifies the internal void pressure as the main cause of deconsolidation and the second approach identifies the fiber reinforcement network as the main cause. Due to of their controversial results and limited variety of materials and processes, there is a big need of a more comprehensive investigation on several materials and processes.

This study investigates the deconsolidation behavior of 17 different materials and material configurations considering commodity, engineering, and performance polymers as well as a carbon and two glass fiber fabrics. Based on the first law of thermodynamics, a deconsolidation model is proposed and verified by experiments. Universal applicable input parameters are proposed for the prediction of deconsolidation to minimize the required input measurements. The study revealed that the fiber reinforcement network is the main cause of deconsolidation, especially for fiber volume fractions higher than 48 %. The internal void pressure can promote deconsolidation, when the specimen was recently manufactured. In other cases the internal void pressure as well as the surface tension prevents deconsolidation. During deconsolidation the polymer is displaced by the volume increase of the void. The polymer flow damps the progress of deconsolidation because of the internal friction of the polymer. The crystallinity and the thermal expansion lead to a reversible thickness increase during deconsolidation. Moisture can highly accelerate deconsolidation and can increase the thickness by several times because of the vaporization of water. The model is also capable to predict reconsolidation under the defined boundary condition of pressure, time, and specimen size. For high pressure matrix squeeze out occur, which falsifies the accuracy of the model.

The proposed model was applied to thermoforming, induction welding, and thermoplastic tape placement. It is demonstrated that the load rate during thermoforming is the critical factor of achieving complete reconsolidation. The required load rate can be determined by the model and is dependent on the cooling rate, the forming length, the extent of deconsolidation, the processing temperature, and the final pressure. During induction welding deconsolidation can tremendously occur because of the left moisture in the polymer at the molten state. The moisture cannot fully diffuse out of the specimen during the faster heating. Therefore, additional pressure is needed for complete reconsolidation than it would be for a dry specimen. Deconsolidation is an issue for thermoplastic tape placement, too. It limits the placement velocity because of insufficient cooling after compaction. If the specimen after compaction is locally in a molten state, it deconsolidates and causes residual stresses in the bond line, which decreases the interlaminar shear strength. It can be concluded that the study gains new knowledge and helps to optimize these processes by means of the developed model without a high number of required measurements.

Kurzfassung

Aufgrund seiner guten spezifischen Festigkeit und Steifigkeit ist der endlosfaserverstärkte Thermoplast ein hervorragender Leichtbauwerkstoff. Allerdings kann es während des Wiederaufschmelzens durch Dekonsolidierung zu einem Verlust der guten mechanischen Eigenschaften kommen, daher ist Dekonsolidierung unerwünscht. In vielen Studien wurde die Dekonsolidierung mit unterschiedlichen Ergebnissen untersucht. Dabei wurde meist ein Material und ein Prozess betrachtet. Eine allgemeine Interpretation und die Vergleichbarkeit unter den Studien sind dadurch nur begrenzt möglich. Aus der Literatur sind zwei Ansätze bekannt. Dem ersten Ansatz liegt der Druckunterschied zwischen Poreninnendruck und Umgebungsdruck als Hauptursache der Dekonsolidierung zu Grunde. Beim zweiten Ansatz wird die Faserverstärkung als Hauptursache identifiziert. Aufgrund der kontroversen Ergebnisse und der begrenzten Anzahl der Materialien und Verarbeitungsverfahren, besteht die Notwendigkeit einer umfassenden Untersuchung über mehrere Materialien und Prozesse. Diese Studie umfasst drei Polymere (Polypropylen, Polycarbonat und Polyphenylensulfid), drei Gewebe (Köper, Atlas und Unidirektional) und zwei Prozesse (Autoklav und Heißpressen) bei verschiedenen Faservolumengehalten.

Es wurde der Einfluss des Porengehaltes auf die interlaminare Scherfestigkeit untersucht. Aus der Literatur ist bekannt, dass die interlaminare Scherfestigkeit mit der Zunahme des Porengehaltes linear sinkt. Dies konnte für die Dekonsolidierung bestätigt werden. Die Reduktion der interlaminaren Scherfestigkeit für thermoplastische Matrizes ist kleiner als für duroplastische Matrizes und liegt im Bereich zwischen 0,5 % bis 1,5 % pro Prozent Porengehalt. Außerdem ist die Abnahme signifikant vom Matrixpolymer abhängig.

Im Falle der thermisch induzierten Dekonsolidierung nimmt der Porengehalt proportional zu der Dicke der Probe zu und ist ein Maß für die Dekonsolidierung. Die Pore expandiert aufgrund der thermischen Gasexpansion und kann durch äußere Kräfte zur Expansion gezwungen werden, was zu einem Unterdruck in der Pore führt. Die Faserverstärkung ist die Hauptursache der Dickenzunahme beziehungsweise der Dekonsolidierung. Die gespeicherte Energie, aufgebaut

während der Kompaktierung, wird während der Dekonsolidierung abgegeben. Der Dekompaktierungsdruck reicht von 0,02 MPa bis 0,15 MPa für die untersuchten Gewebe und Faservolumengehalte. Die Oberflächenspannung behindert die Porenexpansion, weil die Oberfläche vergrößert werden muss, die zusätzliche Energie benötigt. Beim Kontakt von benachbarten Poren verursacht die Oberflächenspannung ein Verschmelzen der Poren. Durch das bessere Volumen-Oberfläche-Verhältnis wird Energie abgebaut. Der Polymerfluss bremst die Entwicklung der Dickenzunahme aufgrund der erforderlichen Energie (innere Reibung) der viskosen Strömung. Je höher die Temperatur ist, desto niedriger ist die Viskosität des Polymers, wodurch weniger Energie für ein weiteres Porenwachstum benötigt wird. Durch den reversiblen Einfluss der Kristallinität und der Wärmeausdehnung des Verbundes wird während der Erwärmung die Dicke erhöht und während der Abkühlung wieder verringert. Feuchtigkeit kann einen enormen Einfluss auf die Dekonsolidierung haben. Ist noch Feuchtigkeit über der Schmelztemperatur im Verbund vorhanden, verdampft diese und kann die Dicke um ein Vielfaches der ursprünglichen Dicke vergrößern.

Das Dekonsolidierungsmodell ist in der Lage die Rekonsolidierung vorherzusagen. Allerdings muss der Rekonsolidierungsdruck unter einem Grenzwert liegen (0,15 MPa für 50x50 mm² und 1,5 MPa für 500x500 mm² große Proben), da es sonst bei der Probe zu einem Polymerfluss aus der Probe von mehr als 2 % kommt. Die Rekonsolidierung ist eine inverse Dekonsolidierung und weist die gleichen Mechanismen in der entgegengesetzten Richtung auf.

Das entwickelte Modell basiert auf dem ersten Hauptsatz der Thermodynamik und kann die Dicke während der Dekonsolidierung und der Rekonsolidierung vorhersagen. Dabei wurden eine homogene Porenverteilung und eine einheitliche, kugelförmige Porengröße angenommen. Außerdem wurde die Massenerhaltung angenommen. Um den Aufwand für die Bestimmung der Eingangsgrößen zu reduzieren, wurden allgemein gültige Eingabeparameter bestimmt, die für eine Vielzahl von Konfigurationen gelten. Das simulierte Materialverhalten mit den allgemein gültigen Eingangsparametern erzielte unter den definierten Einschränkungen eine gute Übereinstimmung mit dem tatsächlichen Materialverhalten. Nur bei Konfigurationen mit einer Viskositätsdifferenz von mehr als

30 % zwischen der Schmelztemperatur und der Prozesstemperatur sind die allgemein gültigen Eingangsparameter nicht anwendbar. Um die Relevanz für die Industrie aufzuzeigen, wurden die Effekte der Dekonsolidierung für drei weitere Verfahren simuliert. Es wurde gezeigt, dass die Kraftzunahmegeschwindigkeit während des Thermoformens ein Schlüsselfaktor für eine vollständige Rekonsolidierung ist. Wenn die Kraft zu langsam appliziert wird oder die finale Kraft zu gering ist, ist die Probe bereits erstarrt, bevor eine vollständige Konsolidierung erreicht werden kann. Auch beim Induktionsschweißen kann Dekonsolidierung auftreten. Besonders die Feuchtigkeit kann zu einer starken Zunahme der Dekonsolidierung führen, verursacht durch die sehr schnellen Heizraten von mehr als 100 K/min. Die Feuchtigkeit kann während der kurzen Aufheizphase nicht vollständig aus dem Polymer ausdiffundieren, sodass die Feuchtigkeit beim Erreichen der Schmelztemperatur in der Probe verdampft. Beim Tapelegen wird die Ablegegeschwindigkeit durch die Dekonsolidierung begrenzt. Nach einer scheinbar vollständigen Konsolidierung unter der Walze kann die Probe lokal dekonsolidieren, wenn das Polymer unter der Oberfläche noch geschmolzen ist. Die daraus resultierenden Poren reduzieren die interlaminare Scherfestigkeit drastisch um 5,8 % pro Prozent Porengehalt für den untersuchten Fall. Ursache ist die Kristallisation in der Verbindungszone. Dadurch werden Eigenspannungen erzeugt, die in der gleichen Größenordnung wie die tatsächliche Scherfestigkeit sind.

Abbreviations

Abbreviation	Meaning
AC	Autoclave
CCD	Charge-coupled device camera
CC	Carbon matrix composite
CF	Carbon fiber
CFRP	Carbon fiber reinforced polymer
DMSO	Dimethylsulfoxide
DSC	Differential scanning calometry
DTA	Differential thermal analysis
EP	Epoxy
GF	Glass fiber
GFRP	Glass fiber reinforced polymer
HP	Hot pressed
ILSS	Interlaminar shear strength
OWRK	Owens, Wendt, Rabel, and Kaelble method
PA	Polyamide
PA12	Polyamide 12
PC	Polycarbonate
PEEK	Polyetheretherketone
PP	Polypropylene
PPS	Polyphenylensulfide
TP	Thermoplastic

TS	Thermoset
UD	Unidirectional
UP	Unsaturated polyester
Organo-sheet	Fully impregnated reinforced thermoplastic sheet

Symbols

Symbol	Unit	Denotation
a	[N/mm^4]	Parameter of polynomial function
A	[Pas]	Parameter of Arrhenius equation
A_m	[MPa]	Interlaminar shear strength in a void free condition
A_{spe}	[m²]	Cross section of the specimen
A_v	[m²]	Void area at any cut in in-plane direction
A_{vo}	[m²]	Surface area
b	[N/mm^3]	Parameter of polynomial function
B	[1/K]	Parameter of Arrhenius equation
B_m	[MPa]	Slope of interlaminar shear strength on void content
c	[N/mm^2]	Parameter of polynomial function
C	[-]	Constant
c_c	[mol/m³]	Gradient of particle density
c_p	[kg*m²/s²/K]	Heat capacity at constant pressure
c_{pf}	[kg*m²/s²/K]	Heat capacity of fibers at constant pressure
c_{pm}	[kg*m²/s²/K]	Heat capacity of matrix at constant pressure
d	[N/mm]	Parameter of polynomial function
D	[m²/s]	Diffusion coefficient
dA_{vo}	[m²]	Incremental new surface area
Δl	[m]	Flow length
Δp	[N/mm²]	Pressure drop

dr	[m]	Incremental void radius step
dt	[s]	Incremental time step
dT	[K]	Incremental temperature step
du_r	[m/s]	Incremental void radius velocity step
dV	[m^3]	Incremental volume change
dx	[m]	Deflection in thickness direction
e	[N]	Parameter of polynomial function
E_{com}	[W]	Energy of thermal expansion of the composite
E_{cry}	[W]	Energy of the melting of the crystals
E_{die}	[W]	Energy of external load
E_{moi}	[W]	Energy of moisture vaporization
E_{net}	[W]	Energy of decompaction of the fiber reinforcement network
E_{sur}	[W]	Energy of void shrinkage and coalescence
E_{sur}	[W]	Surface energy
E_{vis}	[W]	Energy of visco-elastic behavior of the matrix
E_{voi}	[W]	Energy of void expansion because of thermal gas law and internal void pressure
$E^{\|\|}_f$	[GPa]	Young's modulus of the fibers in in-plane direction
$E^{\|\|}_m$	[GPa]	Young's modulus of the matrix in in-plane direction
F_0	[N]	Constant force
F_d	[N]	Irreversible force
F_{die}	[N]	Applied die force
F_{cf}	[N]	Final crystallization force

F_{ci}	[N]	Initial crystallization force
F_s	[N]	Reversible force
F_v	[N]	Force of enforced expansion
H	[mm]	Current height
H_0	[mm]	Initial height
J	[mol/m²/s]	Particle current density
K	[m²]	Permeability
L_0	[mm]	Initial length
m	[kg]	Mass
m_{com}	[kg]	Mass of composite
m_{norm}	[kg]	One kilogram
n	[-]	Number of voids
n_o	[-]	Initial number of voids
n_r	[-]	Number of measurements
p	[N/mm²]	Pressure
p_∞	[N/mm²]	External / atmosphere pressure
p_b	[N/mm²]	Internal bubble pressure
p_e	[N/mm²]	External pressure
p_i	[N/mm²]	Internal pressure
p_o	[N/mm²]	Initial void pressure
p_v	[MPa]	Void pressure
r	[m]	Radius
r*	[-]	Nalimov criterion

R	[m]	Void radius
R_s	[J/kg/K]	Specific gas constant
$\dot{R}$	[m/s]	Radius change velocity
$\ddot{R}$	[m/s²]	Radius change acceleration
s	[-]	Standard deviation
S	[m]	Polymer shell radius
T	[K]	Temperature
t	[s]	Time
t_{sht}	[-]	Student factor
T_o	[K]	Initial temperature
T_1	[K]	Target temperature
u	[m/s]	Velocity of the void surface
u_R	[m/s]	Velocity of the outer shell surface in radial direction
u_r	[m/s]	Velocity of the void surface in radial direction
u_Φ	[m/s]	Velocity of the void surface in tangential direction
v	[m/s]	Average velocity
V	[m³]	Volume
V_c	[m³]	Composite volume
V_{decon}	[m³]	Volume of the deconsolidated specimen
V_{fibers}	[m³]	Volume of the fibers
V_f	[m³]	Volume of the fibers
V_m	[m³]	Volume of the matrix

V_{matrix}	[m³]	Volume of the matrix
V_{mrich}	[m³]	Matrix rich volume
V_{psq}	[m³]	Polymer loss
V_o	[m³]	Initial void volume
V_s	[m³]	Solid specimen's volume
V_V	[m³]	Void volume
x	[m]	Specimen thickness
$\dot{x}$	[-]	Conspicuous value
X_c	[%]	Crystallinity
x_c	[m]	Theoretical void free thickness
x_o	[m]	Initial thickness
$\bar{y}$	[-]	Average value
α	[-]	Void content
α^f_{11}	[-]	Thermal expansion of the fibers in in-plane direction
α^m_{11}	[-]	Thermal expansion of the matrix in in-plane direction
α^c_{11}	[-]	Thermal expansion of the composite in in-plane direction
α_c	[-]	Thermal expansion of the composite in thickness direction
γ	[mN/m]	Surface tension
ΔH^0		Theoretical specific latent heat of a full (100 %) crystallization
$\Delta\varepsilon^p$	[-]	Composite strain
ΔH_M	[J/g]	Specific enthalpy of melt

ΔH_R	[J/g]	Specific enthalpy of recrystallization
ΔV^p	[m³]	Incremental volume change of the polymer
Δt	[s]	Incremental time change
Δx	[mm]	Incremental thickness change
η	[Pas]	Dynamic viscosity
θ	[°]	Tangential direction of the void surface
ρ	[kg/m³]	Density
ρ_p	[kg/m³]	Current density of the polymer
ρ_c	[kg/m³]	Density of the crystals
ρ_a	[kg/m³]	Density of the amorphous phase
τ_{int}	[MPa]	Apparent interlaminar shear strength
τ_{vis}	[MPa]	Shear tension
φ	[-]	Fiber volume fraction
φ_w	[-]	Fiber weight fraction
φ_{moi}	[-]	Moisture weight fraction
Φ	[°]	Tangential direction of the void surface
φ_{mrich}	[-]	Matrix rich volume fraction
σ	[-]	Confidence interval

1 Introduction and Scope

1.1 Introduction

In the last twenty years sustainability became more important in terms of economic and resource efficiency. This fact is strengthened by the shortage of resources and the increasing globalization. Therefore, composites became an interesting resource efficient light weight alternative because of their excellent mechanical performance to density ratio. They have a weight reduction potential of 30 % to 70 % in comparison to metals [1]. However, their processing technologies are relatively expensive and significant improvements have to be done to overcome the higher material costs [2]. Two groups of matrix polymers are available: thermosets and thermoplastics. Thermoset polymers have the advantage of short curing times (several minutes) and they are solid after curing, but the viscosity is highly time-temperature dependent, which is difficult to measure in standardized set ups [3]. Thermoplastic polymers are solid and can be melted by heat over a certain temperature. They do not need to be cured and do not show a complex time-temperature dependency of the viscosity. In the molten state, they can be formed and welded. These are significant advantages against thermoset polymers, but in case of composites these advantages are not unconditional. During reheat thermoplastic composites can lose their former good consolidation, which leads to a reduction of mechanical performance. This effect is called deconsolidation. Many processes are limited by deconsolidation. In order to avoid this effect, the process speed is reduced, which results in a higher cycle time and therefore higher process costs. As a consequence, new composite technologies are hindered to become more broadly used in industry. There is a high need of solutions to overcome this issue, which can only be achieved by a better process understanding and especially a better understanding of the reasons for deconsolidation. This work is focused on that demand and offers solutions by means of an analytical model.

1.2 Motivation and Approach

Composite manufacturing techniques are continuously improving, especially in the area of cycle time and process speed. Because of new heating sources, like diode or solid state lasers, induction, coated infrared radiators or ceramic heating elements, a high amount of energy can be applied to the part. The applied heat is significantly dependent on the electric power. Heating rates from 100 K/min to 100 K/s are possible [4–7]. In contrast to the fast heating, the cooling is limited to convection or conduction. This issue is strengthened by the fact that rollers, which have a small area of contact, are used to achieve consolidation (compaction and solidification) and cooling. Also, the difference between melting temperature and crystallization temperature requires additional cooling below the lower crystallization temperature. In many processes, it is hardly possible to maintain pressure during the whole cooling cycle. This can lead to a loss of consolidation and hence mechanical performance. The required time to maintain pressure is often the limiting factor of a further cycle time reduction and hinders the enhancement of the economic viability [8–10]. Several studies have investigated the loss of consolidation during heating and cooling with different results and different factors causing the loss. These studies investigated a specific material in a specific process, which limits these studies to isolated conclusions. At the moment, there is no comprehensive evaluation available. Additionally, an enormous number of measurements are required to simulate the effect by means of finite element models, which makes it uneconomical for wide industrial use. Therefore, this study investigates a wide range of different materials and configurations processed utilizing different techniques to achieve a general conclusion and a more comprehensive model.

The aim of this work is to investigate deconsolidation and to determine the influencing parameters including manufacturing, post processing, and material. The approach is illustrated in Figure 1.1. Existing models were evaluated to identify the main drivers of deconsolidation for specific materials and process conditions. Based on the literature review, a model for the main drivers is adapted and when necessary developed. The target is to gain an analytical model of deconsolidation using the first law of thermodynamics. For a wide range of materials and conditions, the model was

verified including all important effects such as void dynamics, decompaction of fiber reinforcement network, polymer dynamics, and external loads. In order to achieve a general model, three polymers and three reinforcement types were used with different fiber volume fractions and manufacturing techniques produced. The model should be capable to determine an equilibrium state, where all internal forces of the composite are in equilibrium. The model should also be capable to build up the time dependency of the thickness while deconsolidation. Also, the goal of validating a universal approach with a minimum of input measurements was required to make the model useable for industrial applications. These findings are applied to industrial processes, in order to transform theoretical knowledge into workable applications.

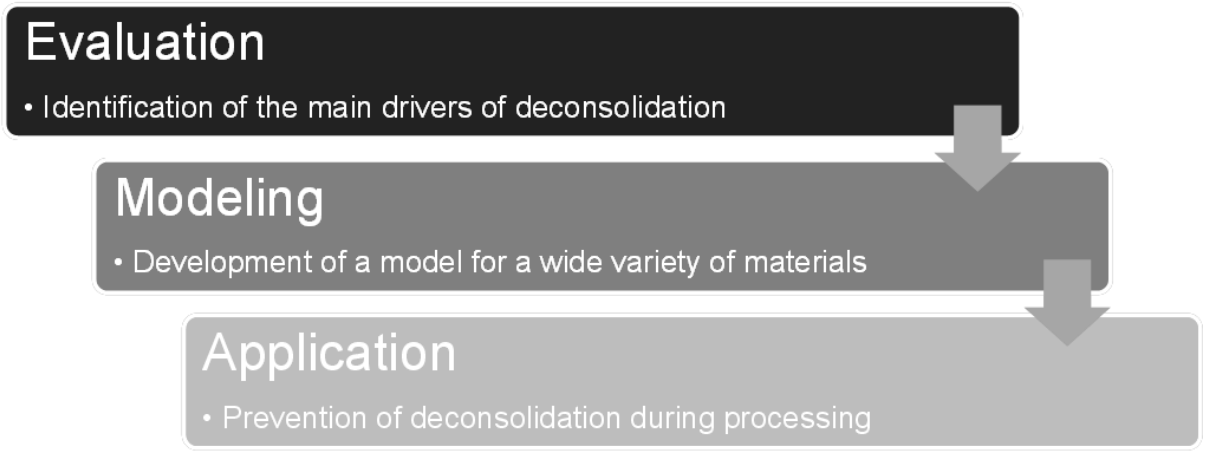

Figure 1.1: Scope of this work including the steps evaluation of existing knowledge, modeling the main drivers, and transferring the knowledge to application

1.3 Layout of the Work

This chapter describes the layout of the thesis, shown in Figure 1.2. The state of the art chapter starts with a general definition of deconsolidation and the necessity of this work because of different reasons for deconsolidation, which is reported in literature. Possible key phenomena are described including void dynamics, fiber reinforcement network, polymer dynamics, and external loads. Deconsolidation in different processes is identified as well as their effect on the part and process conditions. Based on these results, different characterization methods and experiments were carried out to gain an isolated determination of the effects. These experiments included common optical, mechanical, and thermal characterizations, to allow a comprehensible determination of the parameters.

An analytical model based on first law of thermodynamics is developed considering: void expansion, surface tension, fiber reinforcement network, polymer flow, crystallinity, thermal expansion, moisture, and external loads. The model is validated for the equilibrium state and the time dependent progress of deconsolidation including a sensitivity study of the deconsolidation effects. The model is applied to a full process chain from the consolidated part (organo-sheet) to the steps re-heating, where deconsolidation occurs, and cooling, where reconsolidation takes place. In order to simplify the usage of the model, universal applicable input parameters are defined and the accuracy is proven.

The findings of the work are applied to industrial processes such as thermoforming, induction welding, and thermoplastic tape placement. Key effects are found and further investigated to determine the influence on the part quality and process speed. The application shows the relevance of the model for the process development and their possible improvements.

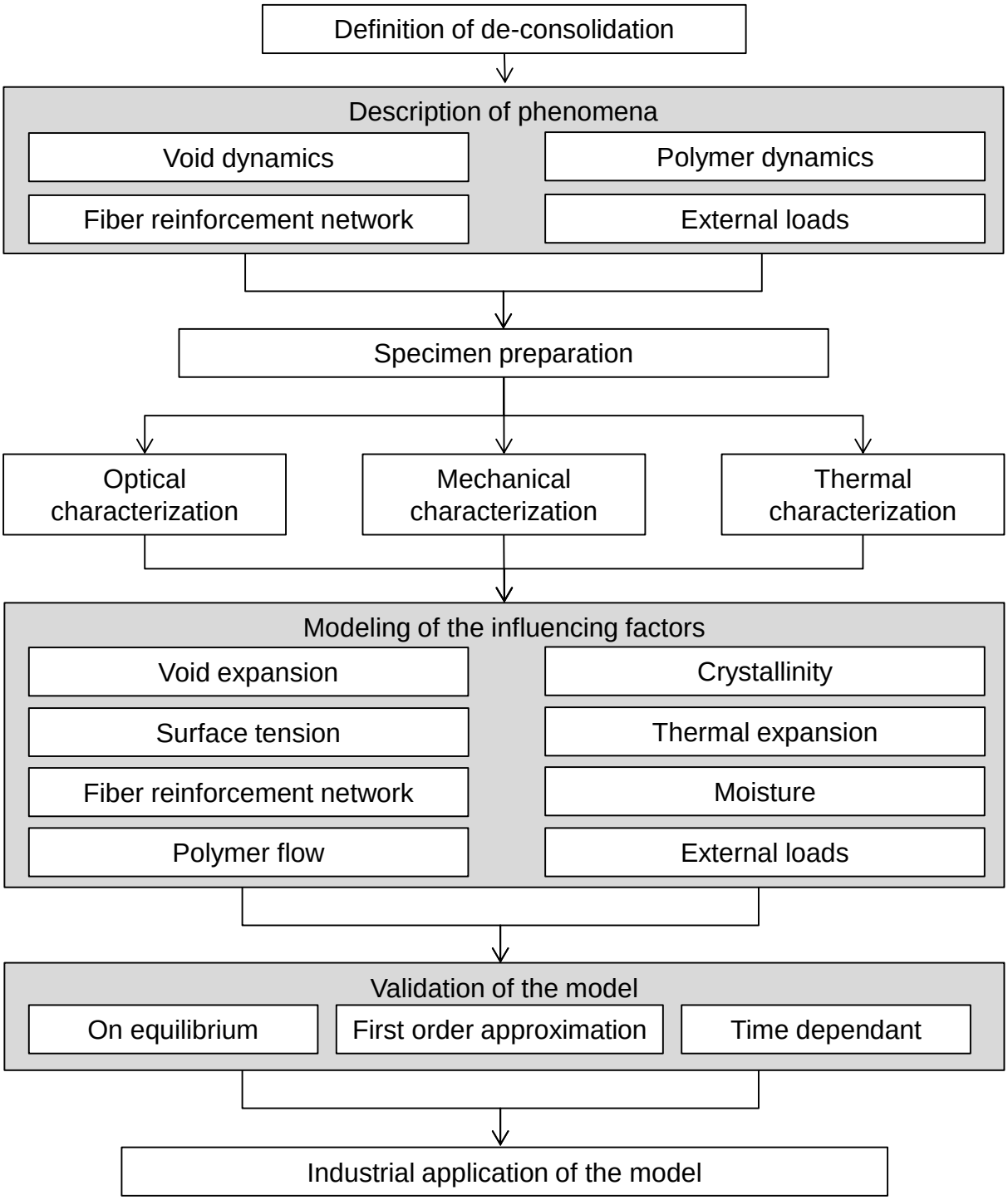

Figure 1.2: Layout of the work from the literature review to the industrial application

2 State of the Art

In the middle of the 1990's, deconsolidation, associated with an increase of void content, came in the focus of research because of the emergence of new continuous thermoplastic manufacturing techniques with a higher mass output than conventional techniques like autoclaving. Henniger et al. defined deconsolidation "as the tendency of a composite to lose consolidation on reheating, hence as a structural disintegration, which is often associated with an increase in void content" [8]. Deconsolidation has been investigated by many different researchers and for many different applications. Ranganatha et al. and Pitchumani et al. developed a model for the thermoplastic tape placement process considering the surface tension of the composite and the ideal gas law as the main factors of deconsolidation, which is damped by the viscosity [11; 12]. More recent, this result has been confirmed by Khan et al [13]. In contrast to these findings, Ye et al. and Wolfrath et al. identified the unloading of the tension in the fiber network as the main factor of deconsolidation. They neglected the ideal gas law and the surface tension, because of minor importance for their case [14; 15]. From literature four different factors can be identified for deconsolidation:

1. Decompaction of fiber reinforcement network
2. Void expansion because of thermal gas expansion (ideal gas law)
3. Void shrinkage and coalescence because of surface tension
4. Viscoelastic behavior of matrix

2.1 Deconsolidation Mechanisms

This chapter deals with possible deconsolidation phenomena and their physical background. Subsequently, the occurrence in process is presented.

2.1.1 Void Dynamics

The ideal gas law can be used to model the behavior of a real gas. It is assumed that a certain number of disordered particles move because of the Brownian motion inside a volume. They hit each other and barriers [16]. The model (2.1) approximates the behavior of real gases for low pressures, which set the volume V, and pressure p in a proportional relationship with the temperature T, the mass m and the specific gas constant R_s [16]. This idealization usually gives an acceptable accuracy, if the pressure is below 1 MPa [16].

$$m \cdot R_s \cdot T = p \cdot V \qquad m \cdot R_s = \frac{p \cdot V}{T} = \text{constant} \tag{2.1}$$

Many authors used the ideal gas law to model the void behavior during deconsolidation. Usually it is assumed that the void expands, when the internal void pressure is above the external pressure or shrinks, when the external pressure is above the internal pressure applied [12; 13]. Some authors used the ideal gas law to approximate the influence of the temperature on the final state of deconsolidation, which leads to a very low influence on void content [17]. Neither of these approaches considers a hindering effect on deconsolidation, when the volume is forced to expand by other effects.

2.1.2 Surface Tension

The surface tension is caused by the tendency of a liquid to reduce the free surface area. Energetically efficient is a sphere because of the high volume to surface ratio. Equation (2.2) shows the general relationship between the surface energy change E_{sur}, the surface tension γ, and the new surface area dA_{vo} [16].

$$E_{sur} = -\int \gamma \cdot dA_{vo} \tag{2.2}$$

The surface tension has been identified as an important factor for deconsolidation [11; 12]. There are two main approaches [11; 12]. Firstly, pure shrinkage of voids by neglecting void movements relative to the polymer and void coalescence. Secondly, Ye et al. concluded for glass and carbon fiber thermoplastic composites that the surface tension can lead to shrinkage and also coalescence of voids. But they concluded that void shrinkage is not a significant reason for deconsolidation and therefore they neglected the effect of surface tension [17; 18].

The surface tension of many polymers is linear temperature dependent between room temperature and above melting temperature [19–21]. As the temperature increases, the internal energy of the polymer increases and relates to the surface entropy. This leads to a lower surface tension [22]. Usually, the dependency of surface tension on temperature is in the range of 0.05-0.08 mN/m/K [22]. The surface tension for polypropylene, polycarbonate, and polyphenylensulfide is listed in Table 2.1.

Table 2.1: Surface tension and its dependency on temperature

Polymer	**Surface tension [mN/m]**	**Temperature dependency [mN/mK]**
Polypropylene	31.57 [21] 29.6 [22] 29.4 [23]	0.059 [21] 0.058 [22] 0.056 [23]
Polycarbonate	42.9 [23]	0.060 [23]
Polyphenylensulfide	49.6 [24]	-
Glass fiber reinforced polyphenylensulfide	43.2 [24]	-

2.1.3 Fiber Reinforcement Network

The fiber reinforcement network has been identified as another major factor affecting deconsolidation [15; 17-18]. Much literature are available dealing with single fiber bundle compaction and multilayer compaction. Cai and Gutowski proposed a model of lubricated fiber bundles based on fiber waviness and friction [25]. The elastic component is based on beam bending in different directions and the viscous component is caused by shear only. Chen et al. used the model to simulate the

deformation behavior of a single woven fabric layer and identified bending, initial fiber packaging, and yarn compaction as the major effects [26]. They also investigated the compaction behavior of multilayer fabrics. In addition to the single layer behavior, nesting occurred, whose influence increased with the number of layers and finally became the dominant factor [27]. The general shape of the thickness over pressure curve has three sections (Figure 2.1). For low pressure, a pressure increase causes a strong linear decrease of thickness. For intermediate pressure, a pressure change shows an exponential transition to high pressure. And finally for high pressure, a pressure change shows a slight linear decrease of thickness [28]. These findings were validated by the contact pressure between adjacent layers of fabric [29].

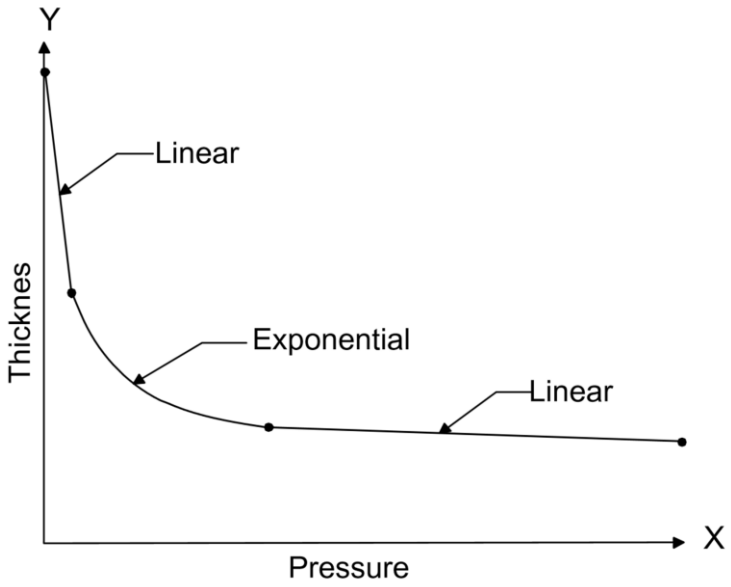

Figure 2.1: Typical compaction curve of a dry woven fabric [28]

Another approach to model multilayer compaction is to use the Maxwell equation. The spring damper approach uses parallel and in sequence shut elements. The range is from one to five different elements [30–32]. Govignon et al. investigated the loading and unloading behavior during dry and wet testing of multilayer fabrics. They identified three sections of the resin infusion process, the dry compaction, the wet decompaction, and the wet re-compaction [33]. Their results fit well to the Maxwell equation, the so called power law. The unloading had a lower force than the loading at the same thickness. Especially, the wetted fibers showed a lower load because of a lubrication effect by the low viscous resin [34; 35]. The compaction behavior can be enhanced by vibration in the dry state, but there is no influence during compaction in the wet state [36]. Nevertheless, Kelly and Bickerton and Walbran et al. found out

that the compaction and decompaction behavior fits better to a polynomial function of 4th order than the usually used power law [37; 38].

2.1.4 Polymer Dynamics

Thermoplastic composites usually expand with increasing temperature, dependent on the fiber/matrix combination and the thermal history. The coefficient of thermal expansion of the matrix is much higher than of the carbon or the glass fibers. The composite has an anisotropic expansion. Fibers have a lower expansion coefficient in longitude direction than in transverse direction [39]. The longitudinal behavior of the composite is dominated by the fibers, compared to the transversal direction, which is matrix dominated [40–42]. Fibers generally show a linear expansion behavior over temperature and no material change or reconfigurations occur during composite processing temperature [43]. The in-plane expansion can be modeled by the rule of mixture as given in Equation (2.3), where α is the coefficient of thermal expansion, E is the young's modulus, φ the fiber volume fraction, V the volume, m stands for the matrix, f for the fibers, and || for longitudinal direction. The longitudinal behavior is dominated by the high stiffness of the fibers.

$$\alpha^{c}{}_{11} = \frac{\alpha^{\parallel}{}_{f} \cdot E^{\parallel}{}_{f} \cdot \varphi + \alpha_{m} \cdot E_{m} \cdot (1-\varphi)}{V_{f} \cdot E^{\parallel}{}_{f} + V_{m} \cdot E_{m}} \tag{2.3}$$

Thermoplastic polymers show a nonlinear expansion behavior over temperature including significant changes at certain temperatures (melting, crystallization, glass transition), which is also dependent on the thermal history [40; 41; 44]. Sorensen et al. have investigated the thermal expansion of carbon fiber reinforced polyphenylensulfide and found out a complex temperature dependent behavior [45]. They have considered the different coefficients of thermal expansion stepwise. The thermal expansion in through thickness direction cannot be easily gained form the individual coefficients of the polymer and the fibers because of the Poisson effect in in-plane direction of each individual ply and the behavior of the matrix rich regions [40; 46]. In order to overcome this issue, a finite element method (FEM) micromechanical model was used based on a unit cell [47]. Nevertheless, if the

temperature dependency of the coefficient of thermal expansion α_c is known (by experiment or FEM), the composite strain ε_c can be calculated (2.4), where T_0 and T_1 are the initial and target temperature [39].

$$\Delta\varepsilon^p = \int_{T_0}^{T_1} \alpha_c(T) \cdot dT \tag{2.4}$$

Another key factor of expansion in through thickness direction is resin shrinkage due to crystallization and melting of crystals because of a different package density of amorphous and crystalline phases. Crystalline structures have a short range order of polymer chains, leading to a higher density compared with disordered structures of amorphous phases. Depending on the thermal history, this can lead to significant thickness changes and lock or release of residual stresses. Because of the high fiber stiffness, the effect of crystallization and melting is low in fiber direction and is often neglected [48].

Because of crystallization, the current density of the polymer ρ_p (2.5) can be modeled by using the rule of mixture of the amorphous density ρ_a, and the crystalline density ρ_c of the polymer. The degree of crystals is X_c [44].

$$\rho_p = \frac{X_c}{\rho_c} + \frac{1 - X_c}{\rho_a} \tag{2.5}$$

The incremental volume change ΔV^p of the polymer can be modeled by Equation (2.6). ρ_{p-1} is the previous incremental polymer density.

$$\Delta V^p = \frac{\rho_{p-1} - \rho_p}{\rho_p} \tag{2.6}$$

The volume change of the polymer can be used to calculate the polymer strain $\Delta\varepsilon^p$ (2.7). The proposed crystallization kinetics, based on the modified standard linear solid, considers the viscoelastic response of the polymer [48].

$$\Delta\varepsilon^{p} = \frac{-1+\sqrt{1+\frac{4}{3}\Delta V^{p}}}{2} \tag{2.7}$$

As shown in chapter 5.1 and in literature, voids in thermoplastic composites commonly have a spherical shape [12–14]. The first report on spherical bubbles in a liquid was published by Rayleigh in 1917 [49]. He investigated the collapse of bubbles in boiling water. As reported by Joseph et al., Poritsky extended the model of Rayleigh with the influence of surface tension and viscosity [50]. Nevertheless, the equation described the phenomenon is called the Rayleigh-Plesset equation given in (2.8) [50–53]; where γ is the surface tension, R the void radius, p_b the bubble internal pressure, p_∞ the external or atmosphere pressure, t the time, and η the viscosity. The dots stand for the first and second derivation of time. Accordingly, the equation is a differential question.

$$\frac{2\cdot\gamma}{R} = p_b - p_\infty - \rho\cdot(R\cdot\ddot{R}+\frac{2}{3}\cdot\dot{R}^2) - 4\cdot\eta\cdot\frac{\dot{R}}{R} \tag{2.8}$$

The Rayleigh-Plesset equation is based on a unit cell, where a void is surrounded by a liquid shell of infinite size. The model is used to approximate the void growth in non-Newtonian liquids doped with a blowing agent [54]. Amon and Denson used the equation to model the bubble expansion in a Newtonian fluid with a biaxial flow [55]. Since then, many authors have used the approach to model void dynamics in thermoplastic processes such as tape placement or during deconsolidation [11; 12; 17; 18].

Another approach to model the matrix flow is based on Darcy's law [15; 56]. Generally, Darcy's law can be used to model flow processes in porous media such as fabrics. This has been described by Gebart and Adams and Rebenfeld [57; 58]. The flow velocity of a low viscous liquid can be calculated by (2.9), where v is the average velocity, K the permeability, ∆p the pressure drop, and ∆l the flow length.

$$v = -\frac{K}{\eta} \cdot \frac{\Delta p}{\Delta l} \tag{2.9}$$

Wolfrath et al. used the equation (2.9) to model the fiber volume evolution of a glass mat thermoplastic composite during deconsolidation [15; 56]. They assumed that the fiber bed is the porous media and the matrix is the liquid. A composite commonly has lower permeability transverse to the fiber direction than in fiber direction [59–61]. When the specimen is subject to pressure in transverse direction, this leads to a preferred flow in in-plane direction. The fibers are usually assumed to be rigid and do not flow with the polymer. This results in a fiber wall friction of the polymer to the fibers, which affects the polymer flow profile [59–61]. Rogers proposed a simple model with no wall slip (Figure 2.2). Therefore, the polymer cannot flow in the contact region. He also assumed a Newton fluid and a plate like shape of the contact region. The model is solved for a constant force F in Equation (2.10), where L is the length of the specimen, H the height, and Δt the time interval.

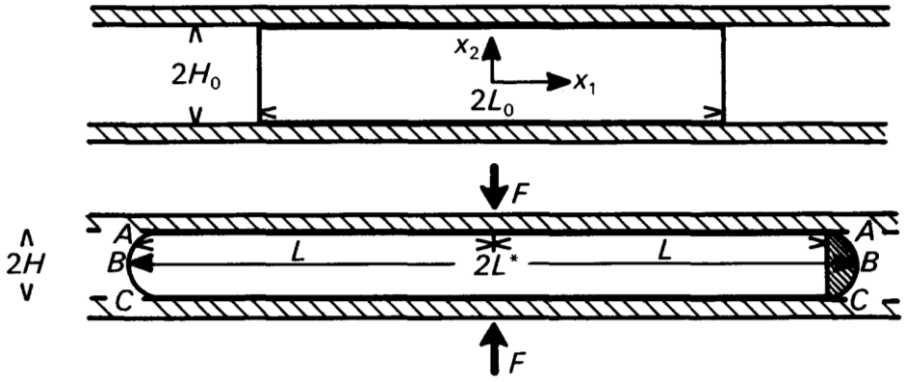

Figure 2.2: Schemata of the squeeze flow between two layers [59]

$$\frac{1}{H^5} - \frac{1}{H_0^5} \approx \frac{5 \cdot F \cdot \Delta t}{2 \cdot \eta \cdot L_0^3 \cdot H_0^3} \tag{2.10}$$

The mobility of polymer chains is dependent on the molecular mass, the chemical composition, and the temperature. Above the melting or glass transition temperature, the polymer chains change into a viscous state with a high mobility of the chains. This allows the flow of the polymer [62]. Below this temperature, the polymer chains can hardly creep, which is a time and stress intensive progress. Above the melting

temperature of semi-crystalline polymers and the glass transition temperature of amorphous polymers, the non-cross-linked thermoplastic changes it state from a solid or viscoelastic state to a viscous state, which is dependent on temperature and chemical structure such as molecular mass or chain configuration [63]. The polymer viscosity can be determined by an Arrhenius type function (2.11), which has been found to give good correlation to the measurement [12; 13; 17; 64]. The polymer constants A and B were determined by empirically calculations. T is the temperature.

$$\eta = A \cdot e^{\frac{B}{T}} \tag{2.11}$$

Polymers are penetrable for moisture, which is absorbed by the surface and diffuses into the polymer. Polymers with polar groups such as polyamides or polycarbonate have a higher penetrability for moisture than nonpolar polymers such as polypropylene [63]. The diffusion in polymers is based on atomic transport between water and polymer molecules driven by Brownian molecular motion [65]. The solution diffusion can be described by Fick's first law of diffusion given in (2.12). J is the particle's current density, D the diffusion coefficient, and c_c the gradient of particle density. In a fiber reinforced polymer the moisture can be solved in the polymer and the sizing of the fibers [65].

$$J = -D \cdot grad\, c_c \tag{2.12}$$

The diffusion coefficient (water vapor permeability) of polypropylene, polycarbonate, and polyphenylensulfide is on different magnitude as well as the saturation point, as listed in Table 2.2. The diffusion coefficient of polypropylene and polycarbonate increases exponential (Arrhenius equation) with temperature. The thickness has a linear influence on the water vapor permeability by a negative slope [62].

Table 2.2: The diffusion coefficient (at 23 °C and 85 % relative humidity) and the saturation point of polypropylene, polycarbonate, and polyphenylensulfide

Polymer	**Water vapor permeability for 100 µm thickness [g/m²/24h]**	**Saturation point in weight [%]**
Polypropylene	~0.7 (100µm) [62]	0.03 [66]
Polycarbonate	15 (100µm) [62]	0.3 [62]
Polyphenylensulfide	-	0.02 [67]

2.2 Effect of Deconsolidation on Mechanical Properties

Interlaminar shear strength is affected by the toughness of the matrix, the interface strength between fibers and matrix, and the void content [68]. Only limited data of the influence of deconsolidation on mechanical properties is available; therefore the influence of void content after consolidation is also reviewed. The fiber volume fraction can also increase the interlaminar strength to a limited extent [68]. St. John and Brown investigated the effect of moisture on the interlaminar shear strength of glass fiber reinforced phenolic composites. The sizing was changed to show the effect of interface on shear strength. An optimized sizing can significantly increase the interlaminar shear strength in dry and especially in wet condition after exposure to water [69], because the moisture leads to a deterioration of the interface. Nevertheless, the effect of an optimized matrix toughness and interface is low in longitudinal direction [70]. The interlaminar shear strength is directly related to the void content by two factors: first, the reduction of net cross section and second, large voids act as crack initiators [71]. Wisnom et al. proposed that many small cracks (voids) have not enough energy to propagate the crack; there is a critical crack size necessary to weaken the specimen in the interface of plies [72]. Some values of the dependency of void content on mechanical properties are listed in Table 2.3.

Table 2.3: The effect of void content on different mechanical properties

Material	Mechanical test	Effect of 1 % void content change	Source
UD CF/PEEK	Double cantilever beam	~0.077 KJ/m²/%	[73]
UD CF/PEEK	Transverse flexure strength	~8.00 MPa/%	[73]
UD GF/PA66	Transverse flexure strength	15.5 MPa/%	[8]
UD GF/PP	Transverse flexure strength	18.6 MPa/%	[8]
UD GF/PP	Flexure strength	7.9 MPa/%	[75]
UD GF/PP	Shear strength according to Lauke [76]	0.7 MPa/%	[74]
UD GF/PA12	Shear strength according to Lauke [76]	4 MPa/%	[74]
UD CF/EP	Interlaminar shear strength	0.49 MPa/%	[77]
UD CF/EP	Interlaminar shear strength	6.79 MPa/%	[78]
UD GF/EP	Interlaminar shear strength	4-10 MPa/%	[79]
Woven CF/UP	Interlaminar shear strength	1.15 MPa/%	[78]
Woven CF/CC	Interlaminar shear strength	1.8-2.8 MPa/%*	[80]
Woven GF/PTFE	Interlaminar shear strength	2.7 MPa/%	[71]

***open porosity**

During impregnation and consolidation the void content decreases. The inverse process is deconsolidation, where the void content increases with a progress of time. Deconsolidation has a negative effect on the mechanical performance especially the interlaminar shear strength [8]. Henninger et al. found out a linear dependency of the interlaminar strength on the void content [8]. Beehag and Ye investigated the pressure necessary to prevent deconsolidation (void content increase) and the effect on the interlaminar fracture [81]. They concluded that for a carbon fiber unidirectional reinforced polyetheretherketone a pressure increase from 0 MPa to 0.2 MPa improved the mode I interlaminar fracture energy (double cantilever beam tests) from 1.5 kJ/m² to 2.2 KJ/m². It stayed constant for higher pressures. They gained a similar result for the transverse flexure strength. There is only limited literature available dealing with deconsolidation and the effect on the mechanics. Therefore, more

literature was evaluated dealing with void content and consolidation. Yoshida et al. proposed an allowable void content level (<1 %) for thermoset materials, which must be kept during manufacturing, to avoid undesired deviations in mechanical performance [78]. The level needs to be defined for each polymer separately because of different slopes of the degradation.

2.3 Composite Processing

A wide variety of manufacturing processes for thermoplastic composites are available. For several processes, deconsolidation is an issue. Two main problems can be identified: first, processes with heating or cooling with no or insufficient pressure, second, continuous processes, where the pressure is applied to a line or to a limited area such as a die or sliding shoe. Usually, the arrangements to avoid deconsolidation leads to a decrease of production speed.

2.3.1 Thermoforming

Thermoforming is the draping of fully impregnated sheets (organo-sheets) to the final shape. The process shown in Figure 2.3 includes the process steps: heating of the organo-sheet above melting temperature (left), transport to the press, forming in a temperated tool (usually far below melting temperature, middle left), cool down (middle right), and trimming (right).

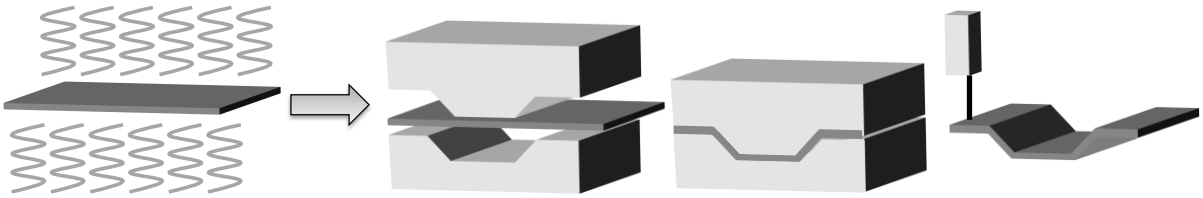

Figure 2.3: Process steps of thermoforming of composites including the steps: heating (left), forming (middle left), cooling (middle right), and trimming (right)

During heating in an infrared field or in an oven and during closing of the die, it is hardly possible to apply any pressure [82], which leads to deconsolidation. The deviation, between the final thickness after processing and the deconsolidated thickness, can cause problems with the temperature distribution because of an

isolation effect of the entrapped air. Also, during forming, the thickness deviation can lead to crushing at sharp edges of the die. The deconsolidated part reconsolidates during forming by the applied pressure. The degree of reconsolidation is dependent on the die temperature and the closing speed [82; 83]. As higher the die temperature as lower the void content, but this can extend the cycle time. A higher closing speed increases the cooling rate, which has a negative effect on the void content [84].

2.3.2 Induction Welding

Induction welding or curing is a joining technology for thermoplastic or thermoset composites, where heat is generated inside the material by inducing an electric current (eddy current) because of an alternated electro-magnetic field (Figure 2.4 left) [85; 86].

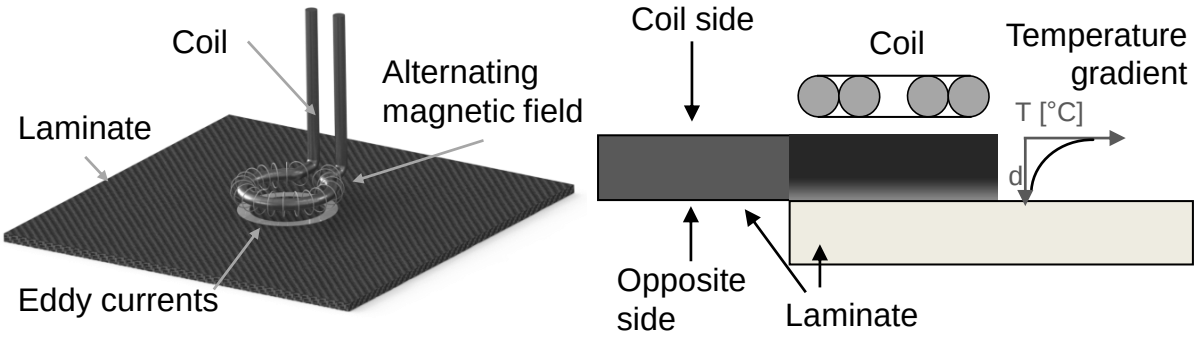

Figure 2.4: Principle of induction welding (left) and temperature distribution during induction welding (right) [87]

The heat can be generated within a conductive composite or within a susceptor in the joint. Pressure is applied by a die or a roller. Deconsolidation commonly occurs in thermoplastic conductive composites without a susceptor because the electromagnetic field is applied from the outside and its intensity quadratically decreases with the distance [14]. Therefore, more heat is generated closer to the coil and has to penetrate to the joint as shown in Figure 2.4 (right), which needs time [87]. Because of the thickness of the composite, it is hardly possible to draw the heat out of the composite in expectable time. If the composite in the inside is still molten after releasing the pressure of the die or roller, the composite deconsolidates. The deconsolidation weakens the joint and can distort the part [14]. Another problem is

the increased thickness, which decreases the electric conductivity because of less contact between the plies.

2.3.3 Thermoplastic Tape Placement

Tape placement is defined as the automated laying of oriented unidirectional preimpregnated fibers (tapes) on a tool [88]. A process schema is shown in Figure 2.5.

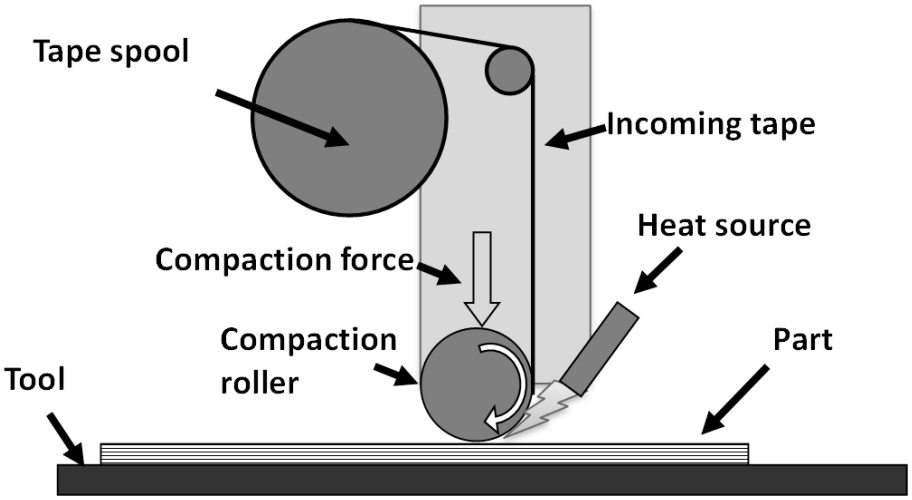

Figure 2.5: Schema of the thermoplastic tape placement process

During processing, the tapes are guided from the spool to the compaction roller, are heated above melting temperature by a heat source e.g. a hot gas torch or a laser beam, and are placed side by side until the layer is finished. A compaction roller draws out the applied energy of the material and consolidates the tapes. For the next layer, the process is repeated. Each orientation of the layer can be set according to the load profile. The placement process allows the production of large, load path optimized parts from fiber reinforced thermoplastic materials. The main drawback of a further velocity increase is deconsolidation as listed in Table 2.4. The roller cannot draw out enough energy of the material, so that the material is still in a molten state after compaction, which leads to a release of stored energy. The former consolidated part deconsolidates [89]. The internal void pressure has been identified as the main driver of deconsolidation for thermoplastic tape placement [10; 12].

Table 2.4: Limiting factor during thermoplastic tape placement

Heating type	Placement velocity	Limiting factor	Author
Hot gas	1.8 - 2.4 m/min	Deconsolidation (void formation)	Tierney and Gillespie [10]
Hot gas	0.9 - 2.1 m/min	Deconsolidation (void formation)	Heider et al. [90]
Hot gas	0.8 - 1.2 m/min	Delamination and deconsolidation (void formation)	Sonmez et al. [91; 92]
Hot gas	3 m/min	Delamination and deconsolidation (void formation)	Khan et al. [9]
Laser	6 m/min	Deconsolidation (void formation)	Brzeski et al. and Schledjewski [89; 93]

2.3.4 Roll Forming

Roll forming is a continuous process with a stepwise progressive forming by rollers to the final cross section. During processing, the material is heated above melting temperature, formed by pairs of rollers, and is cooled to solidify. The sheets change from reconsolidation at the rollers and deconsolidation between the two pairs of rollers [94]. The knowledge of deconsolidation is very important especially during the cooling from the molten state to room temperature because the material cools from the outside to the inside [81]. This gradient can cause deconsolidation and distortion of the part. There are two approaches to decrease deconsolidation and distortion during roll forming. First, the number of pairs of rollers can be increased and second, the process speed can be decreased. Both are economically undesirable [74].

3 Materials and Methods

This chapter describes the materials used, their preparation, and their characterization methods. Also the carried out treatments are explained. And finally, an analysis of errors is given to proof the confidence of the results.

3.1 Materials

Deconsolidation, which occurs during the re-melting of fiber reinforced thermoplastic composites, is not desired. Usually, one fabric and one polymer were investigated in former studies. This limits the validity of general interpretation. Therefore, different materials were selected in this study to cover a wide range of validity for applications and process conditions. The selected materials include a commodity, an engineering, and a performance polymer (polypropylene PP, polycarbonate PC, and polyphenylensulfide PPS), as well as a carbon fiber and two glass fiber reinforced textiles. The textile styles were unidirectional (UD), twill (TW), and satin (SA) with different fiber volume fractions. Some specimens are shown exemplary in Figure 3.1.

Figure 3.1: Some specimens used in this study (from left to right): PP SA 53, PP TW 48, PP UD 58, PC SA 50, and PPS SA 52 (Table 3.1)

These combinations consist of polymers with low, intermediate, and high melting temperatures and viscosities. The fabrics showed different compaction and decompaction behaviors depending on the textile configuration and their displacement. In order to investigate the effect of the manufacturing process on deconsolidation, the specimens were made by autoclaving (AC) and hot pressing (HP). Table 3.1 gives an overview of the materials and their acronyms used in this study.

Table 3.1: Materials used in this study and their acronyms

Textile type	Fiber type	Matrix	Fiber volume fraction	Process	Acronym
Unidirectional	Glass	Polypropylene	58 %	Autoclave	PP UD 58
Unidirectional	Glass	Polypropylene	40 %	Autoclave	PP UD 40
Satin1/4	Glass	Polypropylene	53 %	Autoclave	PP SA 53
Satin1/4	Glass	Polypropylene	49 %	Hot press	PP SA HP 49
Satin1/4	Glass	Polypropylene	48 %	Autoclave	PP SA 48
Satin1/4	Glass	Polypropylene	40 %	Autoclave	PP SA 40
Twill 2x2	Carbon	Polypropylene	52 %	Hot press	PP TW HP 52
Twill 2x2	Carbon	Polypropylene	48 %	Autoclave	PP TW 48
Satin1/4	Glass	Polycarbonate	50 %	Autoclave	PC SA 50
Twill 2x2	Carbon	Polycarbonate	48 %	Autoclave	PC TW 48
Unidirectional	Glass	Polyphenylensulfide	58 %	Autoclave	PPS UD 58
Unidirectional	Glass	Polyphenylensulfide	40 %	Autoclave	PPS UD 40
Satin1/4	Glass	Polyphenylensulfide	53 %	Autoclave	PPS SA 53
Satin1/4	Glass	Polyphenylensulfide	52 %	Hot press	PPS SA HP 52
Satin1/4	Glass	Polyphenylensulfide	52 %	Autoclave	PPS SA 52
Satin1/4	Glass	Polyphenylensulfide	40 %	Autoclave	PPS SA 40
Twill 2x2	Carbon	Polyphenylensulfide	52 %	Autoclave	PPS TW 52

Table 3.2 gives an overview of the polymers used and their main characteristics from the datasheet. The polypropylene was manufactured by Borealis AG, Austria. The copolymer was a low viscosity compound equipped with additives for good coupling between the matrix and glass fibers. It had a low density and low mechanical performance. Polycarbonate type Makrolon 2207 was manufactured by Bayer MaterialScience AG, Germany. Its viscosity was low and the polymer provided a compromise of density, prices, and mechanical performance. The polyphenylensulfide was supplied as a film made out of Ryton PR09-60 supplied from Chevron Phillips LLC, USA. The PPS had excellent mechanical properties and

a high flammability resistance. These polymers can be used for a wide range of applications.

Table 3.2: Polymer properties from the datasheet and literature

Property	**PP**	**PC**	**PPS**
Polymer class	Commodity	Engineering	Performance
Manufacturer	Borealis AG	Bayer Material-Science AG	Chevron Phillips LLC
Type	BJ100HP	Makrolon 2207	Ryton PR09-60
Morphology	Semi - crystalline	Amorphous	Semi - crystalline
Density [g/cm³]	0.904	1.19	1.35
Tensile modulus [GPa]	1.3	2.4	3.4 [62]
Tensile strength [MPa]	25	66	85
Strain at yield [%]	300	6.0	2.5
Flexural modulus [GPa]	1.25	2.35	3.8
Flexural yield strength [MPa]	35	60	130
Thermal expansion [1/K*10^{-6}]	~110 - 170 [62]	60-70 [62]	55 [62]
Glass transition temperature [°C]	0 - -10 [62]	144	85 [62]
Melting temperature [°C]	164	-	285 [62]
Amorphous density [g/cm³]	0.855 [95]	See density	1.32 [96; 44]
Crystalline density [g/cm³]	0.95 [95]	-	1.43 [96]

The properties of the textiles are listed in Table 3.3. The unidirectional textile was highly orientated with a grammage of 456 g/m². The satin glass weave had homogenous orientation in perpendicular directions. It was balanced to the twill carbon weave by the fiber volume fraction and the number of layers. All fabrics used had a silane based sizing. There were no details available on the chemical composition.

Table 3.3: Textile parameters of unidirectional, satin, and twill fabrics

	UD	SA	TW
Weave type	Unidirectional	Satin 1/4	Twill 2/2
Fiber type	Glass	E-glass	Carbon Torayca T300
Grammage [g/m²]	456	299	200
Yarn density in warp direction [Yarns/cm]	4	22	5
Yarn density in weft direction [Yarns/cm]	4	21	5
Linear density in warp direction [g/km]	1088	68	200
Linear density in weft direction [g/km]	17	68	200
Sizing	Silane	Silane	Epoxide

3.2 Specimen Preparation

Two manufacturing processes were used to investigate the effect of consolidation pressure and applied underpressure within a vacuum bag. The flow chart of specimen preparation is shown in Figure 3.2.

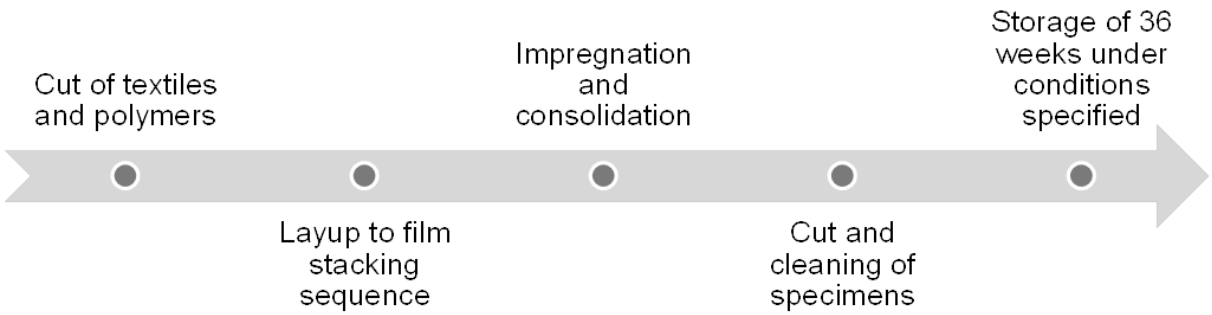

Figure 3.2: Flow chart of the specimen preparation

The fabrics were cut from the roll to a size of 54 x 22 cm² and laid up in a film stacking sequence to accomplish the desired thickness and fiber volume fraction. During processing, the specimen were heated at 10 K/min to target temperature, which was 320 °C for PPS, 280 °C for PC, and 210 °C for PP. The impregnation pressure was maintained for 1 h and followed by cooling at 10 K/min to room temperature. Finally, the pressure was released. During autoclaving, a pressure of

250 Pa was applied in the vacuum bag and an external pressure of 2.4 MPa was applied. For the hot press process, no vacuum bag was used and the applied pressure of the tool was 4.5 MPa.

After manufacturing the specimens were cut to size by a water cooled buzz saw to 50 x 50 mm². The specimens were cleaned with water, dried with tissues, and stored at room temperature. The mean humidity during storage was 55 %. At least 36 weeks of storage were maintained to equalize the internal void pressure and the moisture of the specimens.

3.3 Deconsolidation Treatments

Two different deconsolidation treatments were carried out. During the free deconsolidation treatment, no external force was applied and during the inhibit deconsolidation treatment, different forces were applied. The free deconsolidation experiments were carried out on the hot press shown in Figure 3.3.

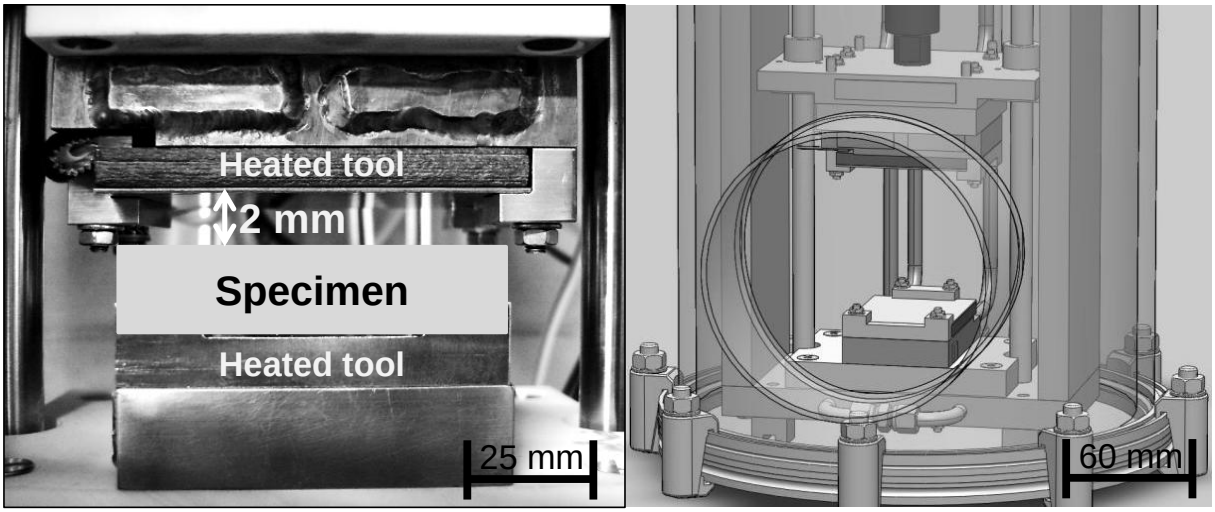

Figure 3.3: The hot press used for deconsolidation treatments

Specimens were placed on a heated tool with a size of 58 x 58 mm². The upper die was positioned 2 mm above the specimen, which ensured no contact to the upper die during all experiments. The temperature profile of the bottom and the upper die was coupled to decrease thermal losses caused by convection.

The specimens were heated at 10 K/s to 25 K below the melting temperature for semi-crystalline polymers and 25 K below the glass transition temperature for

amorphous polymers and maintained at this temperature for 5 min to allow a homogenous temperature distribution through the thickness of the specimen. The temperature was increased to target temperature at 10 K/s and maintained for 10 min. The target temperature was 30 K above the melting temperature for polypropylene and polyphenylensulfide, and 100 K above the glass transition temperature for polycarbonate because of the high viscosity of polycarbonate at 30 K above the glass transition temperatures. These temperatures were chosen to achieve an appropriate speed of the expected effects with sufficient measurement points. Figure 3.4 shows the time temperature chart of the free deconsolidation experiment. Specimens fully deconsolidated within 10 min as shown in chapter 6, when no external pressure was applied. This means all locked forces were released and the specimens were in equilibrium. The specimens were cooled to room temperature at 1 K/s.

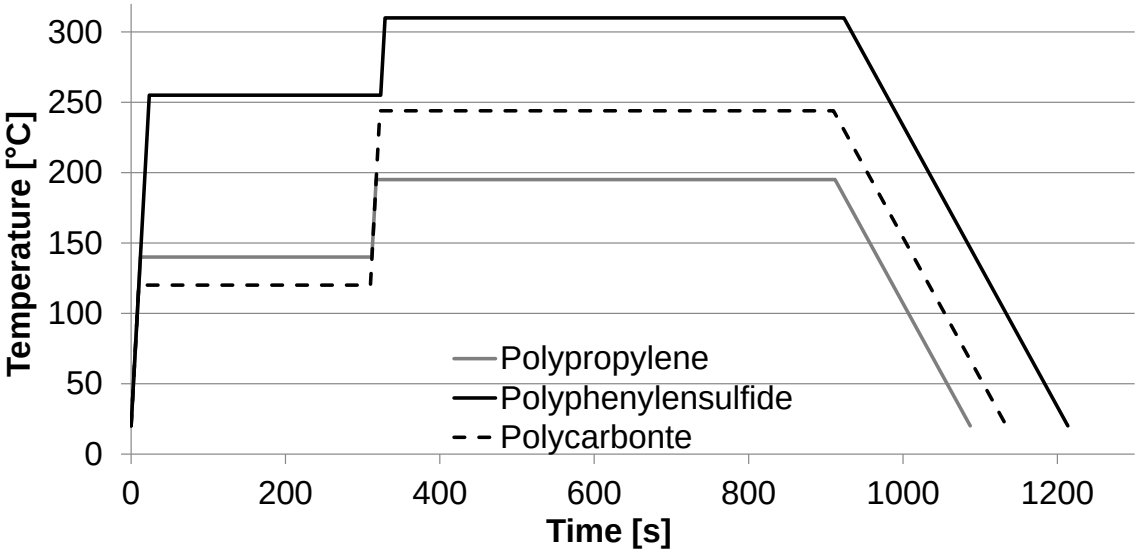

Figure 3.4: Time-temperature chart of the free deconsolidation experiments

Inhibit deconsolidation treatments were carried out on a heated tool. The specimens were subjected to a pressure, which is lower than the proposed pressure to inhibit deconsolidation of << 0.3 MPa [81, 97; 98]. The following pressures were used: 0.0016 MPa, 0.0048 MPa, 0.0064 MPa, and 0.012 MPa. Because of the low pressure, no matrix squeeze out occurred during the treatment. The specimens were heated at 10 K/min from the bottom. The target temperatures were 325 °C for PPS, 260°C for PC, and 210 °C for PP and were maintained for 30 min, to completely equalize the locked forces. These temperatures were set higher than for the free

deconsolidation experiments because of higher thermal losses caused by the applied die by a weight, which acted as a heat sink.

3.4 Material Characterization

Different material characterization tests were carried out, to investigate the material behavior before, during, and after the deconsolidation treatments. Also material characterizations were carried out to determine the initial state of the material (consolidated state), which were needed as the input parameters of the model. These investigations allowed the verification of the model for a detailed prediction of deconsolidation and an approximation using universal applicable input parameters of deconsolidation.

3.4.1 Thickness measurement

The thickness of the specimens was measured optically during the deconsolidation treatment. Before and after the treatment, the thickness was measured mechanically by means of a micrometer screw. Figure 3.5 shows the test set-up of the optical measurement (left). The thickness of every specimen was measured mechanically at five positions (white dots / Figure 3.5 right).

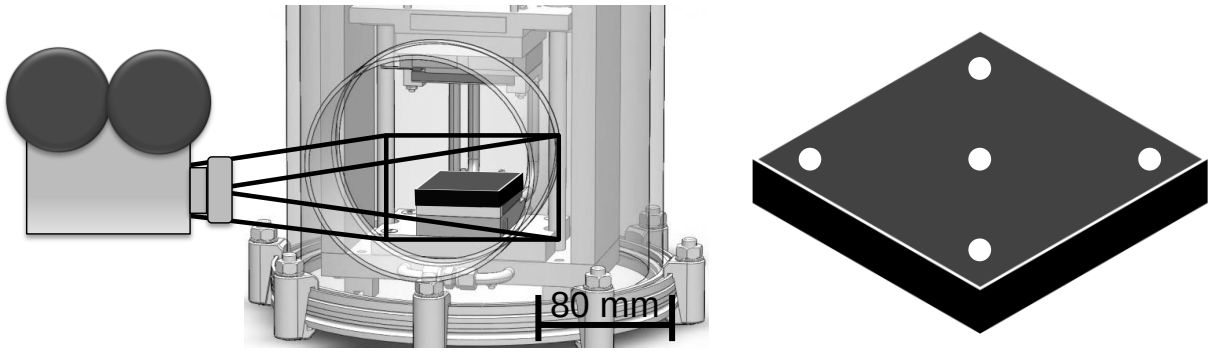

Figure 3.5: Optical thickness measurement during deconsolidation (left) and mechanical thickness measurement before and after deconsolidation at five positions (right)

A micrometer screw with an accuracy of ±1 µm and a pre-defined testing force was used. An average value for each configuration of the measurements was calculated. During the deconsolidation treatments, the specimen was captured by a CCD camera with a resolution of 1024x768 pixels and a frame rate of 1 fps. The post

analysis of the pictures to determine the thickness was done with Motion Studio from Integrated Design Tools Inc, USA. In order to calibrate the measurement, the average thickness of the specimen, determined by the micrometer screw, was taken to set the initial thickness to the pixel size. The software tracked the edges of the specimen over time resulting in the thickness change over the corresponding temperature and time (Figure 3.6). The measurement accuracy was determined by the comparison of the final thickness of the specimen measured with the micrometer screw to the software results. The maximum error was 20 µm.

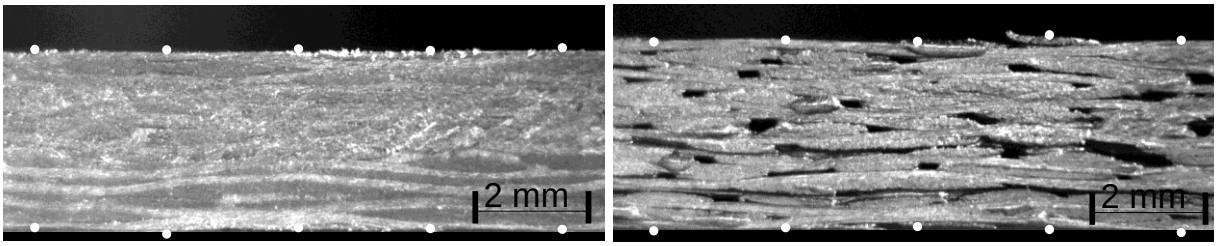

Figure 3.6: CCD camera image at the begin of the measurement (left) and after the measurement (right) with post digital processing (white dots)

3.4.2 Microscopic Characterization

Optical characterizations were used to investigate the void and yarn change before and after deconsolidation. Therefore, micrographs of the consolidated and different deconsolidated states were taken and further analyzed by means of Analysis Docu 5 from Olympus K.K, Japan. The micrographs were taken by a reflected light microscope type Aristomet from Leiz Group, Germany in both plane directions to gain more information about void shape and distribution. Figure 3.7 exemplarily shows the investigated properties, which were void content, size, distribution, and shape (diameter and circumference). Eight micrographs of each configuration out of four samples were taken from polished specimens to ensure statistical reliability. The samples were cut out from the middle of the specimens (50 x 50 mm²). The number of voids was calculated from the void content, the specimen's volume, and the void radius.

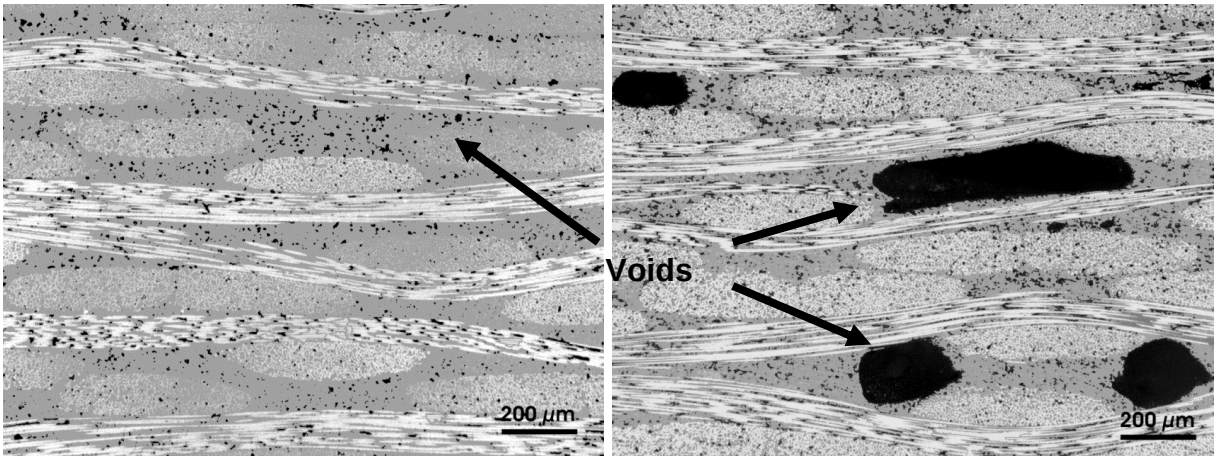

Figure 3.7: Digital image analysis of consolidated (left) and freely deconsolidated (right) PP SA 48

In order to gain a void size distribution, the recorded void sizes were grouped in fixed intervals with an upper and lower limit of void size. This leads to a classification of the void sizes and allows the calculation of the percentage of each void class. This procedure was carried out according to DIN 66141 and Schwister et al. [99–101].

3.4.3 Mechanical Characterization

Interlaminar shear strength

Deconsolidation has a significant effect on the mechanical performance, especially the interlaminar behavior. The interlaminar behavior has been identified to be very sensitive to deconsolidation and void evolution [74]. In order to quantify the effect of deconsolidation on the interlaminar shear strength, specimens were tested according to DIN EN ISO 14130 [102]. The test was repeated for the consolidated and fully deconsolidated stages 10 times and for the intermediate deconsolidated stages 5 times. A Zwick Roell 1474 universal testing machine with a die velocity of 10 mm/min was used. Figure 3.8 shows the test set up. The specimen’s width and length and the bearing distance were adjusted according to the thickness of the specimen.

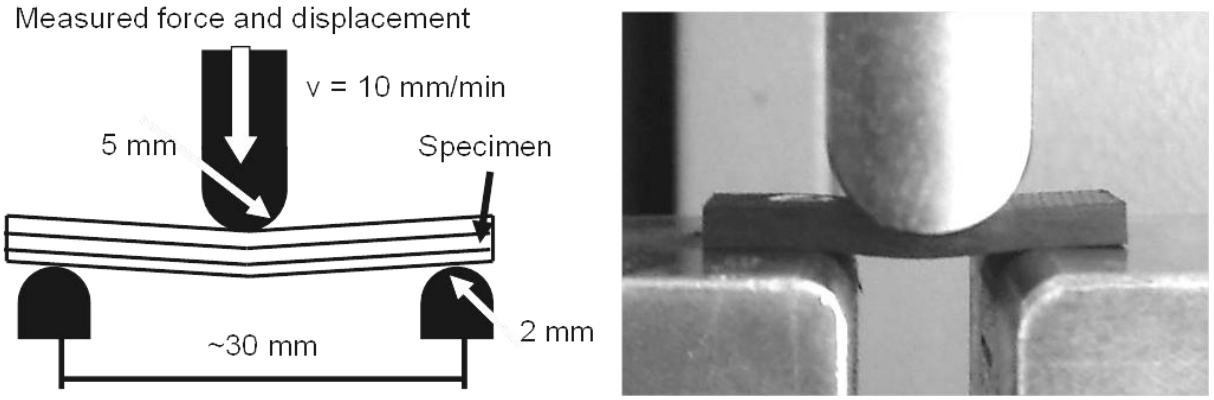

Figure 3.8: Experimental set up of the interlaminar shear strength test

The interlaminar shear strength was calculated from the force at fracture. Also, the fracture type was optically analyzed and classified in the types interlaminar, mixture, bending, and compression fracture.

Compaction and decompaction test of dry fabrics

The compaction and decompaction of the fiber reinforcement network have a high influence on deconsolidation [17]. Therefore, the fiber reinforcement was compacted and decompacted on a universal test machine (Zwick Roell 1474). Only one compaction and decompaction cycle were carried out. To increase measurement accuracy, three blind curves were recorded and all experiments were corrected by the average blind curve. Several layers of fabric were placed onto each other with the same orientation. One configuration deviates from this lay up (PPS SA 53). This configuration had a cross ply lay-up. Each test was repeated three times with a displacement velocity of 0.6 mm/min, which was assumed to be infinitesimal slow. Between compaction and decompaction the holding time was set to 2 min to settle the stack. The difference between wet and dry compaction was considered by the parameters matrix viscosity and polymer flow. Any lubrication effects, which were known from thermoset resins, were neglected.

3.4.4 Surface Characterization

Some authors have identified the surface tension as a main inhibitor of deconsolidation [13; 103]. Polypropylene, polyphenylensulfide, and polycarbonate specimens were investigated according to the Owens, Wendt, Rabel, and Kälble

method (WORK), which was a standard method (DIN 55660-5) [104]. They used the static contact angle measurement by means of an optical tension meter. Contact angles of different liquids on a reference specimen (steel) are shown in Figure 3.9. Eight drops of each liquid (glycerol, ethylene glycol, dimethyl sulfoxide, and diiodmethane) were placed onto the specimen at room temperature. These liquids were standard liquids for contact angle measurements of polymers [105; 106]. The tests were repeated three times.

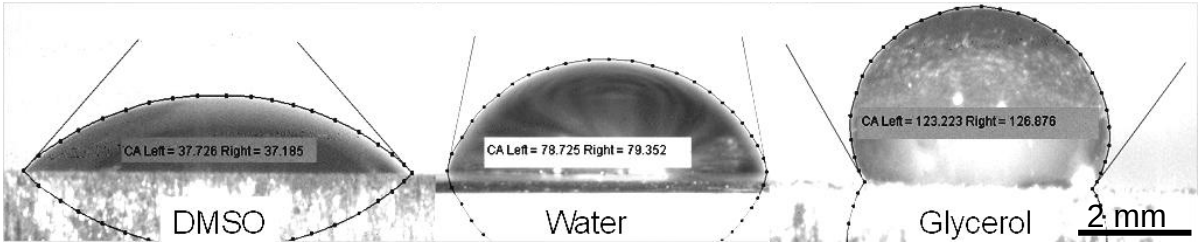

Figure 3.9: Surface angle of a reference specimen

Surface tension of polymers decreases linearly with temperature [107; 19; 20]. These test liquids cannot be used above room temperature because of vaporization. This would falsify the measurement because of energy loss of the vaporized mass. Special equipment and the consideration of vaporization were needed to gain accurate results. Therefore and because of the similar temperature dependency of each polymer group, literature values were used for the temperature dependency.

3.4.5 Thermal Characterization of the Polymer

The crystallinity of polymers has a high influence on their density because of different molecular structures of amorphous and crystalline regions. This leads to a different volume of the specimen. In order to quantify this influence, a differential scanning calorimetry was carried out on a Mettler Toledo DSC 1 for reinforced and neat polyphenylensulfide, polycarbonate, and polypropylene before and after the experiments with different (10 K/min) and similar cooling rates (60 K/min) than in the actual deconsolidation treatment and manufacturing processes. Therefore, the specimens were heated to target temperature and held for 30 min in melt, followed by cooling to room temperature. DSC analysis were carried out according to DIN EN ISO 11357 and repeated two times for two different specimens [108–110]. Pieces of 10 mg were cut from the specimens and placed in an aluminum pan for testing. The

energy change over temperature curve, shown in (Figure 3.10), was taken to determine the enthalpies of recrystallization and melting.

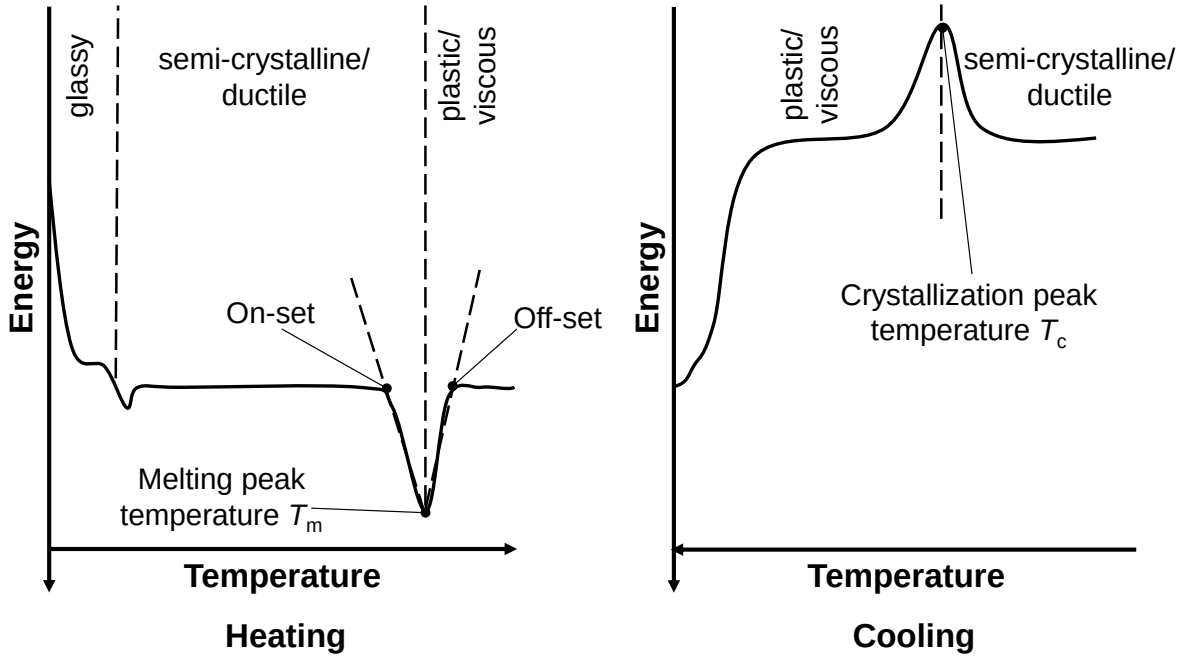

Figure 3.10: Exemplary energy temperature curve for a heating (left) and cooling cycle (right)

The crystallinity was calculated according to (3.1), where ΔH_R is the specific enthalpy of recrystallization, ΔH_M is the specific enthalpy of melt, and ΔH^0 is the theoretical specific latent heat of a full (100 %) crystallization.

$$X_C = \frac{\Delta H_M - \Delta H_R}{\Delta H^0 \cdot (1-\varphi)} \tag{3.1}$$

Additionally, the melting temperature, the crystallization temperature, the on-set and off-set temperature of melting and crystallization were determined from the DSC curve. Melting temperature T_m was defined as the peak temperature of melting and crystallization temperature T_c was defined as the peak temperature of crystallization. The on-set and off-set temperature was the extrapolation of the slope at the inflection to the baseline [111].

Viscosity of polymer has a high impact on flow behavior of matrix during deconsolidation. Rheometer measurements on an ARES from Rheometric Scientific GmbH, Germany served for the determination of the dynamic viscosity. A plate to

plate rheometer set up was used to measure the viscosity at four different temperatures at a frequency of 10 Hz and strain of 5 %, which was found to be at the Newtonian plateau of neat PPS Grade 0214 [112] and BJ100HP polypropylene. The specimens had a diameter of 50 mm with a thickness of 3 mm and were placed for 3 min in the oven of the rheometer to equalize the temperature. After the procedure, the measurement started. Rheometer specimens were made out of neat polymer, which were pressed into shape. Tests were carried out according to [113–115] and were repeated two times. The temperature dependency of the viscosity (2.11) can be calculated by an Arrhenius function [4; 116–118].

The thermal expansion can be measured by two approaches: First, the differential mechanical analysis (DMA), where a low force is applied to the specimen by a pin. The expansion during temperature change moves the pin [111]. Second, the thermal expansion can be calculated from the temperature curve and the corresponding thickness evolution, which was used in this case. Therefore, the temperature curve was split in intervals of 2 K and was divided by the corresponding thickness change (3.2) [119]. The resultant values were plotted over the average temperature of the interval. All values were subjected to a linear regression analysis.

$$\alpha_c(T) = \frac{\Delta T}{\Delta x(T)} \tag{3.2}$$

3.4.6 Water Absorption

The water absorption at 23 °C and 50 % relative humidity was determined by gravimetric measurements on an analytic balance (Excellence Plus XP from Mettler Toledo from Ohio, USA) with an accuracy of 0.01 mg. The specimens were weighted according to ASTM D 570 [120] before and directly after drying. Three specimen of the configurations PP SA 53, PPS SA 53, and PC SA 50 were tested. Their drying conditions are summarized in Table 3.4.

Table 3.4: Conditions of the specimens

Property	At atmosphere	Long term drying	Pre-deconsolidation condition
Relative humidity	50 %	55 %	55 %
Temperature	23 °C	110 °C	140°C (PP), 115°C (PC), 255 °C (PPS)
Drying time	-	24 h	5 min

The specimens were dried at 110°C for 24 h in a convection oven to determine the total water absorption. The percentage of water absorption can be calculated by dividing the weight loss by the initial weight. A second treatment was carried out, which considered the condition before the deconsolidation treatment (pre-deconsolidation condition). Therefore, the specimens were heated to 25 K below the melting temperature (semicrystalline polymers) and glass transition temperature (amorphous polymers) and maintained for 5 min at temperature. This allowed some vaporization and diffusion before the specimen would further be heated above the melting temperature. The specimens' weight was measured before and after holding the specimens below that temperature.

3.4.7 Analysis of Errors

Experiments were repeated several times and mean values of each configuration were calculated. Only mean values and their confidence interval are presented in the results section, except for the decompaction curves. The decompaction curves presented were a selection of single records, which represents most suitable all records of the configuration. Because of material inhomogeneity and process condition deviations, confidence interval (σ) of 99 % and standard deviation (s) were calculated from the recorded data according to Equation (3.3) [121], where t_{stu} was the student factor and n_r was the number of measurements.

$$\sigma = \frac{s \cdot t_{stu}}{\sqrt{n_r}} \tag{3.3}$$

This value gave a possible statistical deviation of the mean values from the estimated mean value. Measurement errors were deleted, if the Nalimov criterion was fulfilled or the specimen showed a defect after the treatment. This could be an unmelted area, impurities or other visible defects. The Nalimov criterion was calculated according to [121] for conspicuous values ẋ (3.4), where ȳ is the average value.

$$r^* = \frac{\left|\dot{x} - \bar{y}\right|}{s} \cdot \sqrt{\frac{n_r}{n_r - 1}} \tag{3.4}$$

The following Table 3.5 summarizes the repeats of experiments and measurements, the confidence interval of each configuration, and the total number of each characterization method.

Table 3.5: Characterization methods and their repeat, confidence interval, and total measurements

Method	Repeat of experiment	Repeat of measurement	Confidence Interval	Total measurements
Thickness micrometer	3	5	±0.07 mm	570
Thickness optical	3	5	±0.015 mm	60
Micrographs Void content	4	2	±0.8 %	64
Interlaminar shear strength	2	5	4.5 MPa	380
Decompaction	3	1	-	9
Surface tension	8	2	4.2 mN/m	48
Crystallinity	1	2	4.3 %	12
Viscosity	4	2	3 Pas	16
Water absorption	3	3	0.016 % (PC) 0.005 % (PPS PP)	36

The maximum confidence interval is given to show the significance of differences and to allow general conclusions, which would not be valid, if the confidence interval was higher than the actual effect.

4 Development of an Analytical Model

The reasons for deconsolidation are controversially discussed in literature. There are different approaches to model deconsolidation, which each only consider a selection of the known effects. Other effects were neglected depending on the chosen approach, material, and process. This may be correct for a specific material or configuration, but limits the model to a single case. In order to propose a general model for deconsolidation for many different configurations and materials, the developed model is based on the first law of thermodynamics. Therefore, the model can be flexibly adapted to the known effects by fundamental equations. The deconsolidation behavior associated with the void content is modeled by means of the energy balance. The model contains the energy of void expansion based on thermal gas law and internal void pressure E_{voi}, void shrinkage and coalescence due to surface tension E_{sur}, decompaction of fiber reinforcement network E_{net}, visco-elastic behavior of the matrix E_{vis}, expansion of the matrix by the melting of crystals E_{cry}, thermal expansion of the composite E_{com}, vaporization of locked moisture E_{moi}, and finally external load E_{die}. For simplification purpose, it is assumed that mass conservation is applicable and the fibers and the matrix are incompressible. The deconsolidation behavior is formulated in Equation (4.1), where the algebraic sign is given by the direction of the force.

$$E_{voi} + E_{sur} + E_{net} + E_{vis} + E_{cry} + E_{com} + E_{moi} + E_{die} = 0 \tag{4.1}$$

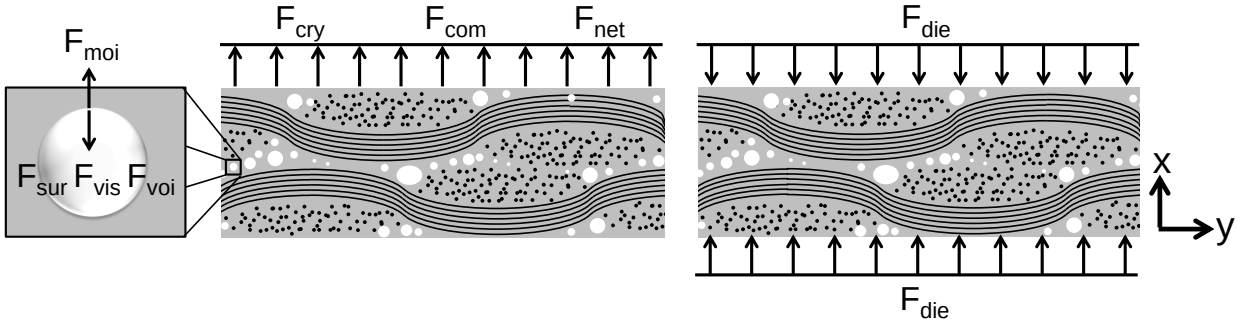

Figure 4.1: Illustration of the model including the corresponding forces of the energy and their effective direction

Because of the low expansion in in-plane direction (Chapter 2.1.4) caused by the stiffness of the fibers, only the thickness evolution is considered in out of plane direction.

4.1 Void Expansion

The thermal gas expansion within the void is often neglected because of the small effect compared to the total void content increase. As shown in chapter 6, the void is forced to expand because of the larger volume of the void in the deconsolidated state compared to in the consolidated state. Thus, the pressure in the void decreases and hinders the composite's expansion. This can be modeled by the ideal gas law. That means that the gas expansion has an inhibiting effect on deconsolidation which is contrary to what was formerly assumed in literature. The forced expansion can be generally modeled by the force-deflection (F_v•dx) approach in (4.2). Energy is dissipated, when the internal and external pressure (p_i and p_e) are different and the volume deflects. A_v is the void area at any cut in-plane direction. During expansion the voids keeps its spherical shape.

$$E_{voi} = \int -F_v \cdot dx = \int -(p_i - p_e) \cdot A_v \cdot dx \tag{4.2}$$

The ideal gas law is shown in (2.1). Combining the ideal gas law with (4.2) results in (4.3), where p_o is the initial void pressure, V_o the initial void volume, and T_o the initial temperature.

$$E_{voi} = -\int \left(\frac{p_o \cdot V_o \cdot T}{V_v \cdot T_o} - p_e\right) \cdot A_v \cdot dx \tag{4.3}$$

The consequence of mass conservation is that the void volume ($V_v=A_V \bullet x$) plus the solid volume (V_s) is the composite volume (V_c) as formulated in (4.4). A_{spe} is the cross section and x_c the theoretical void free thickness of the specimen.

$$\underbrace{V_v} + \underbrace{V_s} = \underbrace{V_c}$$

$$x \cdot A_v + x_c \cdot A_{spe} = x \cdot A_{spe} \tag{4.4}$$

The combination of (4.3) and (4.4) leads to (4.5), which describes the dependency of the void energy on the thickness of the composite and the temperature. The other parameters are measured at the initial state.

$$E_{voi} = -\int \left(\frac{p_o \cdot V_o \cdot T}{x \cdot T_o} - p_e \cdot A_{spe} \cdot \left(1 - \frac{x_c}{x}\right)\right) \cdot dx \tag{4.5}$$

4.2 Surface Tension

The surface energy is formulated in (4.6), where dA_{vo} is the new surface area of voids.

$$E_{sur} = -\int \gamma \cdot dA_{vo} \tag{4.6}$$

It is assumed that the voids are mainly spherical. That allows the definition of an average void radius R, given in (4.7).

$$R = \sqrt[3]{\frac{V_v \cdot 3}{4 \cdot \pi}} \tag{4.7}$$

Voids occur outside yarns in matrix rich areas (chapter 5.1). This is shown exemplary in a micrograph (Figure 4.2 left), where the voids are black between the yarns. The black dots inside the yarns are grinding artifacts. In the schematic illustration (Figure 4.2 right) the yarns are black and the matrix rich areas are grey.

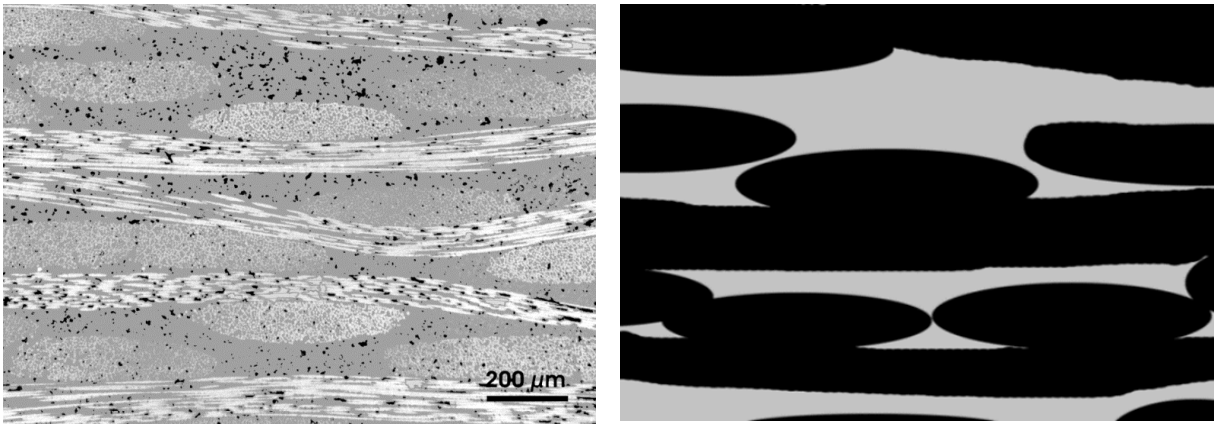

Figure 4.2: A micrograph of PP SA HP 49 with voids in black (left) and a schema with matrix rich areas in grey and the yarn in black (right)

A part of the matrix and all fibers are located in the yarns. By assuming a body-centered cubic lattice with a package density of 68 % corresponding to a good alignment of fibers, the matrix rich volume fraction (φ_{mrich}) can be formulated (4.8). φ is the fiber volume fraction.

$$\varphi_{mrich} = 1 - \varphi \cdot (1 + \frac{1 - 0.68}{0.68}) \tag{4.8}$$

The matrix rich volume is given in (4.9) dependent on the theoretical void free thickness and the cross section of the composite.

$$V_{mrich} = x_c \cdot A_{spe} \cdot \varphi_{mrich} \tag{4.9}$$

The void expansion can lead to a contact between neighboring voids. A coalescence of voids into each other leads to a reduction of surface area, which is thermodynamically favorable. A void movement within the matrix is neglected because of the high viscosity of the polymers. An assumed random void distribution results statically in void contact (4.10) proportional to the number of voids n.

$$n \sim \frac{V_{mrich}}{V_{mrich} + V_V} \tag{4.10}$$

Relating (4.10) to the initial state of the void volume and the void number, leads to (4.11).

$$n = \frac{V_{mrich} + V_o}{V_{mrich} + V_V} \cdot n_o \tag{4.11}$$

It must be pointed out that new voids can be created by outgassing of solvents and moisture or a degradation of the fiber sizing. These effects are neglected because no outgassing of solvent was observed during the treatment and the manufacturing. The effect of moisture is discussed in chapter 4.7 and chapter 6.1. The treatment and processing temperature used for polypropylene and polycarbonate is below the degradation temperature of the sizing. For polyphenylensulfide the treatment and processing temperature was above the degradation temperature. It is assumed that the sizing was completely disintegrated.

Combining (4.4), (4.7), and (4.11) gives the void area A_{vo} (4.12).

$$A_{vo} = \sqrt[3]{4 \cdot \pi \cdot n_o \cdot (x_o - 1 + \varphi_{mrich}) \cdot x_c \cdot (3 \cdot A_{spe})^2 \cdot \frac{(x - x_c)^2}{x - x_c \cdot (1 - \varphi_{mrich})}} \tag{4.12}$$

The differentiation of A_{vo} by dx (4.12) and the substitution of dA_{vo} by dx leads to the integral of the surface work (4.13), which is dependent on the initial state and the thickness of the composite.

$$E_{sur} = -\int \gamma \cdot \sqrt[3]{\frac{4}{3} \cdot \pi \cdot n_o \cdot (x_o - 1 + \varphi_{mrich}) \cdot x_c \cdot A_{spe}{}^2} \cdot \left[\frac{2}{\sqrt[3]{[x - (1 - \varphi_{mrich}) \cdot x_c] \cdot (x - x_c)}} - \sqrt[3]{\frac{(x - x_c)^2}{[x - x_c \cdot (1 - \varphi_{mrich})]^4}}\right] \cdot dx \tag{4.13}$$

4.3 Fiber Reinforcement Network

Decompaction of fiber reinforcement network has a significant effect on deconsolidation. Fiber network can be modeled by a spring-damper system (4.14) with some reversible (F_s) and irreversible forces (F_d), which are elongation and velocity dependent.

$$E_{net} = \int F_s(x) \cdot dx + \int F_d(v) \cdot dt \tag{4.14}$$

Because of the low velocity during the tests, there are minor damping effects. Therefore, damping is neglected. During the compaction of the fiber network, the fibers can rearrange in the mesoscale, which leads to settling caused by friction of plies and fiber bundles. The compaction energy can partially be released during melting of the composite, which was not dissipated by settling and damping. Therefore, the decompaction curve is only validated for a specific initial thickness and fiber volume fraction respectively. For each fiber volume fraction the curve has to be determined.

According to Kelly and Bickerton and Walbran et al., the compaction of fabrics can be best fitted by a polynomial function of 4th order [37; 38]. During decompaction a similar shape of curve was found. Therefore, the same approach is used, shown in (4.15).

$$F_s(x) = a \cdot x^4 + b \cdot x^3 + c \cdot x^2 + d \cdot x + e \tag{4.15}$$

4.4 Polymer Flow

This model considers the intra- and interlaminar voids of the specimen, which already exist at the initial condition. The model does not include fusion bonding of two plies and the build-up of new voids because of the bond line. Polymer flow can generally be modeled by the Navier-Stokes equation, which is validated for liquids assuming mass conservation (Chapter 2.1.4). As reported in 4.2, the voids had a spherical shape before and after deconsolidation. This leads to the transformation of mass

conservation equation in spherical coordinates (4.16) by assuming an incompressible fluid. r is in radial direction, θ and Φ are in tangential direction, and u is the velocity. An illustration of the polymer flow model is given in Figure 4.3.

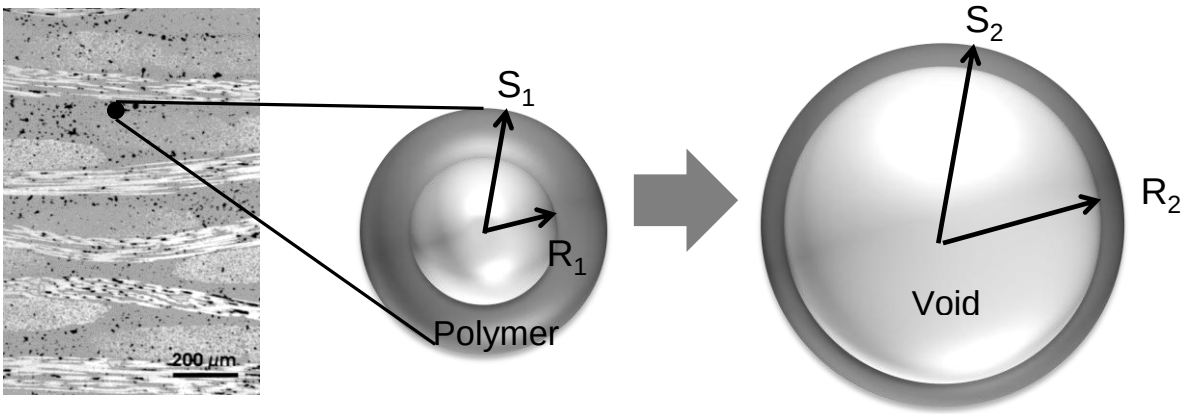

Figure 4.3: Illustration of the polymer flow model (middle: before deconsolidation and right: after deconsolidation)

$$\frac{dp}{dt}+\frac{1}{r^2}\cdot\frac{d}{dr}(\rho\cdot r^2\cdot u_r)+\frac{1}{r\cdot\sin(\Theta)}\cdot\frac{d\rho u_\Theta}{d\Phi}+ \frac{1}{r\cdot\sin(\Theta)\cdot d\Theta}\cdot\frac{d}{d\Theta}(\sin(\Theta)\cdot\rho\cdot u_\Theta)=0 \tag{4.16}$$

Because of the spherical shape of the voids, there is no flow in tangential directions. Therefore, the angle component tends towards zero resulting in (4.17), which is only dependent on the radius, the density, and the velocity in radius direction.

$$\frac{1}{r^2}\cdot\frac{d}{dr}\cdot(\rho\cdot r^2\cdot u_r)=0 \tag{4.17}$$

To fulfill (4.17) for no density changes of the polymer, the velocity multiplied by the radius in square must be constant (4.18), where R is the outer radius.

$$r^2\cdot u_r=R^2\cdot u_R \tag{4.18}$$

Polymer flow is described by the Navier-Stokes equation (4.19) considering no tangential flow.

$$\frac{du_r}{dt} + u_r \frac{du_r}{dr} = \frac{1}{\rho} \cdot \frac{dp}{dr} \tag{4.19}$$

In order to further solve the general equation, a void shell model is introduced (Figure 4.3); each void is surrounded by a polymer shell of the thickness (R-S), where S is the outer diameter of the shell. The indices “1” and “2” stand for the condition before and after an incremental time segment.

Assuming inertia (no density change) leads to (4.20), which is dependent on the void pressure (p_v) and the shear tension (τ_{vis}).

$$\frac{1}{\rho} \cdot \frac{dp}{dr} = 0 -> dp = 0 = p_v + \tau_{vis} \tag{4.20}$$

Because of the radial flow, the shell becomes thinner with an increasing void radius. That can be described by a Newton biaxial flow given in (4.21) [55].

$$\tau_{vis} = 2 \cdot \eta \cdot \frac{du_r}{dr} \tag{4.21}$$

Integration of (4.21) from R to S leads to (4.22) depending on the void radius velocity.

$$\tau_{vis} = 4 \cdot \eta \cdot [\frac{1}{R} - \frac{R^2}{S^3}] \cdot \frac{dR}{dt} \tag{4.22}$$

The void pressure from (4.20) can be related to the shear tension (4.22) of the polymer and the velocity of the void increase (4.23). The formula is similar to the Rayleigh-Plesset equation (2.8) with neglected inertia.

$$p_v = 4 \cdot \eta \cdot [\frac{1}{R} - \frac{R^2}{S^3}] \cdot \frac{dR}{dt} \tag{4.23}$$

The polymer shell radius S (4.24) can be calculated by the matrix rich volume, the number of voids, and the void radius. For small dR (≦ 5 µm), the number of voids is assumed to be constant.

$$(S^3 - R^3) \cdot \frac{4}{3} \cdot \pi \cdot n = V_{mrich} -> S = \sqrt[3]{\frac{3 \cdot V_{mrich}}{4 \cdot \pi \cdot n} - R^3} \tag{4.24}$$

The solution of (4.23) for small dR is gained by (4.24), (4.9), and the integration with respect to dt is given in (4.25). For infinite time the gradient tends to zero (C=0).

$$\int p_v dt = \frac{F}{A_{spe} \cdot \alpha} \cdot \Delta t + C = -\frac{4\eta}{3} \tag{4.25}$$
$$\left[\ln\left\{ \frac{3 \cdot A_{spe}}{4 \cdot \pi \cdot n_1} \cdot (x - x_c) \right\} - \log\left\{ \frac{3 \cdot A_{spe}}{4 \cdot \pi \cdot n_1} (x - x_c \cdot (1 + \varphi_{mirch})) \right\} \right]$$

4.5 Crystallinity

Crystallinity change has a significant influence on the density and therefore, on the specimen's thickness. This leads to a different fiber volume fraction and void content. The crystallinity change would affect all proposed deconsolidation mechanisms. Because the crystallinity is equal before and after deconsolidation (shown in chapter 5.6), it is assumed that crystallinity has no influence on the total thickness change. During deconsolidation it has an influence on the thickness because of density change as a result of melting and crystallization.

Because of the complex calculation of the viscoelastic behavior, caused by the melting or build-up of crystals, the total thickness is only calculated from the general forces displacement approach (4.2). The total thickness of the polymer dependent on the polymer strain and energy change can be used to determine the initial crystallization force (F_{ci}) and the final crystallization force (F_{cf}) before and after melting or crystallization (4.26).

$$E_{cry} = (F_{cf} - F_{ci}) \cdot (1 + \Delta\varepsilon^{p}) \cdot (1 - \varphi) \cdot x \tag{4.26}$$

The total polymer thickness change can be calculated by the specimen thickness and the fiber volume fraction (4.27). For the case of melting, the long term crystallization force is zero and after complete crystallization the final crystallization force is zero.

$$(F_{cf} - F_{ci}) = \frac{E_{cry}}{(1 + \Delta\varepsilon^{p}) \cdot x \cdot (1 - \varphi)} \tag{4.27}$$

4.6 Thermal Expansion

Thermal expansion in thickness direction is a reversible effect, if the initial and the final temperature are the same and no chemical or molecular effects occur. This is the case made under the assumptions in chapter 0. Therefore, the closed integral of the force displacement approach is zero. Nevertheless, the thickness expansion from room temperature to melting temperature because of thermal expansion lays in the same magnitude as deconsolidation. As described in chapter 2.1.4, it is difficult to determine the thermal expansion in thickness direction. This makes it impossible to differentiate these two effects without a simplification. Thus, the effect of thermal expansion is split into two temperature ranges: first, the thermal expansion between room temperature and the on-set of melting and second, the range between the on-set of melting and the processing temperature. The thermal expansion in the first range can be determined by optical measurements because no other effects occur. In the second range, the thermal expansion cannot be determined. In order to overcome this problem, the thermal expansion is extrapolated from the last

determined values in the first range. This leads to an unknown deviation from the real thermal expansion, but the prediction is assumed to be closer to reality than not considering the effect at all. Also, the temperature range is approximately 60 K, which is a fraction of the overall effect.

The energy of the thermal expansion can be measured by a DSC analysis of the heat capacity of the specimen. The knowledge of the energy of thermal expansion and the resultant thermal expansion can be used to determine the expansion force based on the force displacement approach. Thermal expansion leads to different polymer and fiber densities of the specimen between room temperature and process temperature. This changes the initial state of the deconsolidation mechanisms, which are measured at room temperature. It is assumed that the closed loop of heating and cooling to room temperature equalize the effect of thermal expansion. Therefore, it is assumed that the initial state of the deconsolidation mechanisms can be determined at room temperature, if not otherwise mentioned.

The energy of thermal expansion (4.28) can be calculated from the general approach of the forces displacement law, the consideration of the heat capacity c_p, and the mass ratio between 1 kg and the composite mass m_{com}.

$$E_{com} = c_p(T) \cdot \frac{m_{com}}{m_{norm}} \cdot dT = F_{com} \cdot dx \tag{4.28}$$

The heat capacity of the composite (4.29) is dependent on the mass proportion of the fibers and the matrix multiplied with the corresponding heat capacity (c_{pf} and c_{pm}) [122].

$$c_p(T) = (1-\varphi_w) \cdot c_{pm} + \varphi_w \cdot c_{pf} \tag{4.29}$$

4.7 Moisture

During heating of specimens, moisture can vaporize, if a temperature approximately 100 °C is exceeded. According to the vapor pressure curve of water, the accurate

temperature is pressure dependent at which the water vaporizes. This ranges from ~1013 mBar at 100 °C to 221.1 bar at 374.12 °C. Below the melting temperature of the polymer, the solved water inside the polymer can diffuse out, but there is minor volume increase inside the polymer [123]. The high vaporization pressure is released, when the specimen exceeds the melting temperature. It is assumed that no further diffusion occurs above the melting temperature because the high pressure leads to a drastic and stannous volume expansion.

Volume and pressure of vaporized water can be described by the ideal gas law [16]. Including the ideal gas law (2.1) in the general approach for the volume energy (4.30), results in the dependency of the energy on the pressure and volume change (4.31). R_S is 462 J/Kg/K for steam.

$$E_{moi} = \int p \cdot dV \tag{4.30}$$

$$E_{moi} = \int \frac{m \cdot R_s \cdot T}{V} \cdot dV \tag{4.31}$$

(4.31) is only validated for low pressure (<<10MPa) [16]. Especially when the specimen is in the molten state, the moisture has a low pressure because of spontaneous thickness increase. The partial pressure of the material can be calculated by the mass proportion from the complete mass [124]. Combining this with the cross section of the specimen, leads to (4.32), where φ_{moi} is the moisture content. Vaporization pressure can be taken from the vapor pressure chart [124].

$$E_{moi} = -\int p_{moi} \cdot \varphi_{moi} \cdot A_{spe} \cdot dx \tag{4.32}$$

4.8 External Forces

The energy (E_{die}) caused by an external force (F_{die}) like a die, can be calculated with the force displacement approach shown in (4.33). The force of the die acts against

the deconsolidation tendency of the composite, which inhibit the progress of deconsolidation.

$$E_{die} = -\int F_{die} \cdot dx \tag{4.33}$$

The developed model can predict the resultant force of a die, if the thickness is given for example by a fixed position of the die. This would exceed the usual deconsolidation forces caused by thermal expansion and melting of the crystals and lead to matrix squeeze out, which is neglected under the given assumption. The model can be extended by a squeeze flow model, but it has to be pointed out that the made assumption and the validation of the model in chapter 6 have to be repeated.

In order to estimate the influence of squeeze flow, the model of Rogers is used to estimate the polymer loss of the specimen (2.10) [59]. It is defined that a maximum polymer loss out of the composite of 2 weight percent is acceptable to justify the assumption of mass conservation. It is assumed that the fibers do not flow or elongate by the polymer flow. According to the height reduction in the consolidated state (4.34) by an external load, the reduced thickness must result in a polymer flow out of the specimen (V_{psq}). In order to neglect the effect of voids, the theoretical thickness of the void free specimen is used as the initial thickness of the squeeze flow calculation. x_{sq} is the squeezed thickness of the specimen after the application of the external load.

$$A_{spe} \cdot x_c = A_{spe} \cdot x_{sq} + V_{psq} \tag{4.34}$$

5 Results

In order to verify the proposed deconsolidation model and to determine the model parameters, several experiments were carried out. The experimental and approach are described in chapter 3. The results are presented in this chapter.

5.1 Void Expansion and Thickness Increase

The initial state of the specimens is given in Table 5.1 for the fiber volume fraction and the thickness.

Table 5.1: Initial state of fiber volume fraction and the thickness of the specimens

Material	Initial fiber volume fraction [%]	Initial thickness [mm]
PPS UD 58	58.1	3.12
PPS UD 40	40.9	3.23
PPS SA 52 HP	52.6	2.79
PPS SA 53	53.0	2.77
PPS SA 52	52.4	2.80
PPS SA 40	39.9	3.12
PPS TW 52	52.4	2.90
PP UD 58	58.2	3.02
PP UD 40	39.3	2.93
PP SA 53	53.1	2.98
PP SA HP 49	48.6	3.02
PP SA 48	46.5	3.15
PP SA 40	40.6	3.06
PP TW HP 51	50.8	2.92
PP TW 48	48.2	3.16
PC SA 50	50.2	2.92
PC TW 48	48.7	2.88

The results for the thickness measurements of the free deconsolidation experiments are shown in Figure 5.1 for reinforced polypropylene. The unidirectional reinforced polypropylene specimens showed a small expansion after free deconsolidation of less than 6 % caused by their good fiber to fiber alignment and their good fiber bundle packaging next to each other. The specimens with a fabric exhibited a several times higher thickness increase, whether they had a satin 1/4 or twill 2x2 fabrics. Another factor was the fiber volume content. As higher the fiber volume content was as higher the thickness increased, which is more investigated in chapter 6.3.

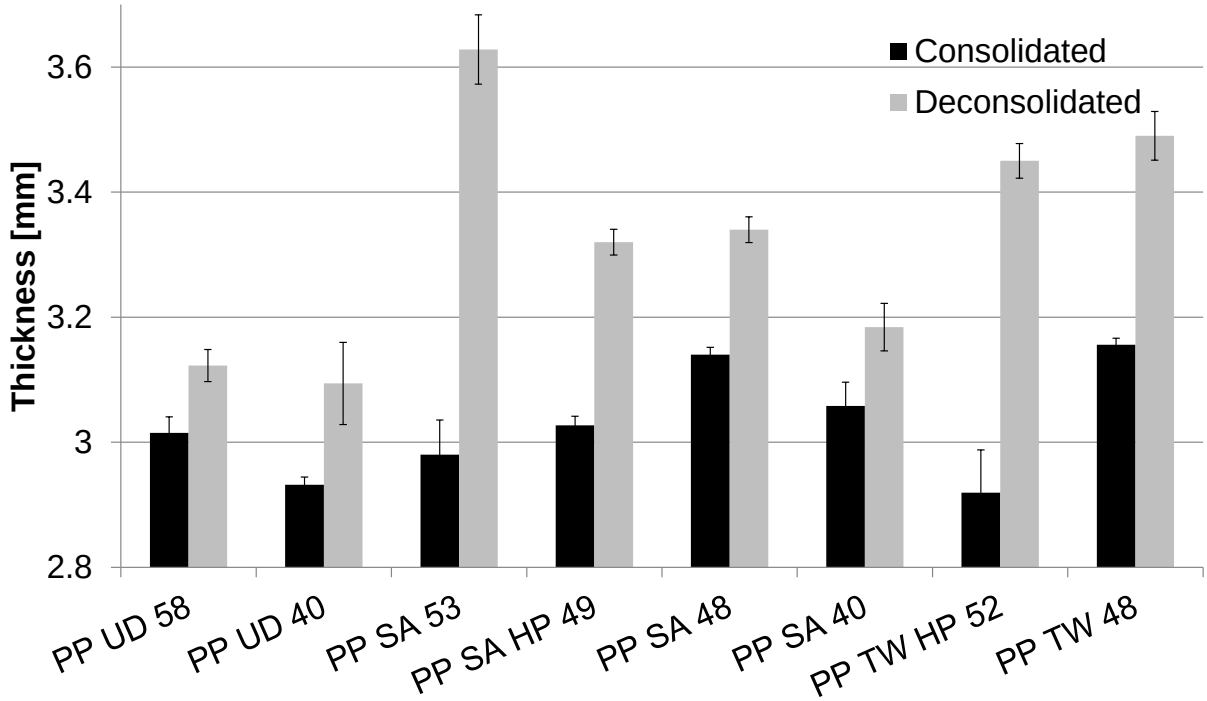

Figure 5.1: Thickness of consolidated and freely deconsolidated reinforced polypropylene

The manufacturing processes of the specimens, differed by the applied underpressure in the vacuum bag and the applied external pressure. They had an effect on the thickness increase caused by the different fiber volume fraction.

Specimens with polyphenylensulfide matrix or the dried specimens with polycarbonate matrix showed a similar tendency with respect to reinforcement type and fiber volume content in their polymer group (Figure 5.2). The overall level was different because of the different number of plies, which were necessary to achieve a similar fiber volume fraction caused by the different initial foil thickness of the film

stacking process. The undried polycarbonate specimens exhibited a higher thickness increase because of the moisture in the specimen. This is discussed in chapter 5.8.

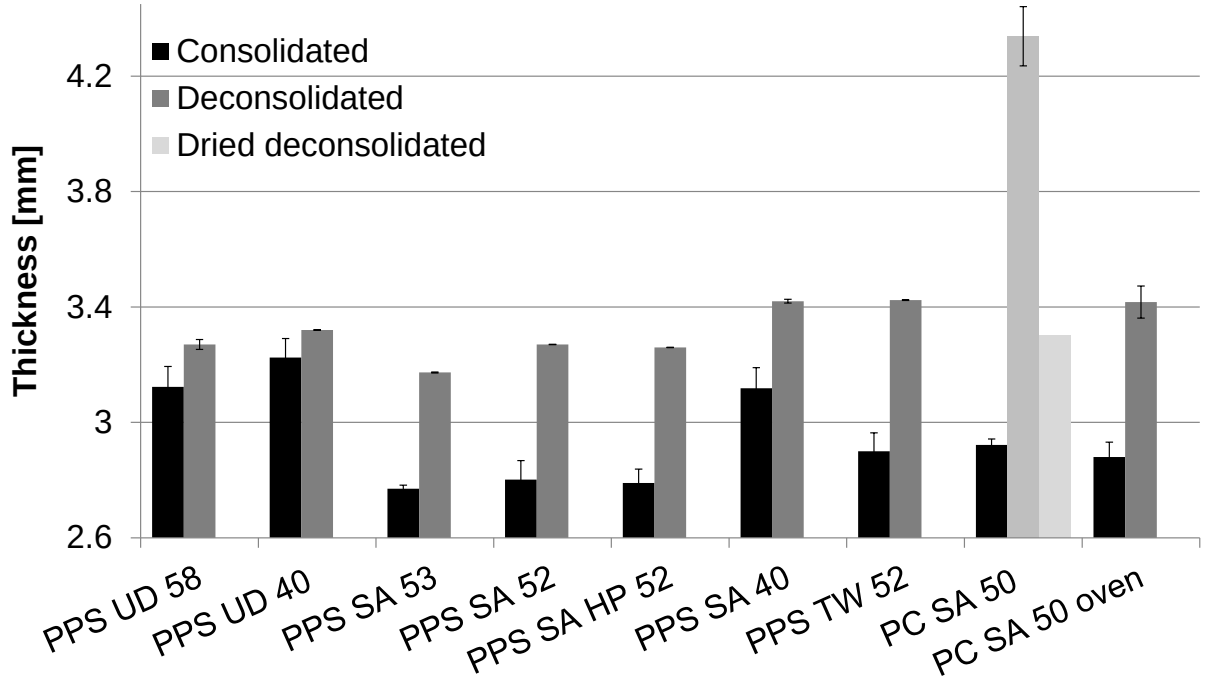

Figure 5.2: Thickness of consolidated and freely deconsolidated reinforced polyphenylensulfide and polycarbonate

Some reinforced polypropylene specimens were deconsolidation treated twice (re-melting) in two separate ways (Figure 5.3). The first batch was deconsolidation treated directly after the first free deconsolidation treatment and the second batch were treated two weeks after the first treatment. The two batches indicated a slight increase of thickness between 40 µm and 44 µm in average over all specimens. Compared with the thickness increase after the first free deconsolidation treatment (200 µm to 530 µm), the repeated treatment did not lead to significant changes, which laid within the range of the confidence interval.

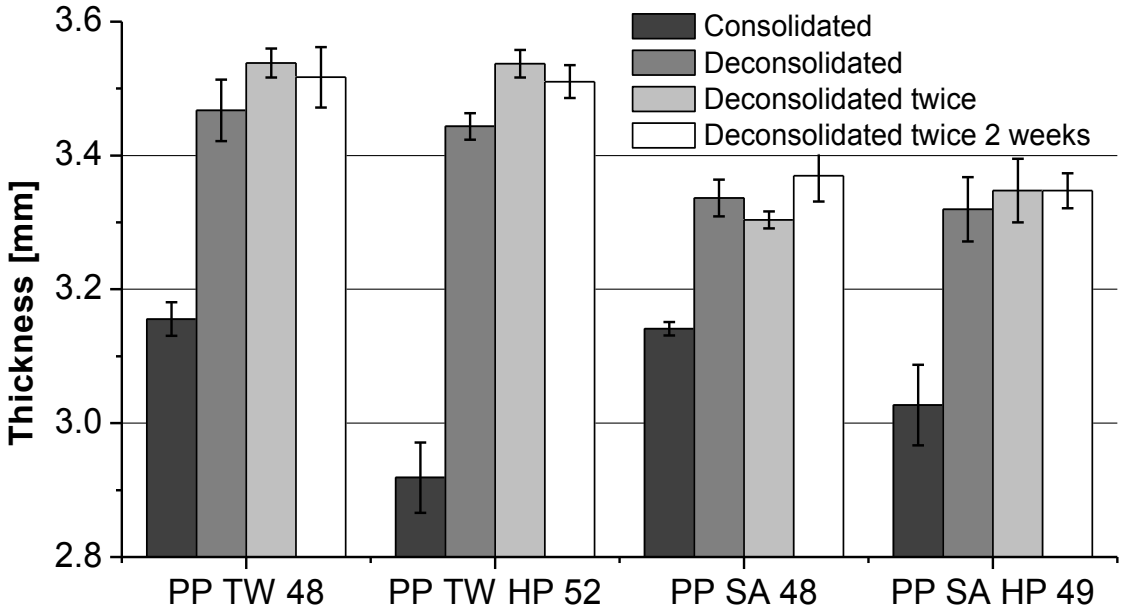

Figure 5.3: Thickness change of repeated freely deconsolidation treated polypropylene

The thickness evolution at different times after manufacturing has been investigated and is shown in Figure 5.4. Therefore, the specimens PPS TW 52 and PPS SA HP 52 were treated (free deconsolidation) a specific time after the manufacturing cycle. The polyphenylensulfide specimens reinforced with the glass satin showed a decrease of specimen's thickness after the treatment different times after manufacture. The thickness after the deconsolidation treatment started at 3.50 mm 30 min after the manufacture and tends to 3.26 mm 36 weeks (6048 h) after the manufacture. The maximum decrease took place between the manufacture and 12 weeks (2016 h) after. In contrast to these specimens, the polyphenylensulfide specimens reinforced with carbon fiber twill had an increase of thickness with time after the manufacture. A steady state was reached 6 h after the manufacture, which was about three magnitudes faster than the glass fabric. The thickness change was approximately 0.12 mm for the carbon fiber reinforced specimen and 0.25 mm for the glass fiber reinforced specimen.

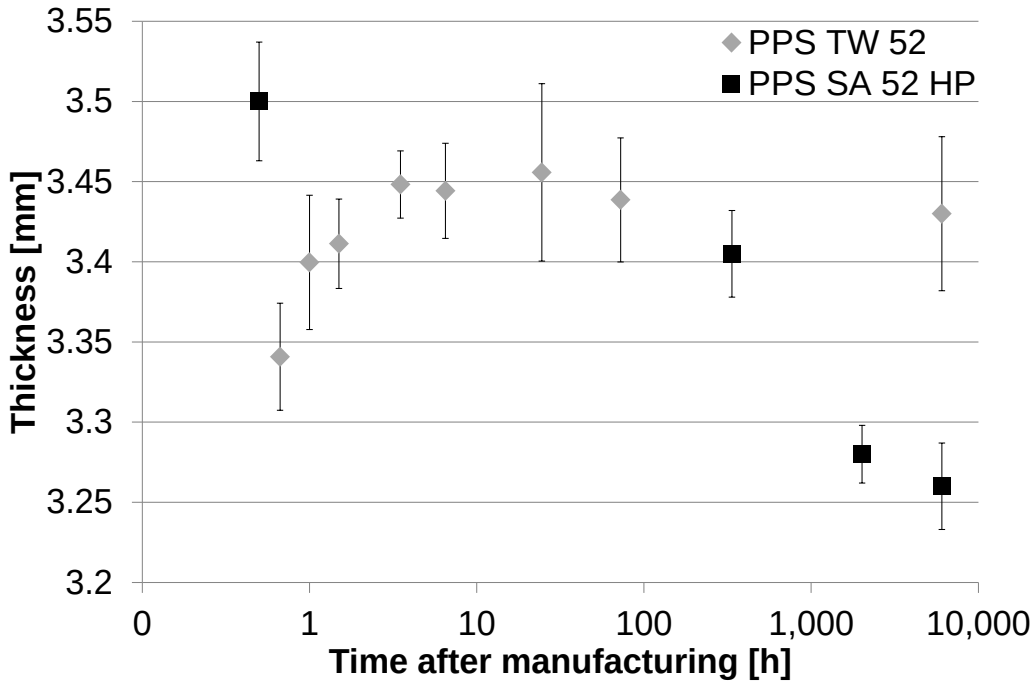

Figure 5.4: Thickness after the deconsolidation treatment at different times after the manufacture for PPS TW 52 and PPS SA HP 52

By assuming mass conservation of the matrix and fibers, the void content (α) can be calculated by (5.1) from the thickness of the specimen (x) and the volume of the matrix (V_{matrix}) and fibers (V_{fibers}).

$$\alpha = \left(\frac{V_{decon}}{V_{matrix} + V_{fibers}} - 1\right) = \left(\frac{x \cdot A_{spe}}{V_{matrix} + V_{fibers}} - 1\right) \tag{5.1}$$

Table 5.2 lists the void content of the initial and the freely deconsolidated specimens determined by thickness and by digital image analysis of micrographs. The initial void content varied from 0.07 % to 3.70 %. There was no clear trend that depends on the reinforcement type, textile binding, or fiber volume content.

Table 5.2: Void content of initial and freely deconsolidated specimens determined by thickness and by digital image analysis

Material	**Initial void content**	**Freely de-consolidated void content**	**Initial void content**	**Freely de-consolidated void content**
	by thickness		**by digital image analysis**	
PPS UD 58	2.02 %	6.42 %		
PPS UD 40	1.09 %	3.92 %		
PPS SA 52 HP	1.43 %	14.93 %		
PPS SA 53	1.08 %	13.65 %		
PPS SA 52	1.08 %	16.00 %		
PPS SA 40	0.90 %	9.65 %		
PPS TW 52	3.10 %	17.93 %		
PP UD 58	0.17 %	5.96 %	0.27 %	4.90 %
PP UD 40	0.41 %	5.62 %		
PP SA 53	1.17 %	18.83 %		
PP SA HP 49	2.98 %	11.45 %	2.87 %	12.90 %
PP SA 48	3.60 %	9.73 %	3.63 %	9.71 %
PP SA 40	3.70 %	7.51 %		
PP TW HP 51	1.39 %	16.55 %	1.38 %	16.61 %
PP TW 48	2.51 %	11.83 %	2.50 %	12.88 %
PC SA 50	0.07 %	11.52 % dried		
PC TW 48	0.52 %	16.59 % dried		

The void content after free deconsolidation was several times higher than the initial void content. Depending on the reinforcement type, three groups can be identified: first, the unidirectional reinforced specimens, which had a void content of 3.9 % to 6.4 %, second, the satin ¼ reinforced specimens with a void content of 7.55 % to 18.83 %, and finally, the twill 2x2 reinforced specimens, which had a void content of 11.83 % to 17.93 %. Within these groups of fabrics, the specimen with a higher fiber volume fraction showed a higher void content. It can also be concluded that a low initial void content does not lead to a low void content after deconsolidation.

In order to get a better understanding about void shape and void size, a digital void analysis was carried out. The void's cross section of PP TW HP 51 showed a pronounced circular shape with accuracy to a circle of 99.2 % and 99.0 % in the initial state and the freely deconsolidated state (Figure 5.5). Occasionally, elliptical voids occurred.

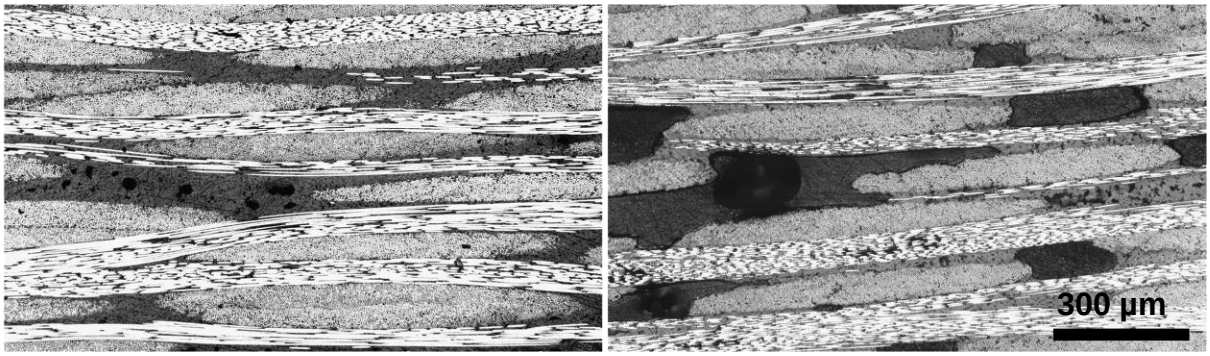

Figure 5.5: Micrograph sections of PP TW HP 51 in the consolidated (left) and deconsolidated state (right)

By assuming a circular void cross section, the area portion of a void class was investigated and is displayed in Figure 5.6.

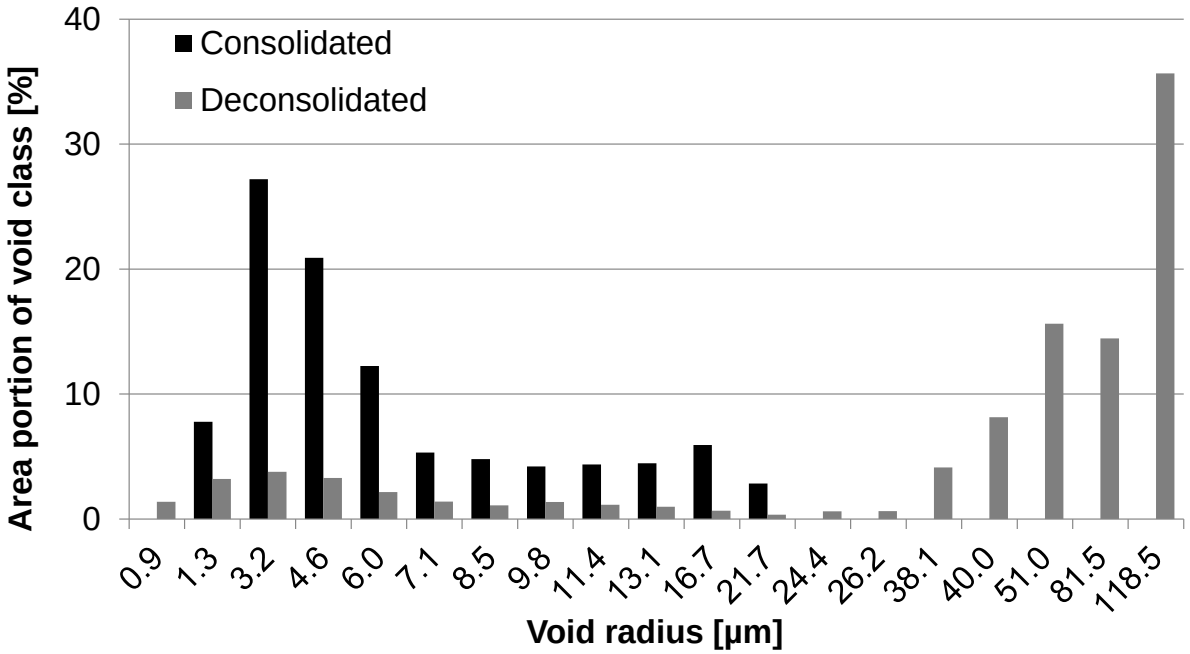

Figure 5.6: Area portion of void class depending on average void radius of the class for PP TW HP 51

In case of the consolidated specimens, a maximum at the void class 3.2 µm was reached. The maximum corresponded well with the average void radius of 2.76 µm determined by the micrographs. The area portion declined until 21.7 µm void radius.

Freely deconsolidated specimens showed the first maximum at 3.2 µm void radius, too, but on a lower area portion caused by a new second maximum at 118.5 µm. The new large voids grew in the matrix rich areas, where they were built up by several smaller voids, which led to a void number reduction.

PP SA HP 49 specimens (Figure 5.7) in the consolidated and freely deconsolidated state had a circular shape of 99.6 % and 99.1 %. A maximum in area portion occurred at 4.6 µm (Figure 5.8). Because of more intersection of the yarns in weave of the satin ¼ compared to the twill 2x2, the PP SA HP 49 specimens had a lower second maximum than PP TW HP 51 in the freely deconsolidated state at 51.3 µm.

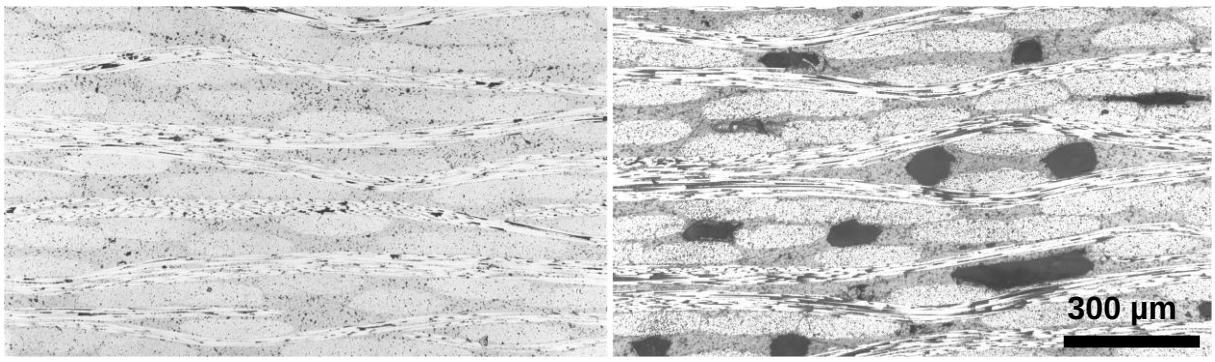

Figure 5.7: Micrograph sections of PP SA HP 49 in the consolidated (left) and deconsolidated state (right)

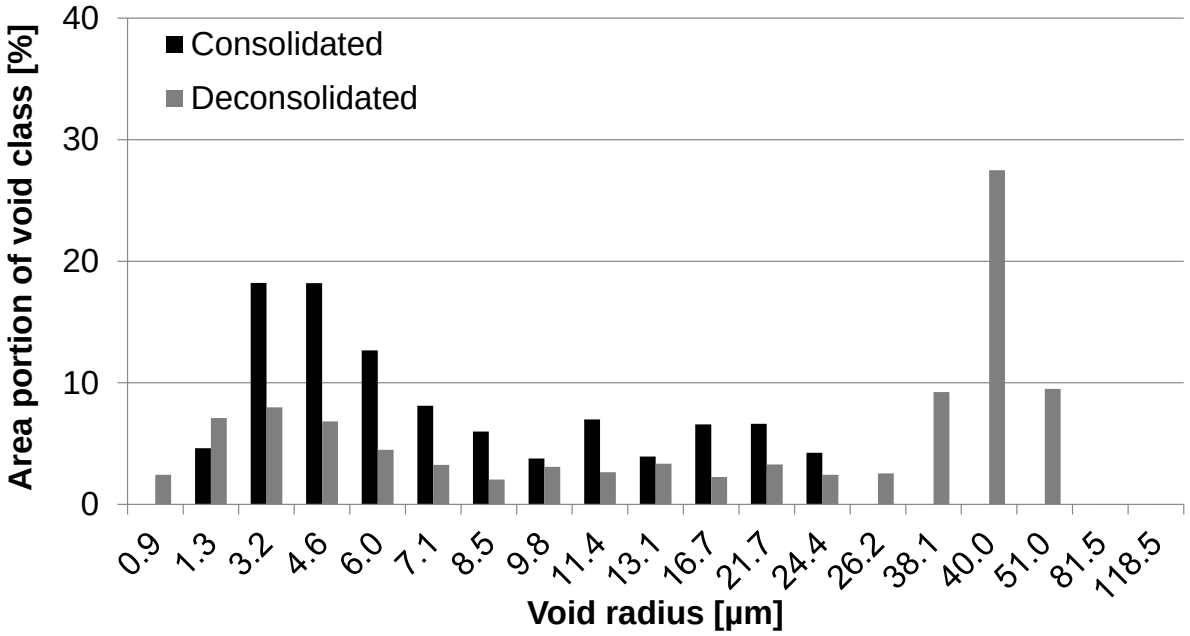

Figure 5.8: Area portion of void class dependent on average void radius of the class for PP SA HP 49

These finding were confirmed by the PP SA 48 specimen shown in Figure 5.9 and in Figure 5.10. Because of the lower thickness and the lower fiber volume fraction, the second maximum in the freely deconsolidated state was less pronounced. PP SA 48 specimens had a circular shape in the consolidated and deconsolidated state of about 99.1 % and 99.6 %.

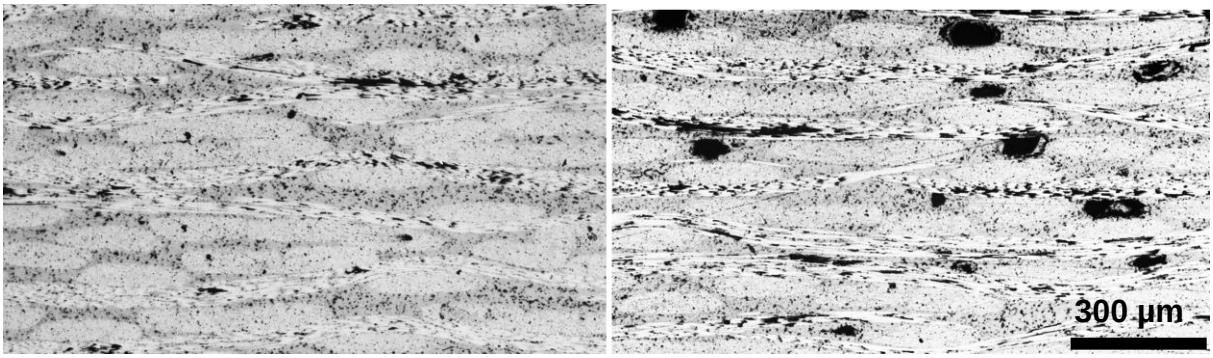

Figure 5.9: Micrograph sections of PP SA 48in the consolidated (left) and deconsolidated state (right)

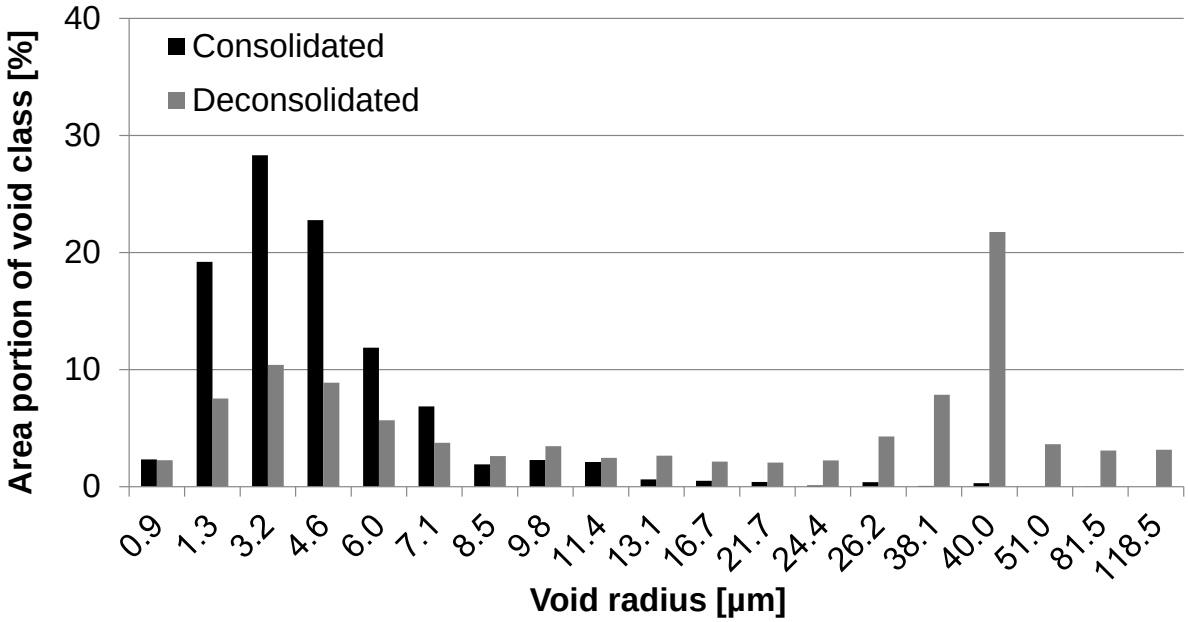

Figure 5.10: Area portion of void class dependent on average void radius of the class for PP SA 48

For the inhibit deconsolidation experiments, different pressures were applied to hinder deconsolidation. The results are shown in Figure 5.11. The void content increases with a lower pressure during the deconsolidation treatment. According to the quadratic behavior, there were minor changes above 0.025 MPa applied pressure. Second, the higher the fiber volume fraction was the stronger was the increase of void content with a decrease of pressure.

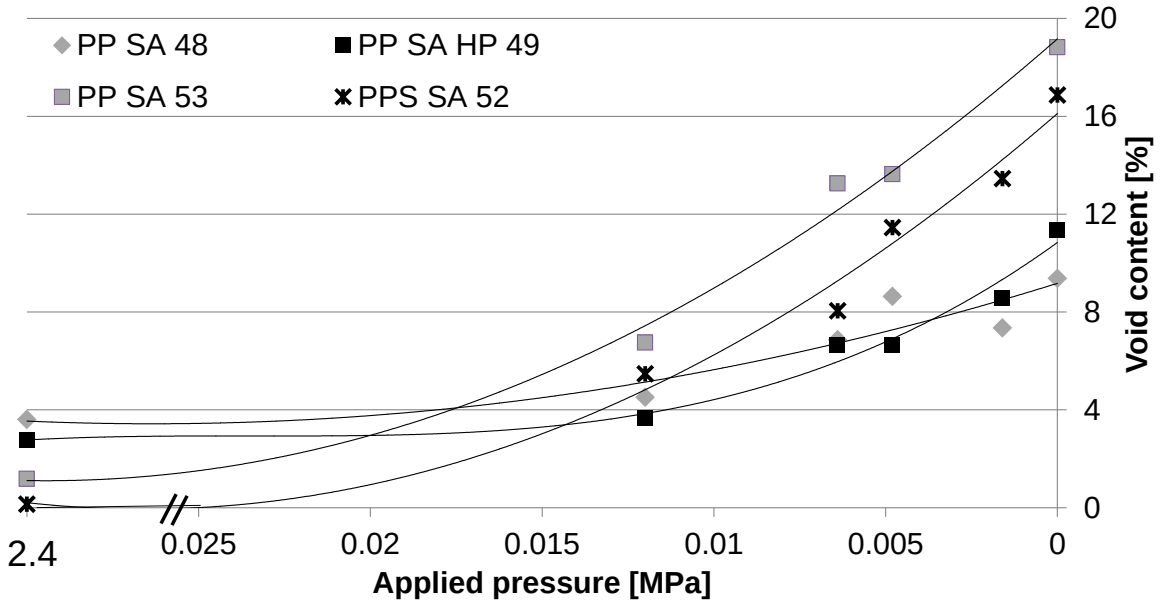

Figure 5.11: Void content dependent on the applied pressure during deconsolidation (the initial state after manufacturing is at 2.4 MPa)

5.2 Surface Tension

The surface tensions at room temperature and the extrapolated surface tension at processing temperature were determined from neat polymers. The results are listed in Table 5.3. No fibers had contact to the surface of the specimen. There was a thin layer of polymer between the atmosphere and the specimen.

Table 5.3: Surface tension of neat polypropylene, polyphenylensulfide, and polycarbonate at room temperature and at processing temperature

	Measured surface tension at room temperature	**Calculated surface tension at processing temperature**
Polypropylene	30.1 mN/m ±4.19 mN/m	18.6 mN/m
Polyphenylensulfide	44.62 mN/m ±0.043 mN/m	31.9 mN/m
Polycarbonate	not performed	25.8 mN/m

No measurements were performed for polycarbonate. The surface tension at room temperature was taken from the literature [23]. The complete disperse behavior of polypropylene resulted in a high confidence interval, because it was not possible to detect a contact angle with the polar liquid water. The disperse part of the surface

tension of polyphenylensulfide and polycarbonate was on a similar level and the total surface tension was higher caused by the polar and disperse nature of the surface.

5.3 Fiber Reinforcement Network

In order to determine the influence of the fiber reinforcement network, dry fabric compaction and decompaction tests were carried out on the universal test machine. Compaction and decompaction pressure were calculated from the measured force divided by the specimen's cross section (50 x 50 mm^2), which is assumed to be constant during testing. The decompaction pressure dependent on the fiber volume fraction was measured for the unidirectional, the twill 2x2, and the satin ¼ fabrics after compaction and holding at maximum fiber volume fraction for 2 min.

The results are shown in Figure 5.12 for the unidirectional, the twill 2x2, and the satin ¼ fabrics with an initial fiber volume fraction of 58 %, 50.7 %, and 50.3 %. At the beginning of the decompaction test, the load cell had a delay because of an averaging of 4 measurement cycles (48 ms), which caused a buckle at the highest pressure. The unidirectional fabric had a sharp decrease of pressure at a high fiber volume fraction and was shifted to a higher fiber volume fractions compared with the twill 2x2 and the satin ¼ fabric caused by the excellent packaging and alignment of the unidirectional fibers. The twill 2x2 and the satin ¼ curves were aligned relatively parallel to each other, but the twill 2x2 curve was on a higher pressure level. Maximum decompaction pressures for different fiber volume fractions were relatively low between 0.12 MPa and 0.02 MPa, which were below the processing pressure during manufacturing of the samples.

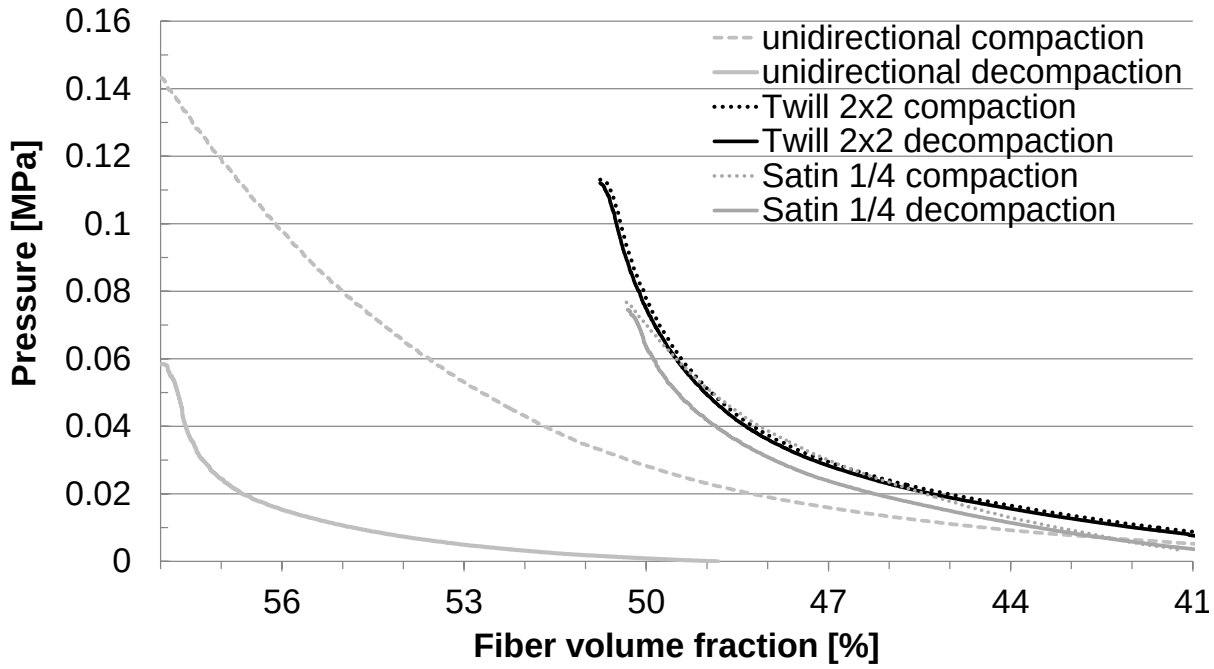

Figure 5.12: Compaction and decompaction pressure dependent on the fiber volume fraction

Settling effects of the fabrics occurred between the end of the compaction cycle and the start of the decompaction cycle. During holding time the measured force decreased by maintaining a constant die position, which corresponded to a constant specimen's thickness. The corresponding pressure of the unidirectional glass fiber reinforced fabric, settled of 0.0912 MPa. The twill carbon fabric and the satin glass fabric settled from 0.01216 MPa and 0.0767 MPa (maximum compaction pressure) to 96 % and 97 %.

The polynomial parameters of the fit (4.15) are given in Table 5.4. It can be seen that the unidirectional fabric had approximately 50 times higher values compared to the carbon twill fabric. In contrast, the glass fiber satin fabric had three times lower values compared to the twill. It must be pointed out that the maximum observed deviation between different decompaction curves of one type were 10 %, which was strongly dependent on the specimen preparation. The lay-up must be maintained constant; it is recommended to have no deviations greater than 1° of the ply orientation.

Table 5.4: Polynomial parameters of the fabrics

Fabric	a	b	c	d	e
Unidirectional	343996.93583	-4339643.87271	20529282.3012	-43162079.658	34029584.22
Twill	6090.12766	-83843.25403	432597.9158	-991541.367	851985.19
Satin	2030.36385	-27723.297	141927.7516	-322954.909	275694.66

5.4 Mechanical Performance

The mechanical performance of the specimens was determined by a matrix dominated test the apparent interlaminar shear strength. Therefore, the deconsolidation treatments were carried out at 5 different applied pressures. Because of the low counter pressure, no matrix squeeze out occurred and therefore no mass loss took place, which would falsify the results.

Figure 5.13 shows a decrease of interlaminar shear strength of reinforced polypropylene with an increase of void content. A regression analysis revealed that the determination coefficient for linear slope was high (0.84-0.95). These results indicate a linear dependency of the shear strength on the void content over a wide range of void contents (0 % - 20 %), which corresponds well with the literature as reported in chapter 2.2.

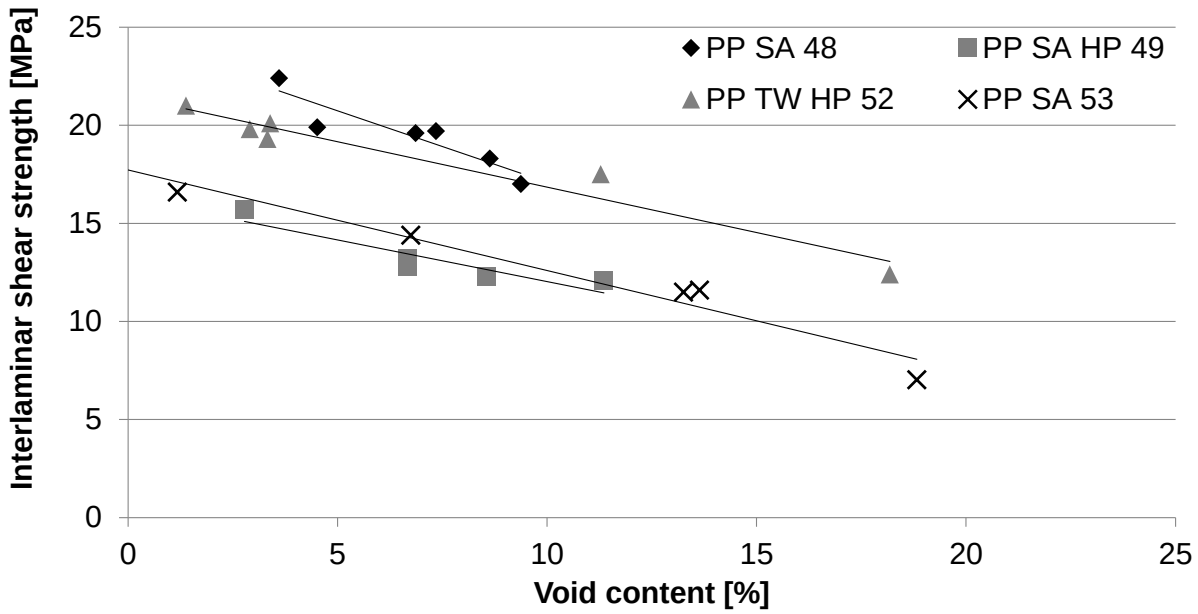

Figure 5.13: Change of interlaminar shear strength dependent on void content for reinforced polypropylene

In order to investigate the effect of void content on interlaminar shear strength for a wider range of materials, the free deconsolidation treated specimens were tested, shown in Figure 5.14 for reinforced polypropylene and in Figure 5.15 for reinforced polyphenylensulfide and polycarbonate.

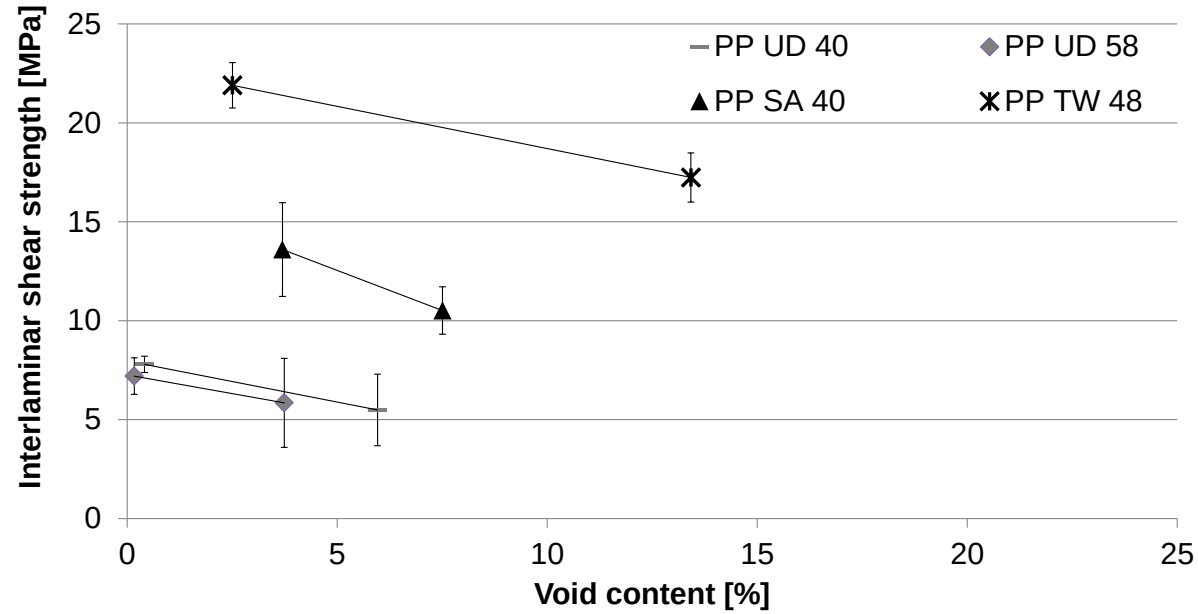

Figure 5.14: Loss of interlaminar shear strength with increasing void content for reinforced polypropylene

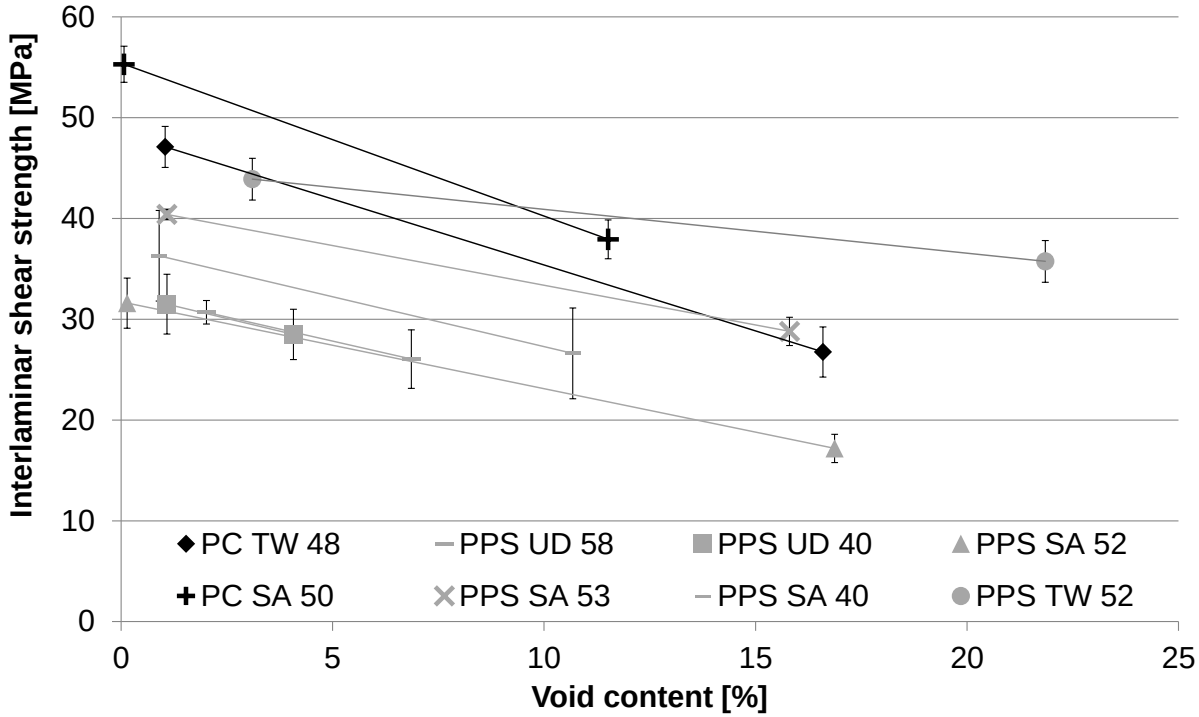

Figure 5.15: Loss of interlaminar shear strength with increasing void content for reinforced polyphenylensulfide and reinforced polycarbonate

Only the reinforced polyphenylensulfide specimens failed interlaminar according to the standard DIN EN ISO 14130. Therefore, the interlaminar shear strength of the reinforced polypropylene and polycarbonate was named as apparent interlaminar shear strength. The level for the reinforced polyphenylensulfide and polycarbonate was about two times higher because of the higher strength and stiffness of the polymer. The slope of the linear regression line for reinforced polypropylene was 0.56 MPa/%. The reinforced polyphenylensulfide and the reinforced polycarbonate had a two times higher slope (in average 1.03 MPa/% and 1.31 MPa/%). The interception with the y-axis, which corresponds to the interlaminar shear strength of a void free specimen, varied within each polymer group by 30 %. Unidirectional reinforced specimen achieved the lowest level of each group, caused by the straight interface between the layers. The linear dependency is formulated in (5.2), where τ_m is the interlaminar shear strength, A_m is the interlaminar shear strength in a void free condition (interception with y-axis), and B_m is the dependency of the interlaminar shear strength on the void content (slope).

$$\tau_m = A_m + B_m * \alpha \tag{5.2}$$

The slope was dependent on the void content and the polymer. There were minor changes within a polymer group, which were independent from the fiber volume fraction, the lay-up, the reinforcement type, and the manufacturing process. The interlaminar shear strength after free deconsolidation (at full deconsolidation) was dependent on the void free interlaminar shear strength, which described the maximum possible shear strength and was dependent on the fiber volume fraction, the lay-up, the polymer, the reinforcement type, and the manufacturing process. Table 5.5 lists the coefficients for all investigated materials.

Table 5.5: Dependency of the interlaminar shear strength on void content and their regression parameters

Acronym	**A_m void free interlaminar shear strength [MPa]**	**B_m dependency of void content [MPa/%]**	**Interlaminar shear strength at full deconsolidation [MPa]**
PPS UD 58	32.8	1.05	26.0
PPS UD 40	32.6	1.06	28.5
PPS SA 53	41.4	0.92	28.5
PPS SA 52	31.7	1.01	17.2
PPS SA 40	37.3	1.11	26.6
PPS TW 52	45.8	0.58	35.6
PP UD 58	7.3	0.51	5.8
PP UD 40	7.8	0.48	5.5
PP SA 53	17.2	0.54	7.0
PP SA HP 49	17.3	0.46	12.1
PP SA 48	24.3	0.59	17.0
PP SA 40	18.7	0.81	10.5
PP TW HP 52	21.7	0.51	12.4
PP TW 48	23.2	0.50	17.2
PC SA 50	55.4	1.35	37.9
PC TW 48	47.8	1.27	26.8

5.5 Polymer Flow

Neat polymer flow was characterized by viscosity measurement on a plate to plate rheometer for polyphenylensulfide and polypropylene. The results of neat polypropylene and polyphenylensulfide and the values from the datasheet for polycarbonate are shown in Figure 5.16.

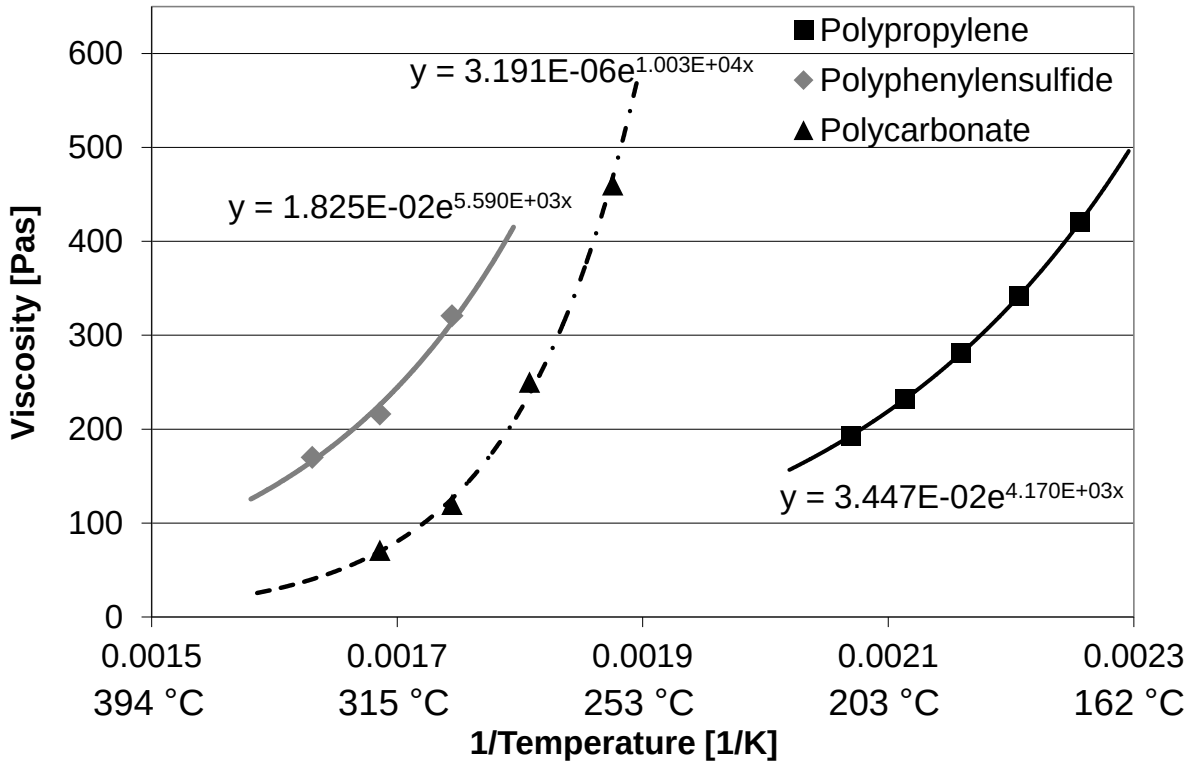

Figure 5.16: Viscosity of neat polypropylene, polycarbonate [125], and polyphenylensulfide dependent on temperature

The viscosity of polypropylene and polyphenylensulfide between processing temperature and melting temperature are in the same range. The viscosity change of polycarbonate in that range was significantly higher. It was between 2-3 times higher. For polyphenylensulfide, 340°C was the highest possible measurement temperature because of thermal degradation of the specimen at higher temperatures. Therefore, no correct measurement at 360°C was possible.

5.6 Crystallinity

The effect of crystallinity was investigated for polypropylene and polyphenylensulfide for 60 K/min and 10 K/min, which laid in the range of the cooling rate of the deconsolidation treatment and the manufacturing. The results, listed in Table 5.6, correspond to the values in the datasheet and indicate that there was no significant effect of the tested cooling rates for neat and reinforced polypropylene on the degree of crystallinity. Nevertheless, there was a strong dependency of the crystallinity on the reinforcement, which was promoted by the fibers. Varga and Karger-Kocsis and Arroyo et al. reported that glass fibers act as a nucleation for crystal build up [126; 127]. The degree of crystallization of glass fiber reinforced polypropylene was accelerated by 33 %. Because of the independency of the crystallinity on cooling rate for polypropylene and polyphenylensulfide in the range of 10 K/min to 60 K/min, the effect on the thickness change and respectively on the deconsolidation in the freely deconsolidated state (on equilibrium) was neglected [128].

Table 5.6: Melting temperature, on set of crystallization, degree of crystallinity, and initial crystallization force

Material	Melting temperature [°C]	On-set of crystallization (10 K/min) [°C]	Crystallinity (60 K/min) [%]	Crystallinity (10 K/min) [%]	Initial crystallization force [kN]
PP neat	162	131	45	45	49.721
PP SA 48	166	134	69	71	79.964
PP TW 48	164	135	61	60	67.031
PPS neat	282	255	37	39	147.299
PPS SA 48	282	253	39	42	158.894
PPS TW 52	283	250	36	39	147.299

In order to calculate the crystallinity, it was important to determine the enthalpy of fusion for 100 % crystallinity. Because of the impossibility of measuring a 100 % crystalline specimen, many authors have extrapolated this value from measurements of lower degrees of crystallinity, which results in a high deviation of this value [129]. Spruiell and Janke and Chung et al. reviewed the literature and assumed 112 J/g as

a correct value for PPS [130; 129]. For syndiotactic polypropylene and theoretically 100 % crystallinity, the enthalpy of fusion was 50 J/g [131]. Initial crystallization force can be calculated by the degree of crystallinity and Equation (4.27). The level of forces caused by the melting of crystals was two magnitudes higher than all other deconsolidation forces except thermal expansion. It was mainly dependent on the enthalpy of fusion and the degree of crystallinity. The neat polyphenylensulfide specimens had more similar initial crystallization forces than the reinforced specimens. Because of the nucleation effect of the reinforcement in polypropylene specimen, the initial crystallization force for the neat polypropylene was lower.

5.7 Thermal Expansion

Thermal expansion was calculated from the thickness evolution versus time and temperature (Table 5.7). The thermal expansion in melt was extrapolated as described in chapter 4.6. Heat capacities were calculated by the rule of mixture according to chapter 4.6. A curve of the heat capacity for glass and carbon fibers is given in [122] and [132]. The data of heat capacity are given in [23] for neat polypropylene and neat polycarbonate and in [67] for neat polyphenylensulfide.

Table 5.7: Heat capacity and thermal expansion of the composites between room temperature and processing temperature

	PP SA 48	**PC SA 50**	**PPS TW 52**
Heat capacity	135.19 [J/g]	225.22 [J/g]	217.89 [J/g]
Thermal expansion	0.057 [mm]	0.095 [mm]	0.13 [mm]

5.8 Moisture

Water absorption of the reinforced polymers is listed in Table 5.8. The reinforced polypropylene and polyphenylensulfide specimens showed a low weight loss of 0.066 % and respectively 0.053 % after 24 h drying. The reinforced polyphenylensulfide and the polypropylene reached a similar value after 5 min dwelling below melting temperature. The values were comparable to the condition of the specimens before the thickness increase during the deconsolidation treatment. Therefore, it can be concluded that no significant moisture was left in the specimen before the specimen exceeded the melting temperature.

Table 5.8: Moisture and weight loss after drying for 24 h and 5 min

Material	Weight loss of polymer* [%]	Weight loss after 24 h drying [%]	Weight loss after 5 min drying [%]
PP SA 53	-	0.066 %	0.066 %
PC SA 50	0.12 % [125]	0.116 %	0.025 %
PPS SA 53	0.06 % [67]	0.053 %	0.051 %

* According to the datasheet of neat polymer at 23 °C and 50 %

The reinforced polycarbonate specimen revealed a relative high weight loss of 0.116 % after drying for 24 h, which was similar to the value for the neat polymer at 23 °C and 50 % relative humidity [125]. After 5 min drying, the specimens had partially reached the 24 h value. This corresponds to a weight of water of 12.25 mg. According to (4.31), this resulted in a volume of steam of 27.6 cm³. Considering a specimen volume of 8.0 cm³ this was 2.45 times more volume than the actual specimen's volume. The thickness increase after deconsolidation was smaller than the calculated steam volume because of the release of pressure during deconsolidation caused by a formation of venting channels (Figure 5.17). The shape of the voids divided from the found circular shape. They were more flat, tube like and were located between the layers with a length of several millimeters.

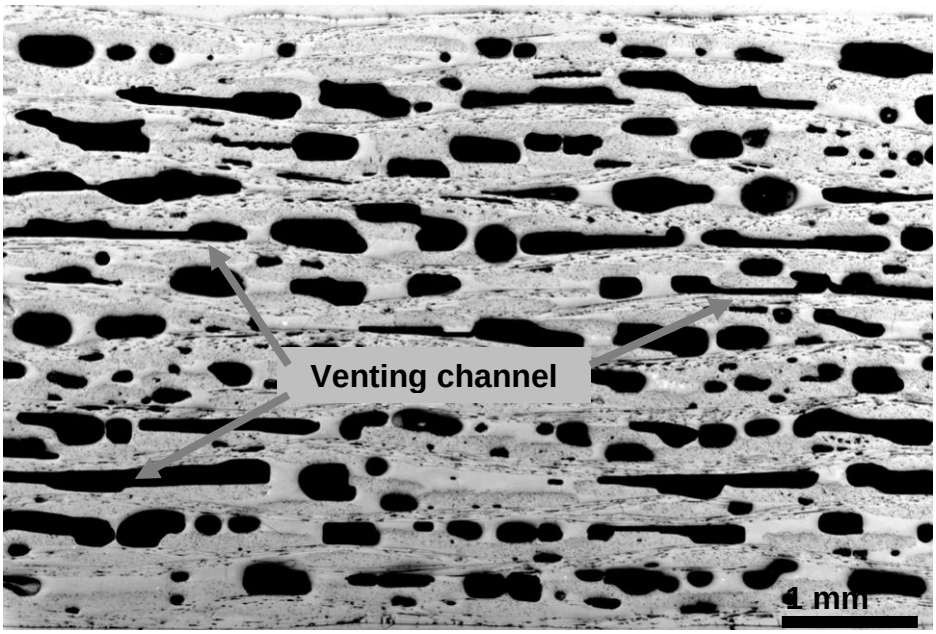

Figure 5.17: Micrograph of an undried PC SA 50 specimen after free deconsolidation

6 Discussion and Validation of the Model

The proposed model is verified for the accurate prediction of the final state of deconsolidation and the time dependency of the thickness during deconsolidation. Also, a first order approach of deconsolidation is verified by means of a minimum of input measurements.

6.1 Discussion of the Influences on Deconsolidation

The principle effects of each deconsolidation mechanism are discussed in this chapter, as well as how they are affected by the input parameters and possible errors during measurement or determination. Figure 6.1 shows the dependency of the normalized forces on the thickness increase of the effect void expansion, surface tension, and fiber reinforcement network. The normalized forces were calculated by the forces of the effect divided by the initial force of the fiber reinforcement network.

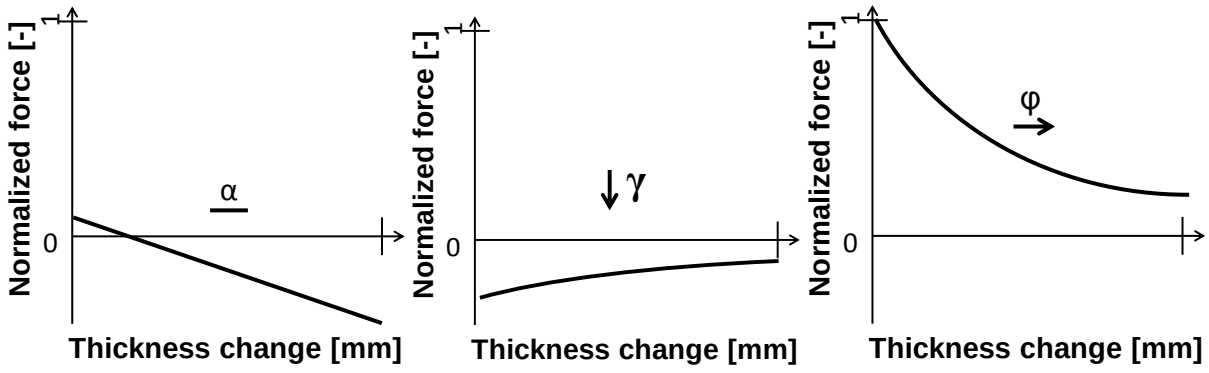

Figure 6.1: Dependency of the normalized forces on the thickness increase of void expansion (left), surface tension (middle), and fiber network (right)

The **void expansion** is affected by a pressure gradient between internal void pressure and external pressure. If a specimen is directly reheated above melting temperature the internal void pressure, which is nearly the applied pressure during manufacturing, promotes deconsolidation and can lead to a void content increase of several times. If an underpressure within a vacuum bag is applied during manufacturing, the internal void pressure can even decrease deconsolidation. After manufacturing of the specimen, the gradient declines with time and finally disappears. An applied external underpressure during deconsolidation can also increase the gradient and therefore promotes deconsolidation.

Reheating temperature affects **void expansion** leading to an acceleration of deconsolidation because of gas expansion. The thermal gas expansion from room temperature to processing temperature can decrease the energy in the range of 40 % to 60 %. The void energy declines with the thickness increase caused by an underpressure inside the void (Figure 6.1 left). Therefore, the energy decreases with larger thicknesses. That reduces deconsolidation. The initial void content has a minor effect because the volume expansion and internal void pressure are proportional to each other. In addition to this effect, the mentioned thermal gas expansion of a higher void content has a higher change in energy than a lower void content.

The **surface energy** is proportionally dependent on the surface tension in melt and the surface area. A polymer with a lower surface tension in melt has a lower surface energy and therefore a lower hindering effect on deconsolidation. Also, the temperature has an influence on surface tension because the surface tension declines with temperature, which less hinders deconsolidation. The second factor of the surface energy (4.13) is affected by the initial surface area, which is dependent on the number of voids and the third root of the average void radius. If the void content increases, some voids coalescence into each other and decrease the void volume to surface area ratio. This effect is dependent by root from the surface work with an increase of void volume (Figure 6.1 middle).

The **fiber reinforcement network energy** decreases by a polynomial function of 4^{th} order with the thickness (Figure 6.1 right). For textiles small changes of thickness have a very high effect on the energy. The effect is decreasing with the thickness as the decompaction pressure also decreases. Zero for infinite thickness is the boundary value. Settling effects were investigated for the reinforcement types used. The twill and satin reinforced specimens had a minor settling effect between 3-4 % of the maximum decompaction pressure. Therefore, the same decompaction curve dependent on the fiber volume fraction of each reinforcement type was used to model all deconsolidation configurations. An exception is the unidirectional reinforced specimen because the settling of the pressure is 54 % of the maximum decompaction pressure. This simplification would falsify the accuracy of the model. It must be pointed out that this simplification must be validated for each fabric because of tremendous difference in the decompaction behavior of fabrics.

Figure 6.2 shows the dependency of the normalized forces on the thickness increase of the crystallinity, thermal expansion, and moisture. It must be pointed out that the scale of the normalized forces of the crystal melting and the thermal expansion is 3 magnitudes higher. Nevertheless they act in a very short range of thickness change and are usually reversible.

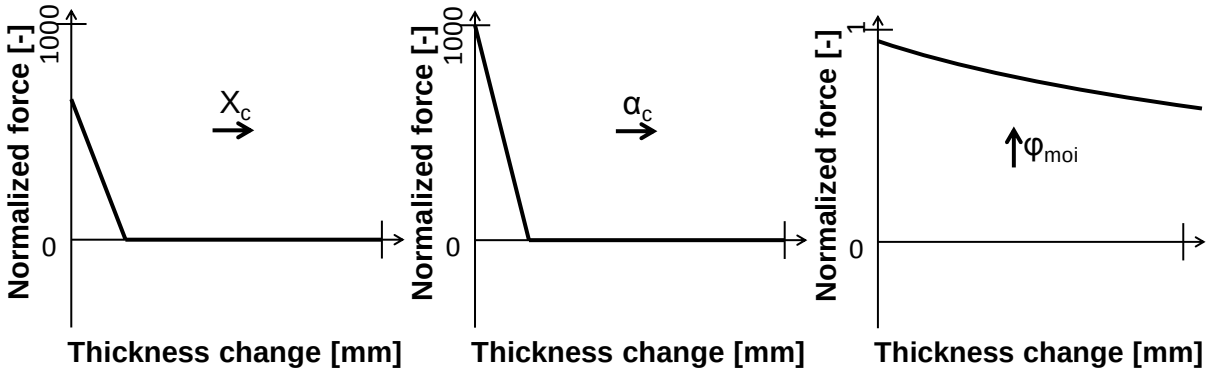

Figure 6.2: Dependency of the normalized forces on the thickness increase for crystal melting (left), thermal expansion (middle), and moisture (right)

The **polymer flow** equation has the type of natural and common logarithms. The forces applied by the other deconsolidation mechanisms cause a polymer flow and are proportionally dependent on the viscosity and are inversely proportional to the time interval. Higher viscosities lead to higher forces and longer deconsolidation times lead to lower forces. A thickness increase results in a higher value of the natural logarithm and the common logarithm. Because of the small inner value of the common logarithms and the lower growth of the common logarithm compared to the natural logarithm, a thickness increase at higher void contents results in a higher force. That means thinner polymer shells of voids cause higher flow velocities in the shell.

As described in chapter 4.5, it is assumed that the **crystallinity** has no effect on deconsolidation itself because of the same crystallinity before and after the treatment at the investigated conditions. If the crystallinity is different, the initial condition of the deconsolidation mechanisms has to be determined at melting temperature, which can be easily done by setting the polymer density and therefore the polymer volume to an amorphous state. This would also lead to a different void fraction and fiber volume fraction in melt. The **thermal expansion** has a similar effect as crystallinity because of the reversible nature of the expansion for the same start and end

temperature. Because the start and end temperature is room temperature, there is no need of a correction under usual conditions. But as described in chapter 4.6, it can be considered during the deconsolidation treatment, with no influence after the treatment.

The **moisture** mechanism is formulated by the ideal gas law, which is proportionally dependent on the moisture content. Because of the tremendous expansion of water above the boiling point, it is very important that the specimen do not have any water just before the melting temperature of the polymer. This can be achieved by an appropriate dwelling time below the melting temperature, which is dependent on the polymer diffusion. Another possibility is the drying according to a standard as described in chapter 3.4.6. The investigation is carried out by means of an open mold, where moisture can be released by the sides and the top of the specimens. There are several processes such as stamp forming, autoclaving, or induction welding with a top die, where the pressure cannot be released to the top or sides. This increases the time of moisture release, leading to a higher moisture content at processing temperature and therefore to an extensive build-up of steam and voids respectively.

Another mechanism is caused by **external forces**. External forces have a proportional effect on the die energy as well as the thickness increase itself. It retards the thickness evolution because of a lower available energy.

6.2 Free Deconsolidation Treatment on Equilibrium

The model for the free and inhibited deconsolidation treatment is solved on equilibrium meaning the sum of all forces is zero (dE/dx=0). The equilibrium is reached after infinite time. The input and output parameters of the model are shown in Figure 6.3.

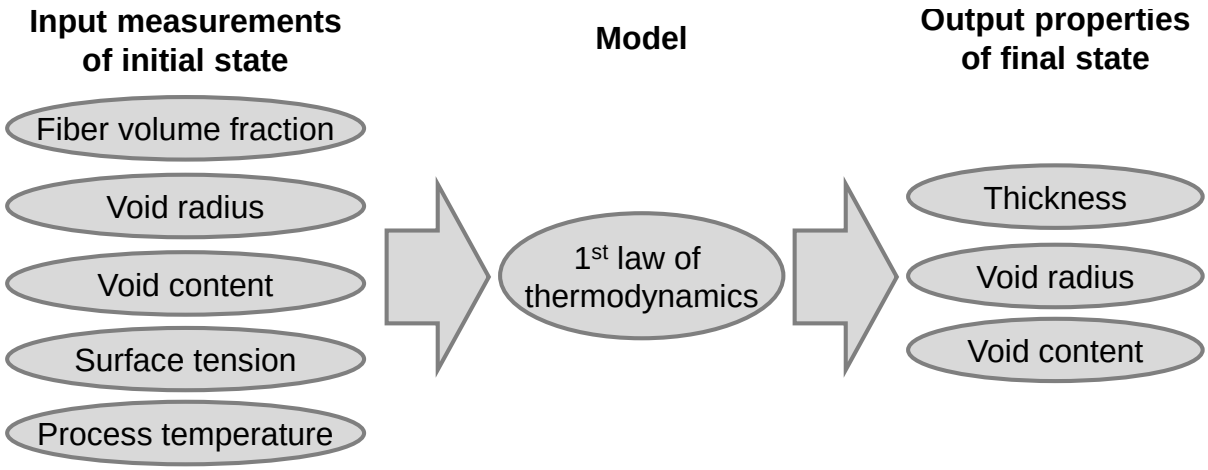

Figure 6.3: Flow chart of the model on equilibrium

All input parameters can be determined by measurements or set by the process (e.g. temperature). The model determines the thickness of the specimen, which is used to calculate the average void radius and void content under the assumption of mass conservation. The initial input parameters for PP TW 48, PP SA 48, PP TW HP 52, PP SA HP 49, and PP UD 58 are listed in Table 6.1, gained from the void analysis described in 5.1 and 3.4.2.

Table 6.1: Initial fiber volume fraction, thickness, void number, void radius, and void content for PP TW 48, PP SA 48, PP TW HP 52, PP SA HP 49, and PP UD 58

	PP TW 48	**PP SA 48**	**PP TW HP 52**	**PP SA HP 49**	**PP UD 58**
Fiber volume fraction [%]	48.2	46.5	50.8	48.6	58.2
Thickness [mm]	3.16	3.15	2.92	3.02	3.02
Initial void number [10^6]	1245	2671	1172	1628	7.28
Initial void radius [µm]	3.36 ±0.13	2.96 ±0.08	2.76 ±0.21	3.14 ±0.24	8.74 ±0.12
Initial void content [%]	2.5 ±0.3	3.6 ±0.3	1.4 ±0.4	2.8 ±0.8	0.27 ±0.2

Table 6.2 lists the results of the model solved for the free deconsolidation treatment on equilibrium. The calculated thicknesses agree well with the measured thickness and are in the range of the confidence interval. A further calculation of the void radius and void content indicates a slight underestimation because of the lower estimated number of voids. This is caused by an overestimation of coalesced voids, which is dependent on a homogenous void distribution and the coalescence criteria “contact of neighboring voids”. The homogeneous void distribution does not take into account the separation of voids by the fabric layers and the roving undulation. It is interesting to note that the autoclaved specimens, which have a lower initial fiber volume fraction and a higher initial void content, show a lower final void content in the freely deconsolidated state than the hot pressed specimens.

Table 6.2: Results of the model solved for the free deconsolidation treatment on equilibrium

Property	**PP SA HP 49**	**PP SA 48**	**PP TW HP 52**	**PP TW 48**	**PP UD 58**
Calculated thickness [mm]	3.30	3.33	3.41	3.49	3.16
Measured thickness [mm]	3.32 ±0.036	3.34 ±0.020	3.44 ±0.015	3.47 ±0.034	3.13 ±0.04
Calculated void radius [µm]	5.6	4.3	7.7	6.4	25.6
Measured void radius [µm]	5.5 ±0.49	5.0 ±0.25	7.9 ±0.74	7.6 ±0.74	18.2 ±0.40
Calculated void content [%]	10.8	9.0	15.5	11.8	4.9
Measured void content by micrographs [%]	12.9 ±0.62	9.7 ±1.24	16.6 ±0.63	12.8 ±0.87	4.9 ±1.50
Measured void content by thickness [%]	11.45 ±0.07	9.73 ±0.10	16.55 ±0.24	11.83 ±0.11	5.96 ±0.60

The calculated effect of the fiber network, the void expansion, and the surface tension on the thickness during deconsolidation is shown in Figure 6.4 for PP SA 48 and PP SA HP 49, which is only possible to be determined by means of the model.

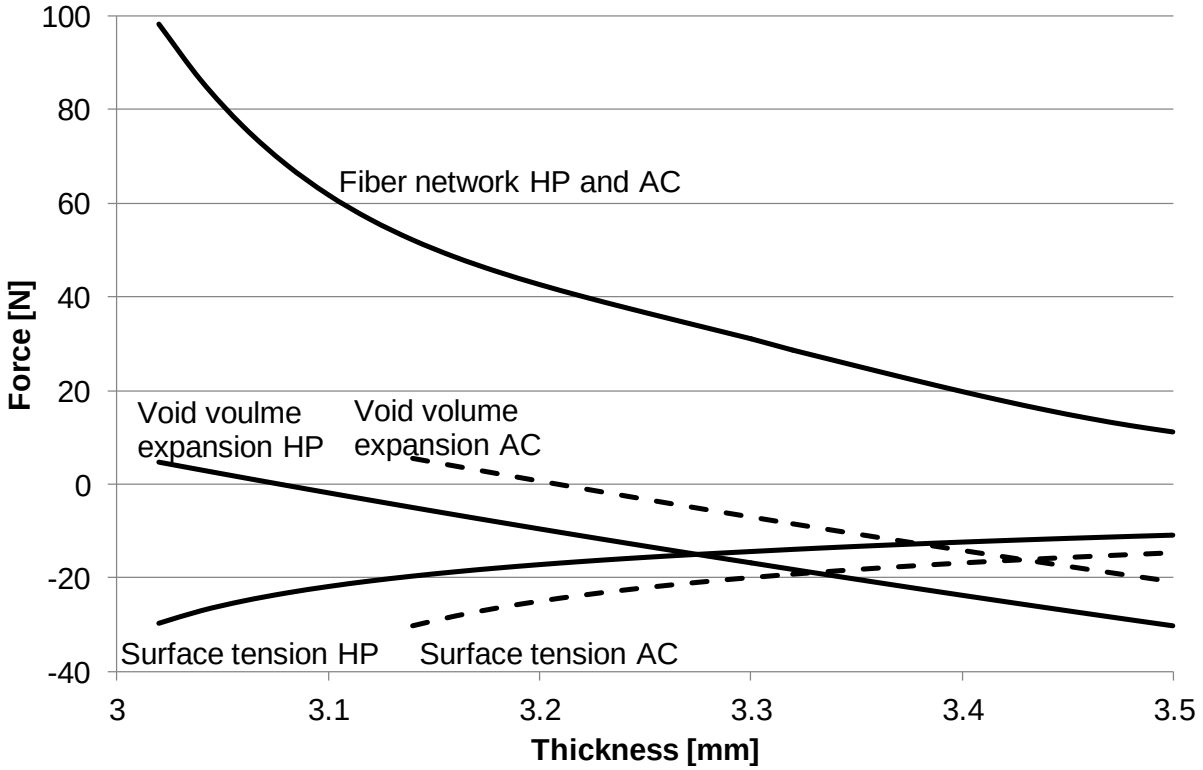

Figure 6.4: Calculated dependence of the thickness on the fiber network, the void expansion, and the surface tension of PP SA 48 (AC) and PP SA HP 49 (HP)

The void expansion initially has a promoting effect on the deconsolidation because of the thermal gas expansion as it is reported by Ye et al. [17]. But the direction of the effect changes into the opposite as the thickness increases until it is the dominating inhibitory effect. This is caused by the forced volume expansion, which leads to an under pressure inside the voids. The force is inversely proportional to the thickness and the void content. The slope is determined by the initial void content, the initial thickness, and the processing temperature. Surface tension has initially an inhibitory effect on deconsolidation. As the thickness increases the effect decreases slowly because the voids coalesce and the volume to surface ratio increases. The boundary value for infinite thickness is zero. The initial values are mainly dependent on the void content and the surface tension of the polymer. Nevertheless, the strongest effect on deconsolidation is caused by the fiber network dependent on the fiber volume fraction and the reversible energy storage in the fiber network respectively. The effect decreases with an increasing thickness because of the polynomial dependence on the fiber volume fraction and therefore the thickness.

In order to quantify the sensitivity of the void content on the initial condition and the processing temperature, the input parameters are individually changed by 10 %. The sensitivity was calculated by the property change divided by the original value. The results are listed in Table 6.3.

Table 6.3: Sensitivity of the void content on an initial condition or processing temperature change of 10 %

Property	PP SA HP 49 [%]	PP SA 48 [%]	PP TW HP 52 [%]	PP TW 48 [%]	PP UD 58 [%]
Void radius	+2.0 / -2.5	+3.4 / -4.5	+1.7 / -0.9	+1.6 / -2.0	+0.5 / -0.5
Void content	+2.5 / -2.4	+4.1 / -4.3	+0.8 / -0.6	+2.3 / -1.7	-0.5 / +0.4
Surface energy	-2.3 / +2.2	-4.2 / +3.6	-0.7 / +0.9	-1.5 / +2.0	-0.5 / +0.5
Fiber volume fraction	+58 / -64	+72 / -	+41 / -38	+54 /-97	+54 / -
Processing temperature	+0.7 / -0.6	+1.0 / -1.3	+0.3 / -0.1	+0.8 / -0.3	+0.1 / 0.0

The initial void radius and void content, which are related to the void number, have a minor effect on the final void content of less than 4.3 %. A minor effect has the surface energy, which is promoted by a high initial void content and the surface tension at processing temperature. Also, the processing temperature has a minor effect on deconsolidation. As reported earlier, the fiber volume fraction has the strongest effect. Even a small change of 10 % leads to a remarkable effect of 40 % to >100 % change of void content. This is caused by the polynomial dependency of 4^{th} order of the force on the thickness.

6.3 Using Universal Applicable Input Parameters to Approximate the Thickness after free Deconsolidation (First Order Approximation)

As shown by the sensitivity study, the fiber volume fraction is the predominant initial parameter of deconsolidation. This leads to the approximation of the final void content by using universal initial parameters plus the measurement of the decompaction behavior, which can be determined by a given decompaction function of the fiber reinforcement network. The universal parameters defined from the

sensitivity analysis are given in Table 6.4. The value for the surface tension is below the measured values because of better fitting to the measurement. Nevertheless the influence is rather low.

Table 6.4: Universal applicable input parameters of the model

Universal input parameter	Value
Void radius	3.0 µm
Void content	2.0 %
Surface tension	16 mN/m

The results of the void content after free deconsolidation using the universal input parameters are listed in Table 6.5 and show a good agreement with the determined void content by thickness measurements.

Table 6.5: Determination of the void content after the free deconsolidation using universal input parameters

Material	Measured void content	Estimated void content
PPS UD 58	6.42 %	6.0 %
PPS SA 53	13.65 %	Not available
PPS SA 52	16.00 %	15.3 %
PPS TW 52	17.93 %	16.9 %
PP UD 58	5.96 %	6.6 %
PP SA 53	18.83 %	15.9 %
PP SA HP 49	11.45 %	10.3 %
PP SA 48	9.73 %	7.9 %
PP TW HP 51	16.55 %	16.3 %
PP TW 48	11.83 %	11.5 %
PC SA 50	11.52 % dried	12.7 %
PC TW 48	16.59 % dried	17.5 %

The increase of void content is slightly under estimated, if the initial void content is higher than the universal applicable void content. Specimens with a lower void content show a slight over estimation, which is expected from the results of the sensitivity study. It can be concluded that the void content can be estimated using the

universal input parameters after the free deconsolidation treatment with a reasonable accuracy. This result confirm the low absolute influence of the initial values of the surface tension, void content, and void radius. It must be pointed out that the proposed mechanisms are not neglected. They are still considered in the model and have a significant effect on deconsolidation. The universal applicable input parameters can be used to optimize a process or find a weak spot with a minimum of experiments. The application using these parameters is demonstrated in chapter 7.

6.4 Dependency of Deconsolidation on External Pressure

The knowledge of the necessary external pressure to prevent deconsolidation is very important. As shown in chapter 0, the void content can be decreased by applying an external pressure during the deconsolidation treatment. The developed model is capable of considering external pressure, which is solved for different external pressures for PPS SA 52, PP SA 49 HP, and PP SA 48 (Table 6.6). The initial thickness before testing was 2.80 mm for PPS SA 52, 3.15 mm for PP SA 49 HP, and 3.02 mm for PP SA 48.

PPS SA 52 shows a good agreement between the measurement and the calculation using universal input parameters up to 0.0048 MPa. Because of the high thickness decrease between 0.0048 MPa and 0.0064 MPa to 3.04 mm and the low confidence interval, it is assumed that an unknown error occurred. A repeat showed no improvement. This specimen showed no obvious defects or unmelted areas. Nevertheless, the application of 0.012 MPa is not sufficient to maintain the initial thickness of the specimen. PP SA 48 and PP SA 49 HP show an excellent agreement between the measurement and the calculation for all applied pressures. The model is solved for the inhibit deconsolidation treatment for many configurations, to calculate the external pressure, which is necessary to prevent deconsolidation. As reported in literature, a low pressure is sufficient to prevent deconsolidation (<<0.3 MPa), which is one magnitude lower than the usual manufacturing pressure [98; 97]. The maximum necessary inhibit deconsolidation pressure in this study to maintain the initial thickness is 0.15 MPa.

Table 6.6: Measured and calculated thickness of applied external pressure for PPS SA 52, PP SA 48, and PP SA 49

	External pressure [MPa]	**Measured thickness on equilibrium [mm]**	**Calculated thickness on equilibrium [mm]**
PPS SA 52	0	3.27	3.24
	0.0016	3.23	3.22
	0.0048	3.16	3.18
	0.0064	3.04	3.15
	0.012	2.96	3.10
PP SA 48	0	3.32	3.34
	0.0016	3.30	3.32
	0.0048	3.31	3.27
	0.0064	3.25	3.24
	0.012	3.17	3.15
PP SA 49 HP	0	3.32	3.31
	0.0016	3.31	3.29
	0.0048	3.26	3.24
	0.0064	3.25	3.22
	0.012	3.16	3.14

Matrix squeeze out can be an issue for deconsolidation, if a significant amount of polymer flows out of the specimen and therefore mass conservation is not applicable. The matrix squeeze out of PP SA 53, PPS SA 53, and PC SA 50 after 10 min is calculated at processing temperature and for different pressures listed in Table 6.7.

Table 6.7: Calculated polymer loss for different cross sections during compression with different pressures for PP SA 53, PPS SA 53, and PC SA 50

	External pressure [MPa]	**Polymer loss for 50x50 mm²**	**Polymer loss for 500x500 mm²**
PP SA 53	0.004	0.035 %	0.0035 %
PP SA 53	0.04	0.35 %	0.035 %
PP SA 53	0.4	3.14 %	0.34 %
PPS SA 53	0.004	0.033 %	0.0033 %
PPS SA 53	0.04	0.32 %	0.033 %
PPS SA 53	0.4	2.97 %	0.32 %
PC SA 50	0.004	0.090 %	0.0090 %
PC SA 50	0.04	0.88 %	0.090 %
PC SA 50	0.4	7.19 %	0.88 %

The specimens have nearly a linear dependency of polymer loss on external pressure. PC SA 50 shows the highest polymer loss of 7.19 % at 0.4 MPa by a cross section of 50x50 mm² because of a three times lower viscosity than PP SA 53 and PPS SA 53 at processing temperature. Nevertheless, the polymer loss is approximately two times higher. Also, PP SA 53 has a slightly higher polymer loss than PPS SA 53 because of the stronger influence of the thickness than the viscosity (2.10). It can be concluded that polymer loss after 10 min is less than 2 % for the maximum deconsolidation pressure (0.15 MPa), a specimens cross section of 50x50 mm². These results justify the assumption made of mass conservation. If the applied pressure is higher than 0.15 MPa, which the case is during reconsolidation at thermoforming for example for small specimens, matrix squeeze out must be considered. It must be pointed out that a 10 times higher cross section leads to a ten times lower matrix loss. This fact must be considered by the application of the model. That means the limiting pressure increases from 0.15 MPa for 50x50 mm² cross section to 1.5 MPa for a cross section of 500x500 mm².

6.5 Time Dependency of the Thickness Evolution during Deconsolidation

Thickness evolution is modeled by the Navier-Stokes equation considering the 1st law of thermodynamics, the viscosity, and the temperature. The flow chart is given in Figure 6.5 and the formulation is solved incrementally with a thickness change of 5 µm. It is assumed that the void content and the void number do not change significantly during one step. Therefore, the void content and the void number are calculated before each increment.

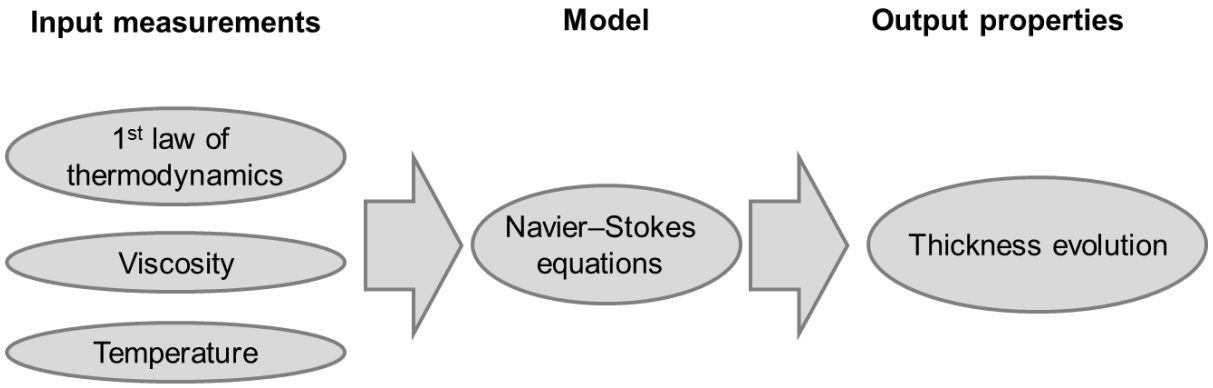

Figure 6.5: Flow chart of the time dependent thickness evolution model

Figure 6.6 shows the measured and calculated thickness evolution and the corresponding temperature of PP SA HP 49. It must be pointed out that the following curves start 30 s before reaching the melting temperature. Deconsolidation starts when the melting temperature is reached and is strongly declining until the thickness on equilibrium is reached. Within 11.1 s, 50 % of the thickness increase is achieved and 90 % is achieved after 51.9 s. The calculated thickness evolution agrees well with the measurement. Only near the melting temperature, the curve slightly deviates from the measurement because of the inhomogeneous temperature distribution through the thickness, which cannot be considered by the model. Deconsolidation can be inhibited by a lower processing temperature because of the exponential dependency of the viscosity on the inverse temperature. But nevertheless, this possibility is less effective because after 11.1 s 50 % of deconsolidation is reached, which corresponds to a temperature of 178 °C, which is 14 K higher than the melting temperature.

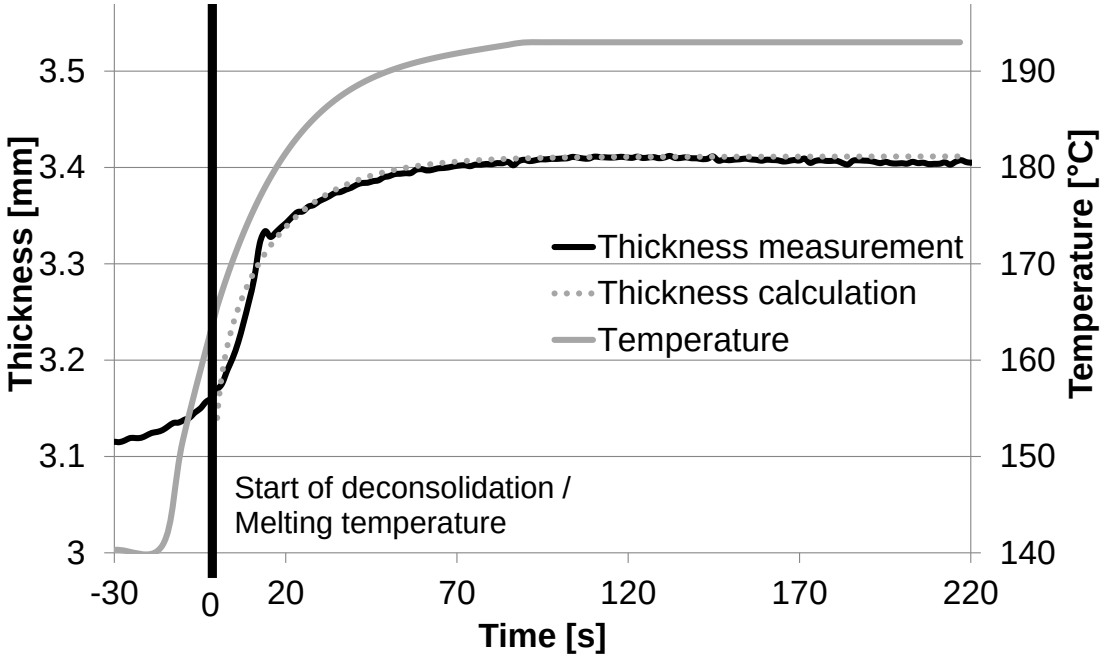

Figure 6.6: Time dependent thickness and temperature evolution for PP SA HP 49

The sensitivity of a 50 % viscosity change on the thickness evolution is shown for PP SA HP 49 in Figure 6.7.

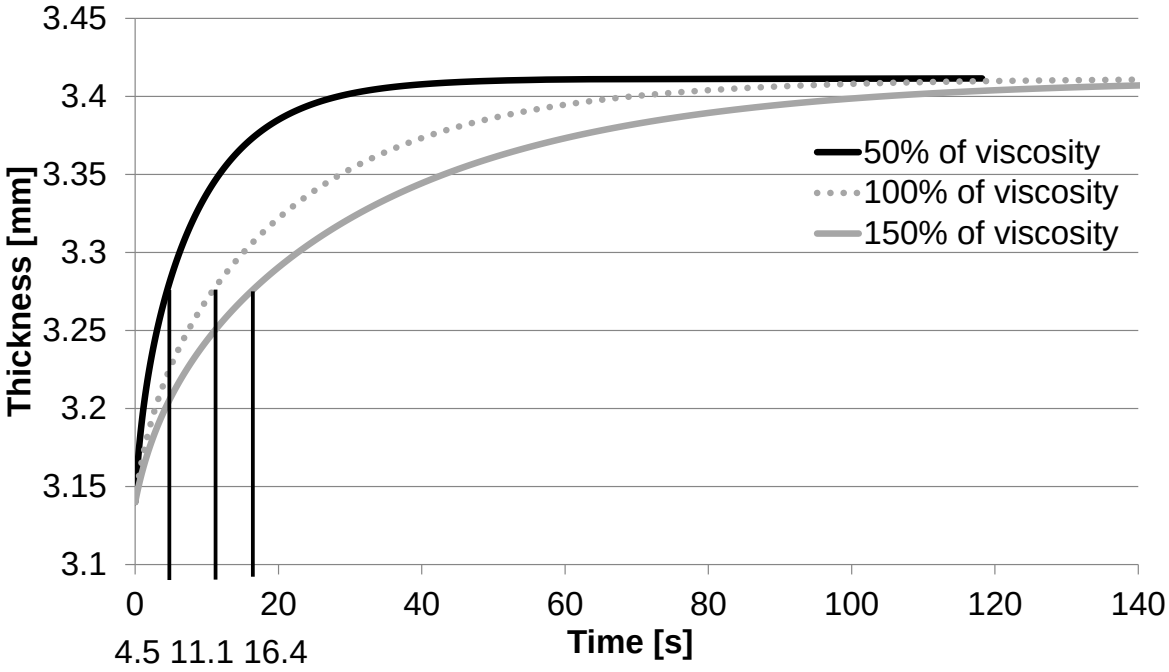

Figure 6.7: Sensitivity of the calculated time dependent thickness evolution of PP SA HP 49 for a 50 % viscosity change

Deconsolidation is promoted by a lower viscosity. As given in (4.25), the incremental thickness increase is linear dependent on the viscosity, which means a 50 % lower viscosity achieves the same step in half of the time. For a lower viscosity, 50 % of the

deconsolidation is achieved after 4.5 s and for a 50 % higher viscosity after 16.4 s. This can be generalized by saying that a different polymer grade of the same group with a higher viscosity can inhibit deconsolidation. It must be pointed out that the impregnation can be more difficult with high viscose polymer grade.

The thickness evolution of the measurement and the calculation for PP TW 48 is shown in Figure 6.8. The measurement signal shows a higher noise caused by the poor contrast of the black specimen and the black background.

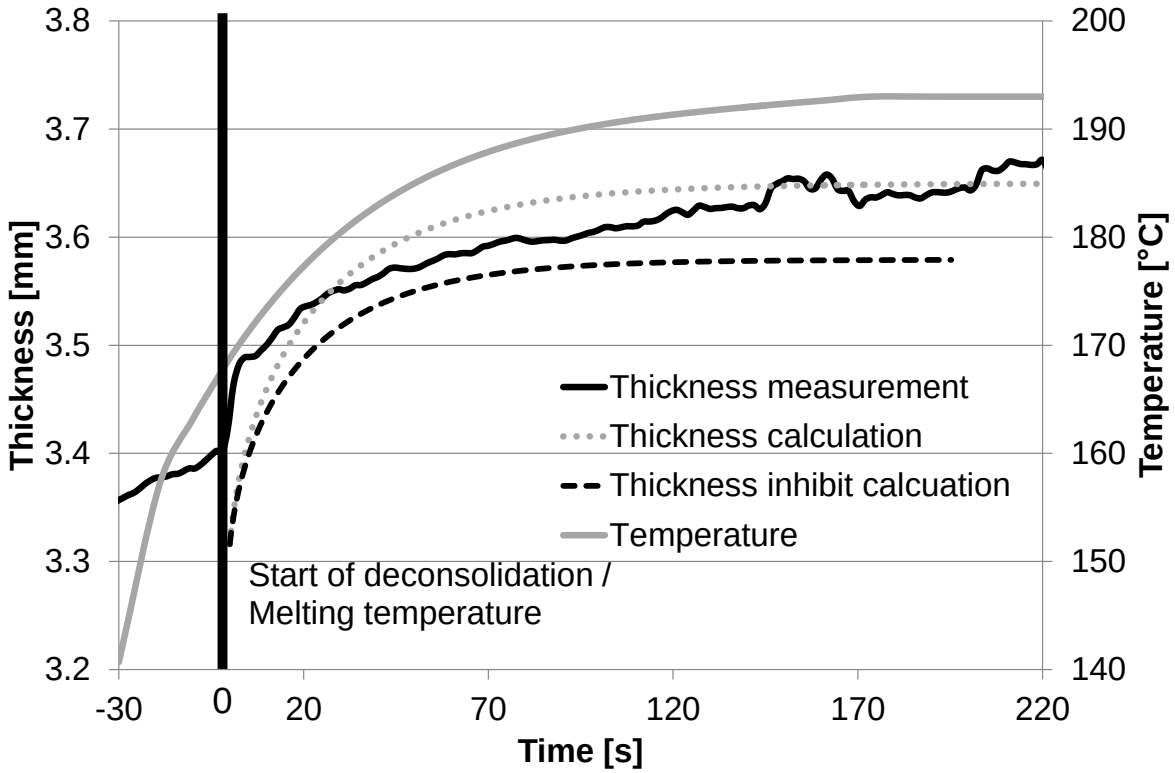

Figure 6.8: Time dependent thickness and temperature evolution for PP TW 48

There is a step before the melting temperature, which could be caused by a slightly inhomogeneous temperature distribution because of heating from one side. Nevertheless, the tendency of the overall trend is not affected. The calculated curve has a good agreement to the measurement. 50 % of the thickness increase is reached after 10.8 s, which is similar to the specimen with the glass fiber satin ¼ reinforcement. This is caused by a similar sum of initial pressure of about 0.028 MPa, even if the total deconsolidation increase is 0.27 mm compared to 0.34 mm.

An external pressure hinders deconsolidation, as shown in chapter 4.6. Therefore, the time dependent influence is investigated for an external pressure of 0.0048 MPa.

Initially the influence of an external pressure is low because the deconsolidation pressure is much higher up to 50 % of the thickness increase. As the extent of deconsolidation increases, so does the inhibit curve deviates from the free deconsolidation curve. Both curves line up to boundary values and have a similar velocity.

6.6 Using Universal Applicable Input Parameters to Approximate the Thickness Evolution (First Order Approximation)

Temperature and therefore viscosity has a great influence on the time dependent thickness evolution during deconsolidation. The temperature during processing is often easy to measure. Nevertheless, the corresponding viscosity data is not available. Therefore, the temperature at a deconsolidation extent of 50 % (50 % of the maximum thickness increase) is used to determine the viscosity at one condition. This leads to a simple approximation of the thickness evolution determined by universal initial parameters given in Table 6.4. The PPS SA 53 needs approximately 100 s to reach the processing temperature even if the tool temperature needs 5 s (Figure 6.9). This is caused by a gap between the specimen and the bottom tool. The temperature was measured at the surface of the specimen (bottom and top) and below the surface of the tool. This effect is considered by the online thickness measurement because the software detects the edges of the specimen. The accurate calculation and the calculation by means of the universal applicable input parameters of the thickness are in good agreement to the measurement. The curves show a progressive thickness increase with a high increase initially, which changes to a nearly linear slope. 50 % of deconsolidation is reached after 18.2 s and the final thickness is achieved after 220 s. There are only minor differences between the accurate and the approximated values because of the relative low temperature difference between the actual measured temperature and the fix temperature of 295 °C for viscosity calculation.

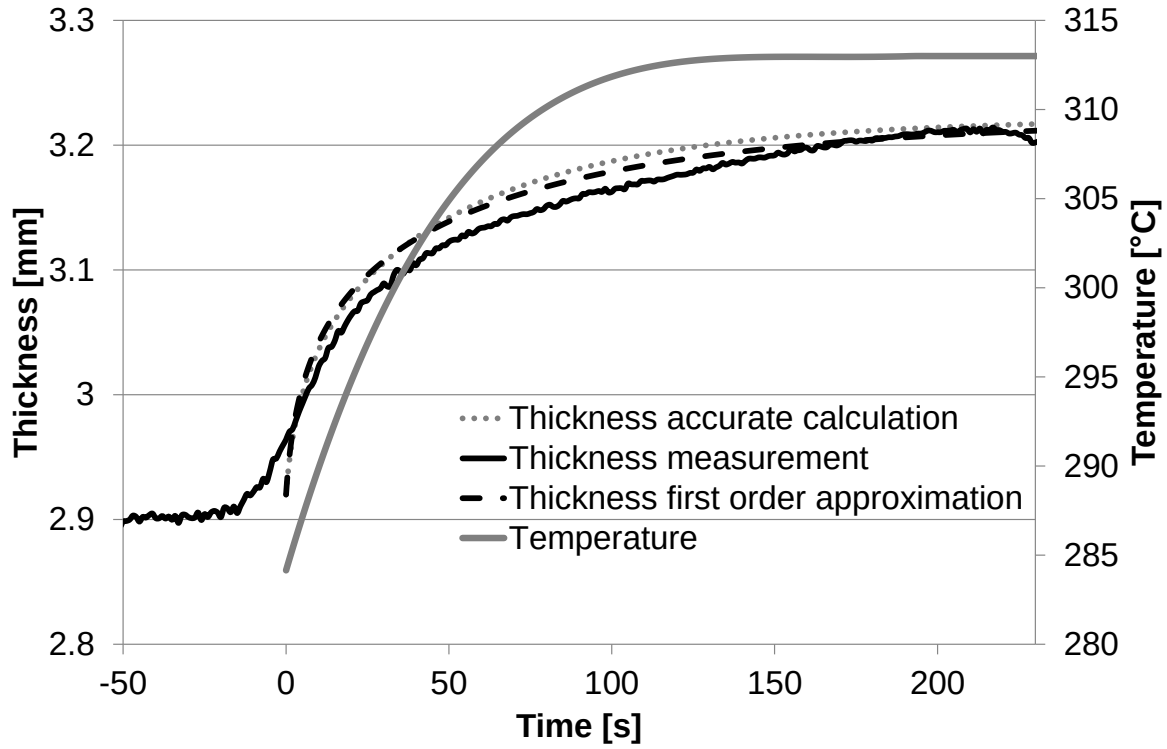

Figure 6.9: Time dependent thickness and temperature evolution for PPS SA 53

PC TW 48 specimens show a similar gap between the tool and the specimen compared to the PPS SA 53 specimens. The gap causes a lower heating rate than set and leads to a delay of processing temperature, which was achieved after 150 s (Figure 6.10). The thickness evolution of the specimen above glass transition temperature shows a linear slope, which is different to all other measured curves. Three repetitions were carried out and all curves show a similar linear behavior. It is assumed that PC TW 48 does not have a sharp starting point of deconsolidation as it is for semi-crystalline specimens, which could be due to the transient softening near the glass transition temperature. Also, the high increase of deconsolidation could lead to an insulating effect corresponding to a higher local temperature gradient than observed for the other configurations. Nevertheless, the agreement of the calculation to the measurement is on an acceptable level. 50 % of the total thickness increase is reached at 18.8 s after the start of deconsolidation.

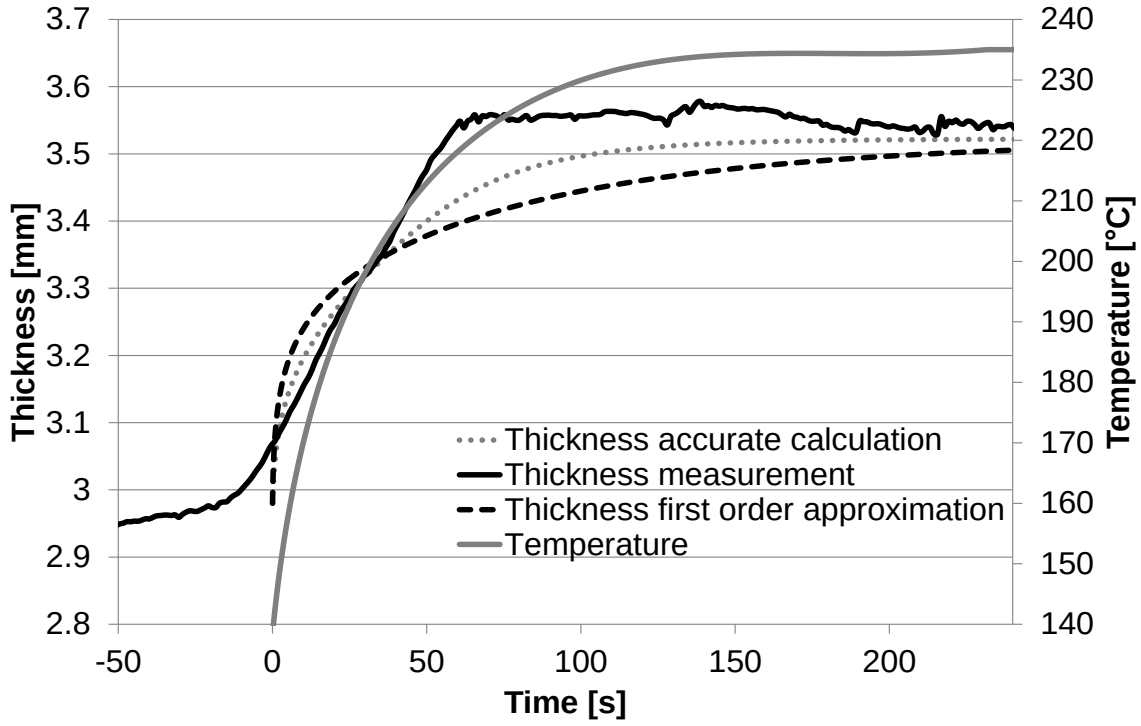

Figure 6.10: Time dependent thickness and temperature evolution for PC TW 48

The universal parameters lead to an acceptable agreement to the measurement. The temperature used was 177 °C (at 50 % of deconsolidation), which deviates from the glass transition temperature 33 K and 60 K from the processing temperature. This leads to a tremendous deviation of the set viscosity from the actual viscosity.

In order to investigate the effect of the approximation, the initial viscosity and the viscosity at processing temperature are compared to the viscosity at different stages of deconsolidation (30 %, 50 %, 70 %), as it is listed in Table 6.8.

Table 6.8: Viscosities at different stages of deconsolidation for PP SA HP 49, PP TW 48, PPS SA 53, and PC TW 48

Property [Pas]	PP SA HP 49	PP TW 48	PPS SA 53	PC TW 48
Viscosity10 K above melting	374.9	375.1	347.8	582.9
Viscosity at 30 % of deconsolidation	410.5	391.7	385.2	525.0
Viscosity at 50 % of deconsolidation	372.1	372.8	348.8	324.6
Viscosity at 70 % of deconsolidation	322.7	331.2	306.1	181.8
Viscosity 20 s after melting	332.2	332.1	344.0	310.8
Viscosity at processing temperature	264.9	264.8	245.4	103.3

The temperature 10 K above melting temperature corresponds approximately to the off-set temperature of melting at 60 K/min heating rate. The polypropylene specimens exhibit a viscosity decrease of ~110 Pas, but already 50 % of deconsolidation took place at a corresponding viscosity of 372.1 Pas and 372.8 Pas. Because of the proportional dependency of the deconsolidation speed on the viscosity, the mistake of the calculated speed up to 70 % of deconsolidation is very low (<2 %). The interval between 70 % and 100 % has a deviation of viscosity of 21 % in average. The deviation is more pronounced at the later stage of deconsolidation because of the higher deviation of viscosity to the fix value. Polyphenylensulfide specimens show a similar behavior. Because of the low deviation of viscosity, 10 K above melting temperature and the processing temperature has an average mistake of deconsolidation of 5 %. The second interval shows a higher deviation of 20 %. Polycarbonate specimens had a deviation of the deconsolidation speed of 9 % in average for the interval of 0 % to 70 %. The second interval has an average mistake of 56 %, which leads to a tremendous deviation from the real behavior.

It can be concluded that the universal applicable input parameters can be used to calculate the thickness evolution and give a good agreement to the actual thickness evolution, when the difference of the final processing temperature and the start of melting is low. The corresponding viscosity should show a deviation between start and end of less than 30 %. Different heating rates can minimally affect the accuracy of the first order approximation, which is the case of the shown polyphenylensulfide example. If the viscosity deviation between start and end is higher than 30 %, tremendous deviation of the approximated behavior to the real behavior is found. In this case the real viscosity must be taken into account.

6.7 Modelling of a Full Deconsolidation Cycle

A full deconsolidation cycle is simulated and compared to the measurement for PP SA HP 49. The coefficient of thermal expansion is temperature dependent and increases with an increase of temperature. As described in chapter 4.6, it is difficult to determine the coefficient of thermal expansion close to the melting temperature and in the melt because other effects like crystal melting and deconsolidation occur.

Therefore, the coefficient of thermal expansion is considered up to the on-set of melting. Because the thermal expansion is a reversible effect, the heating and cooling behavior is equal. A linear regression analysis gives a good agreement to the measurement. The interception with the y axis is at $4.27*10^{-5}$ 1/K and the slope is $0.0842*10^{-5}$ 1/K². Because of the low values of the thickness change per Kelvin, some scatter occurred during thickness measurements. But nevertheless, the values are in the same range of a similar glass fiber reinforced polypropylene grade investigated by Thomason and Groenewound [133].

A full deconsolidation cycle for PP SA HP 49 is shown in Figure 6.11. The demould temperature was 60 °C. The first part of the curve up to the plateau at 135°C is only affected by thermal expansion and has a good agreement to the measurement. When nearing the second heating part, the curve shows a deviation of less than 0.015 mm, which could be caused by the melting of very short polymer chains closely before the on-set of melting. The second segment is affected by thermal expansion and crystal melt and shows a good agreement with the measurement. Only the shape of the curve deviates from the real behavior because of the simplification of a linear melting behavior between the on-set and off-set of melting.

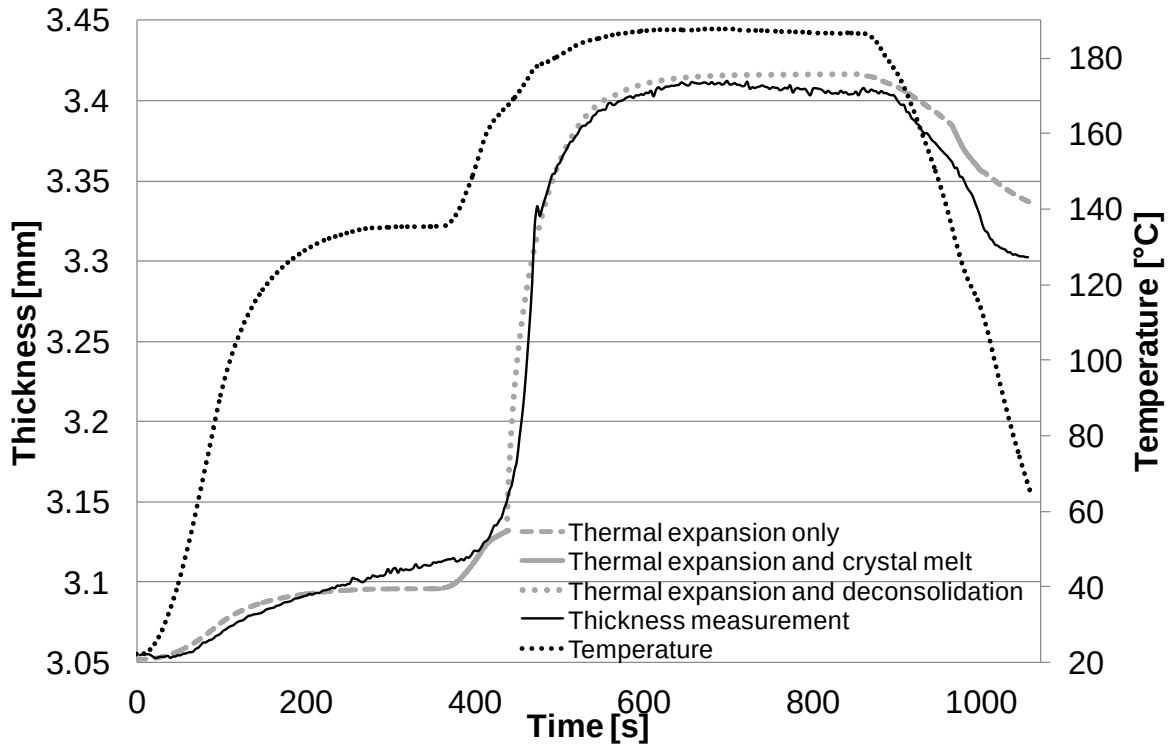

Figure 6.11: Thickness and temperature evolution of PP SA HP 49 for a full deconsolidation cycle

The real behavior has a complex time-temperature dependency. Thermal expansion and deconsolidation occur in the next segment and have a good agreement with the measurement. The cooling to demould temperature exhibits a higher deviation between the real and simulated behavior of 0.04 mm.

Table 6.9 lists the thickness change of each individual effect and their temperature range of act. It is obvious that deconsolidation is the dominant thickness change. In case of a constant crystallinity before and after the treatment, deconsolidation is the dominant irreversible effect. Nevertheless, the resultant force of the thermal expansion and crystal change is several magnitudes higher than the force of deconsolidation.

Table 6.9: Influence on thickness of thermal expansion, crystal change, deconsolidation, and thermal expansion in melt for PP SA HP 49

	Thermal expansion up to melt	**Crystal melt / build up**	**Deconsolidation**	**Thermal expansion in melt**
Thickness change [mm]	± 0.044	± 0.017	+ 0.27	± 0.013
Temperature range of act during heating [°C]	20 - 165	135 - 165	165 - 195	165 - 195
Temperature range of act during cooling [°C]	135 - 20	135 - 115	195 - 165	195 - 165

6.8 Modelling of the Reconsolidation Treatment

The model enable a calculation of reconsolidation, if no matrix squeeze out is considered. Therefore, the reconsolidation behavior of PP SA HP 49 for different reconsolidation pressures is calculated (Figure 6.12).

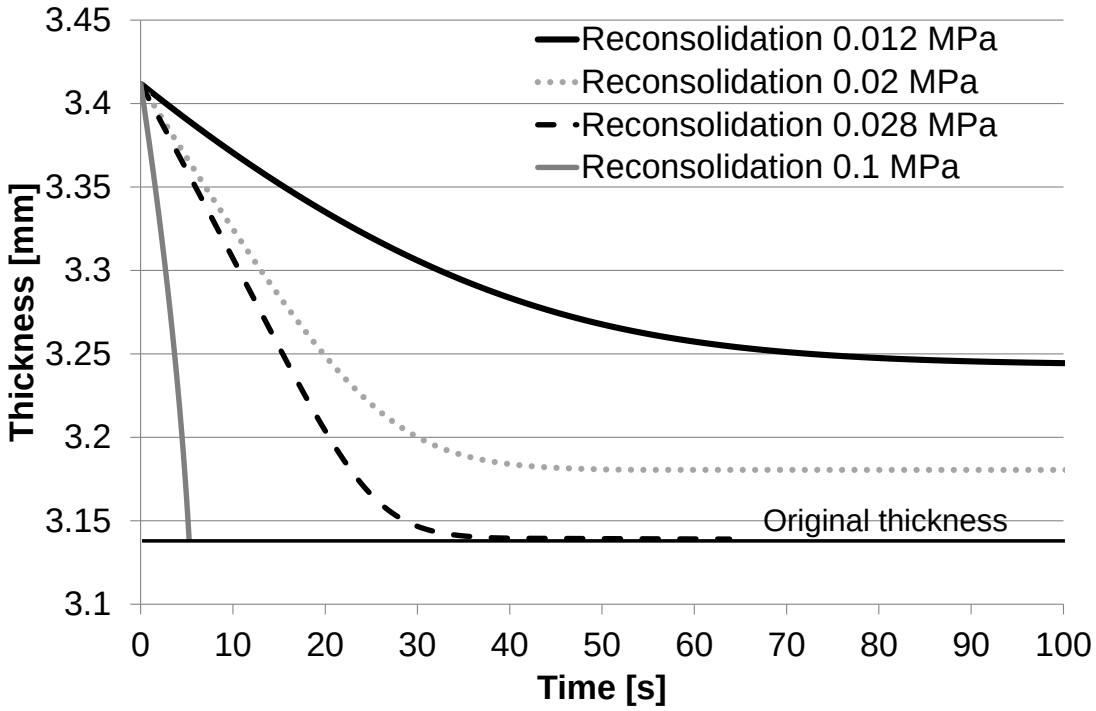

Figure 6.12: Calculated time dependent thickness evolution of different reconsolidation forces for PP SA HP 49

The specimens are theoretically subjected to different pressures at processing temperature. No heat up and cool down is considered. 0.012 MPa and 0.02 MPa can decrease the extent of deconsolidation. These pressures need a shorter time than the actual deconsolidation from a formerly well consolidated material. At pressures of 0.028 MPa the initial consolidation level is reachable. It is interesting to note that the reverse behavior is faster than the initial deconsolidation behavior as a result of the lower viscosity during processing. The reconsolidation takes up to 40 s, which would be too long for a usual thermoforming process. Therefore, the reconsolidation forces were increased until the specimen fully achieved the initial state within 5 s, which is the case at 0.1 MPa. Because the reconsolidation pressure of a thermoforming process is one magnitude higher, the specimens are well consolidated even if the deconsolidation pressures are much higher because of the limited effect of the mechanism (see Figure 6.4). It must be pointed out that matrix squeeze out can occur at pressures higher than 0.15 MPa.

6.9 Long Term Deconsolidation Behavior

Internal void pressure can be affected by thermal gas expansion and pressure history of the specimens. Internal void pressure can be increased by the manufacturing process (consolidation and impregnation) and by the cooling procedure of the specimen. During impregnation and consolidation, air can vent out of the specimen as long as a linked path is available. At some extend of impregnation, no paths are available and the air is locked inside the specimen. A further compaction leads to an increase of internal void pressure because of the decreased void volume. The internal void pressure is indirectly calculated for the deconsolidation treatment at different times after the manufacturing. During the storage of the specimen after manufacturing, the internal void pressure can balance to the atmospheric pressure. The model is solved for a completely balanced internal void pressure (1 bar) after 36 weeks (standard configuration) (Table 6.2). In order to investigate the effect of internal void pressure, the deconsolidation treatment is carried out at different times after manufacturing. The internal void content is recalculated by the model. Based on the measured thickness of the treated specimens at different times after manufacturing, the corresponding internal void pressure is calculated. Therefore, the measured thickness is set as target thickness including all other initial values except the internal void pressure. The results of the model are shown in Figure 6.13, where the hot pressed specimens have higher and the autoclaved specimen lower internal void pressures directly after the manufacturing. This effect is caused by the manufacturing pressure because of the high external pressure by the hot pressing and the depression inside the vacuum bag by the autoclaving. Hot pressed specimens have a logarithmical decrease of internal void pressure after manufacturing. 36 weeks (6,048 h) after the manufacturing, they have an internal void pressure of 1.14 bar. Because of the confidence interval of the thickness measurement, it could also be 1 bar. Nevertheless, the point lines up with the other calculated pressures. Therefore, it is relatively certain that there is still a higher pressure within the void than ambient pressure. The autoclaved specimens (PPS TW 52) have a depression in the void. This is 30 min after the manufacturing at 1 mbar, which is already 4 times higher than the underpressure within the vacuum bag. The underpressure within the void is completely released 6 h after the manufacturing.

Deviation of pressure release between satin and twill fabric is assumed to be affected by the weave structure.

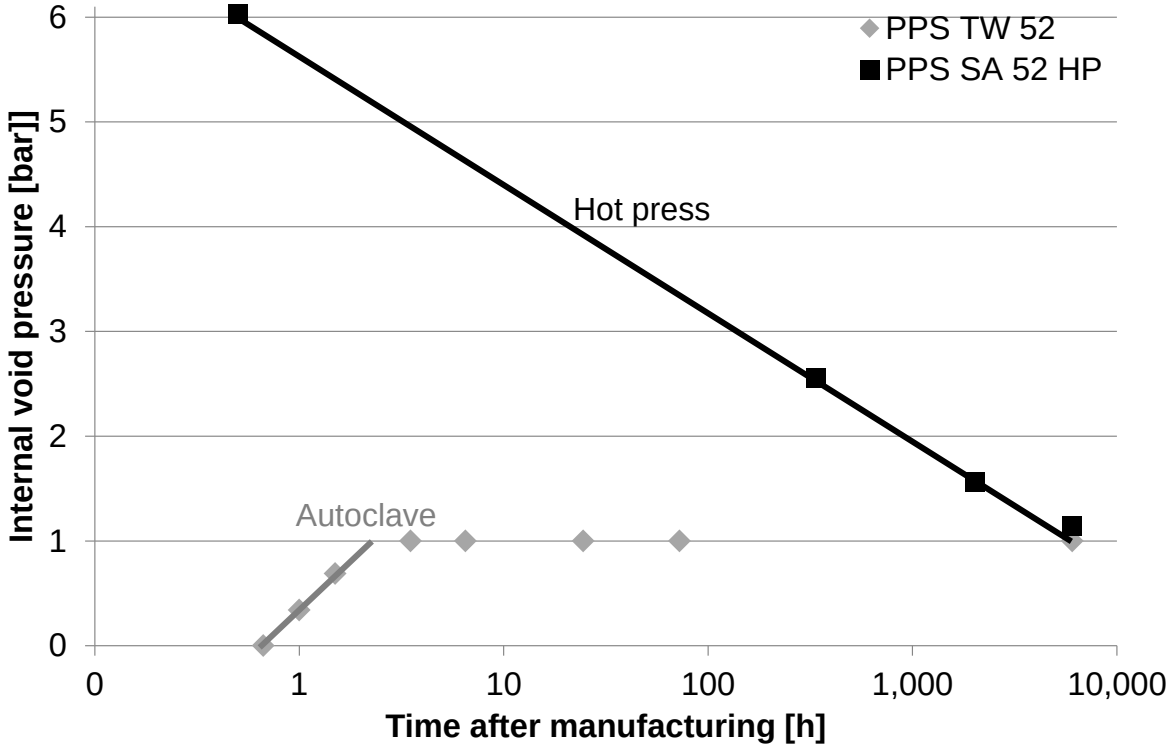

Figure 6.13: Internal void pressure dependency on time for PPS TW 52 and PPS SA 52 HP

The second investigation of internal void pressure is carried out at different times after the first deconsolidation treatment. After a deconsolidation treatment, the specimen cool to room temperature and the internal void pressure increases because of thermal gas expansion, thermal decompression of the composite, and crystallinity build-up. On the other hand the deconsolidation treatment and its resultant thickness increase leads to a forced void volume increase and therefore to an underpressure inside the void volume. In order to investigate the resultant internal void pressure, the specimens are tested 5 min and 2 weeks after the last deconsolidation treatment. Two cases are determined by the model: no internal void pressure release and a complete internal void pressure release (PP SA HP 49). If the internal void pressure is not released, there is no change of forces compared to the first deconsolidation treatment, which means no thickness and void content change takes place. If the internal void pressure is completely released before the next deconsolidation experiment, the PP SA HP 49 specimen increases from 3.30 mm to 3.53 mm, which corresponds to a void content increase from 10.8 % to 16.5 %. The

force evolution over thickness for the first and the second deconsolidation treatment is shown in Figure 6.14.

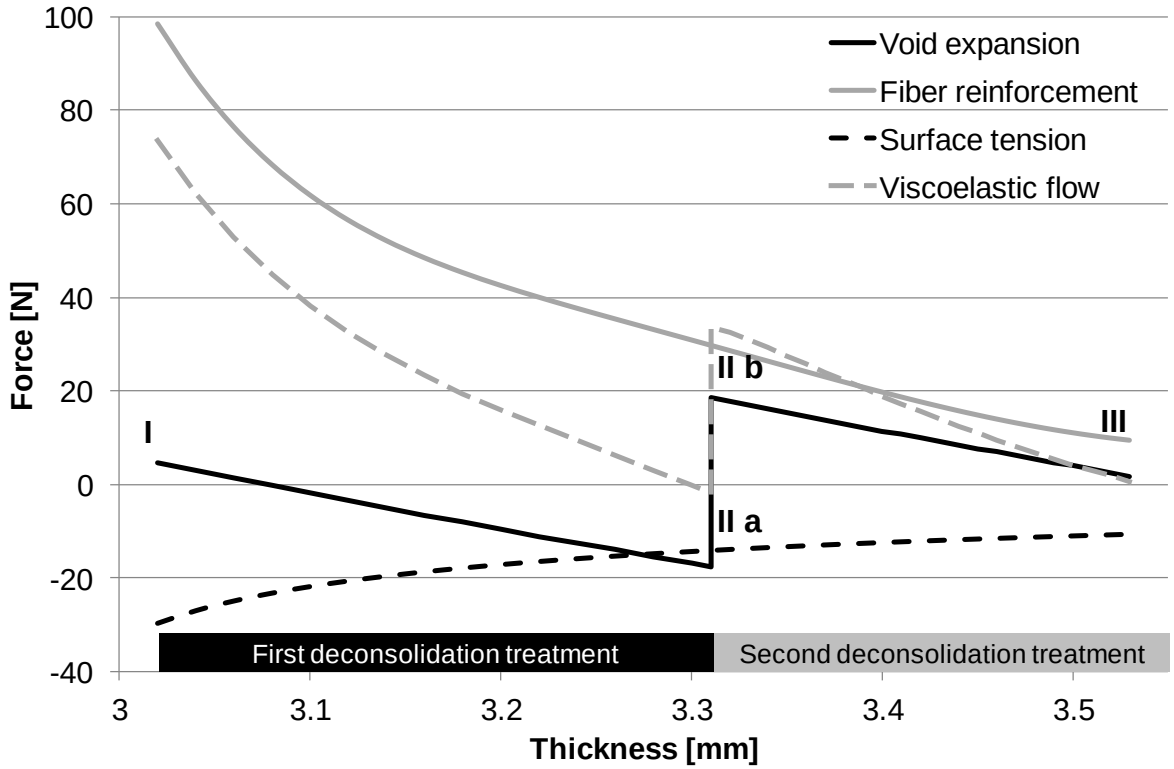

Figure 6.14: The calculated dependence of the thickness on the fiber network, the void expansion, and the surface tension of PP SA HP 49 for the first and the second deconsolidation treatment

Because of the internal void pressure release, the internal void pressure curve is positive before the second treatment and on a higher level than before the first treatment. The positive force leads to significant polymer flow and a drastic thickness increase during the second treatment.

The calculated internal void pressure for the three cases before, at the end, and after the deconsolidation treatments are listed in Table 6.10. It is obvious that the internal void pressure at the end of the first deconsolidation treatment on equilibrium is below atmospheric pressure (0.41 bar). The cool down to room temperature leads to an internal void pressure decrease of 63 % to 0.26 bar. In case of no pressure release, the pressure after the second treatment is equal to that after the first treatment. For a complete pressure release, the condition before the second treatment is equal to that before the first treatment. The results of the second deconsolidation treatment revealed that there are minor differences between the thickness of the specimens

5 min and 2 weeks after the first deconsolidation treatment. This result indicates that there is no significant internal void pressure release within 2 weeks for such a low pressure difference. The two types of internal void pressure determination show a similar trend and are strongly dependent of the textile and pressure difference.

Table 6.10: Internal void pressure for no and complete pressure release after the treatment at different steps

Treatment step	**Internal void pressure for no release [bar]**	**Internal void pressure for full release [bar]**
I After manufacturing	1	1
II a At the first deconsolidation treatment on equilibrium	0.41	0.41
III b After the first deconsolidation treatment and cooling to room temperature	0.26	0.26 →1
III At the second deconsolidation treatment on equilibrium	0.41	1.05
Directly after the second deconsolidation treatment and cooling to room temperature	0.26	0.66

Thermoplastic composites have a tendency to creep above their glass transition temperature because of the glassy nature of the matrix at elevated temperatures [134–137]. Creeping can be observed in the long-term behavior (several hours up to days) and above a threshold pressure of typically greater than 10 MPa. Voids can accelerate creep because they act as stress concentrators [137]. As described in chapter 4, there is no deconsolidation assumed from room temperature and glass transition to melting temperature. This simplification is correct for the short and long exposure above glass transition temperature and melting temperature because the low pressure caused by the deconsolidation mechanism of < 0.15 MPa.

7 Industrial Implementation of the Achievements

The successfully developed deconsolidation model offers a wide range of applications and has a high relevance to the industry because of the simple determination of the input parameters of the first order approximation. This chapter shows the application of the universal applicable input parameters used to predict thermoforming, induction welding, and tape placement. Also recommendations are given for the process development. The following checklist (Figure 7.1) gives advice ranked by the importance for process and material optimization in regards of deconsolidation and reconsolidation.

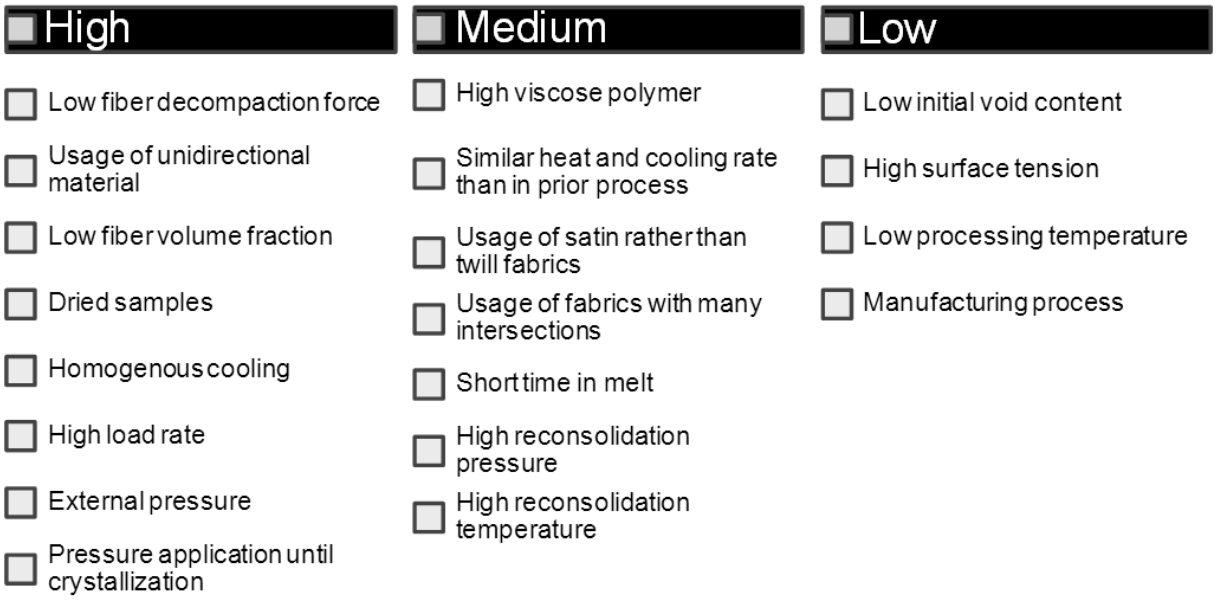

Figure 7.1: Checklist for process and material optimization in regards of deconsolidation and reconsolidation

7.1 Thermoforming

Thermoforming is a common manufacturing process of composite parts. The process takes use of the separation of the complex impregnation and forming. The impregnation is usually a time intensive process, though the forming is very fast. An exemplary temperature-pressure chart is given in Figure 7.2. The temperature was measured in the middle of the composite.

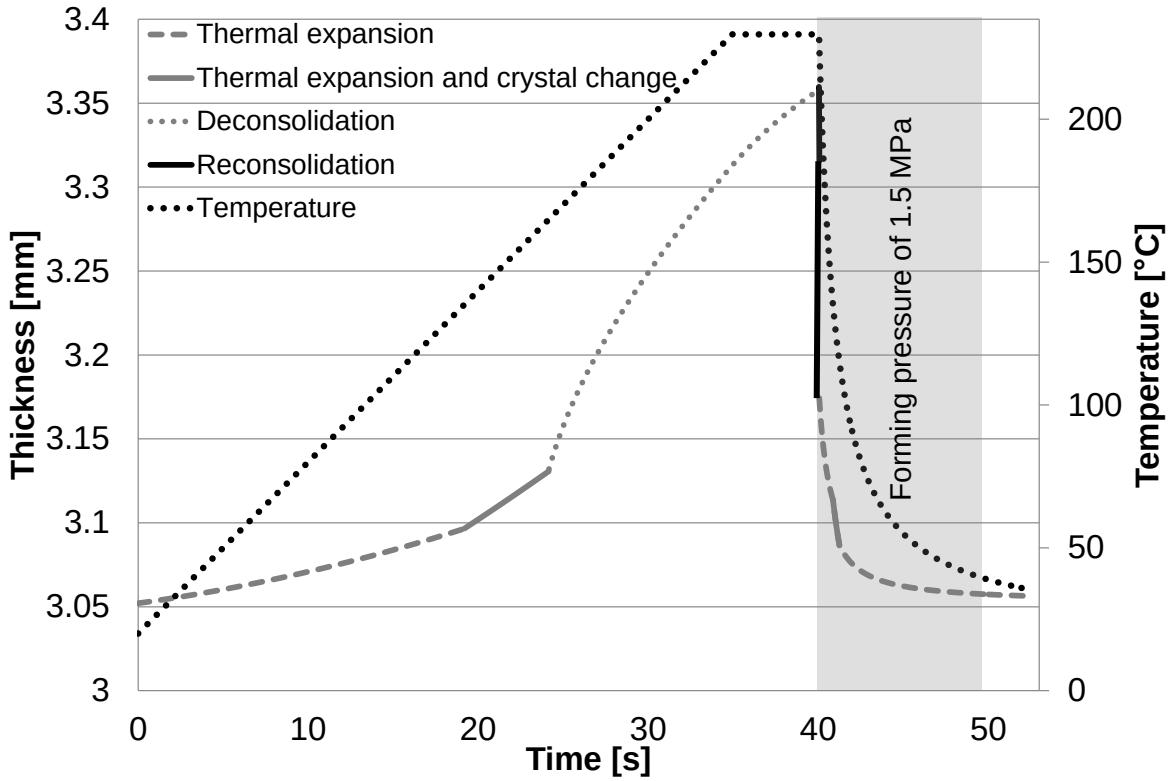

Figure 7.2: Thickness evolution of a typical thermoforming cycle for polypropylene (PP SA HP 49)

It is assumed that the pressure is directly available at the forming stage and no cooling occurs during transportation. Because of the complex time-dependent cooling rate, it is assumed that the specimen completely crystallizes. The overall time of 53 s is split in three separate steps (heating, transport, forming / consolidation). During heating and transport, the specimen can deconsolidate as the melting temperature is exceeded. Higher heating rates lead to a shorter time of the specimen in a molten state, which decrease the degree of deconsolidation. A higher target temperature and a longer transport time extend the time in a molten state resulting in a higher degree of deconsolidation. In the forming and consolidation step, the part has to be reconsolidated, formed, and cooled to demoulding temperature. Reconsolidation mainly occurs when the part is formed to shape and has contact to the upper and lower tool. Therefore, it is important how long the reconsolidation takes dependent on the cooling rate affected by the mold temperature and the load rate. As shown in Figure 7.2, the thickness of the specimen increases in the first section (heating) because of thermal expansion and crystal melt. If the melting temperature is exceeded, the specimen starts to deconsolidate, which continuous during holding and transport to the mold at target temperature. For an instantaneously available

pressure of 1.5 MPa, the specimen is reconsolidated in 0.083 s. In a real thermoforming process, the pressure is built up because of the limited velocity of the die. Therefore, the influence of load rate was simulated in a typical range of 0.5 s to 3.0 s for complete pressure build-up [83]. The load rate is dependent on the feed rate and the forming length. If the forming length increases by a constant feed rate, the load rate decreases and more time is needed for complete pressure build-up [138].

The results of different pressure build-ups are shown in Figure 7.3 with the corresponding temperature curve. In each case the reconsolidation is finished before the maximum pressure is reached. For a pressure build-up time of 0.5 s and 1 s, the final thickness is reached before the full pressure is applied. The time needed to achieve the initial state before deconsolidation at melting temperature is 0.38 s and 0.65 s at a corresponding pressure of 1.14 MPa and 0.97 MPa. For the 2 s, and 3 s curve, the material is already solid before the specimen is completely reconsolidated and the initial thickness is not achieved. It must be pointed out that some reconsolidation can be achieved between the crystallization temperature and the glass transition temperature, when the degree of crystallinity is low or zero. This effect is not part of the developed model and is neglected.

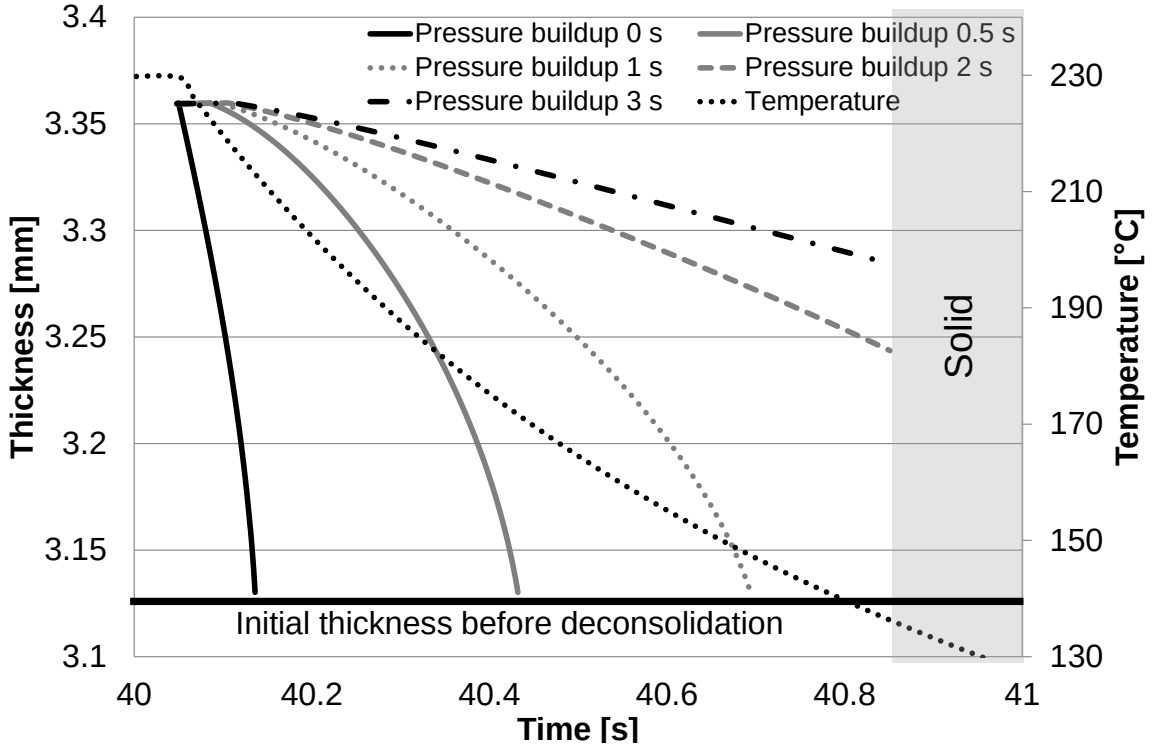

Figure 7.3: Laminate thickness evolution by different load rates and their corresponding time to achieve full pressure for PP SA HP 49

As shown, a pressure build-up of 2 s is too slow for complete reconsolidation. During forming, pressure can be applied as a result of the change of shape. The locally required pressure can lead to an inhomogeneous degree of reconsolidation or even an in-plane transport of voids. It can be concluded that the final pressure is less important than the load rate, if a certain pressure is exceeded. A too slow load rate leads to a solid material before the final pressure is reached. The cooling rate can also affect the final state of reconsolidation, which is set by the available time until the solidification of the specimen. A lower cooling rate results in a longer available time for reconsolidation. Also, the viscosity is influenced because of the dependency on temperature. The cooling rate is influenced by the material, the specimen's thickness, the tool material, and the tool temperature. A higher tool temperature causes a lower cooling rate and results in a longer cycle time. A compromise between cycle time and tool temperature must be found. A temperature gradient can also locally affect the reconsolidation. There is a temperature gradient from the outside to the inside of the specimen. Therefore, the inside of the specimen can be molten while the outside is already solid.

The effects of common parameters of thermoforming on deconsolidation and reconsolidation are listed in Table 7.1. As described, a lower heating rate, a higher processing temperature, and a longer transport time lead to a higher degree of deconsolidation.

Table 7.1: Influence of different parameters on deconsolidation and reconsolidation for thermoforming

Higher parameter	**Deconsolidation**	**Reconsolidation**
Heating rate	↘	↗
Processing temperature	↑	↗
Transport time	↑	↘
Forming pressure	→	↗
Load rate (pressure buildup)	→	↑
Cooling rate	→	↘
Part complexity	→	↓
Decompaction force of the textile	↑	↘

During reconsolidation the higher degree of deconsolidation has to be overcome, which requires a longer time to fully recover the deconsolidation. The decompaction force is the main driver of deconsolidation. During reconsolidation the influence is rather low because of the two or three magnitudes higher reconsolidation force. But nevertheless, the level of reached deconsolidation has to be overcome during reconsolidation, which indirectly makes it to an important factor of reconsolidation.

7.2 Induction Welding

Susceptor-less induction welding offers the possibility for intrinsic heating of the material without the requirement of any additional material. The newly developed susceptor-less continuous induction welding of carbon fiber reinforced thermoplastics uses an air jet to locally cool the top side of the specimen [5]. It is aimed to avoid deconsolidation of the part by a temperature gradient through the thickness of the part to the bond line. The set-up of the process is shown in Figure 7.4. The air jet applies the cooling stream in the middle of the coil just in front of the compaction roller.

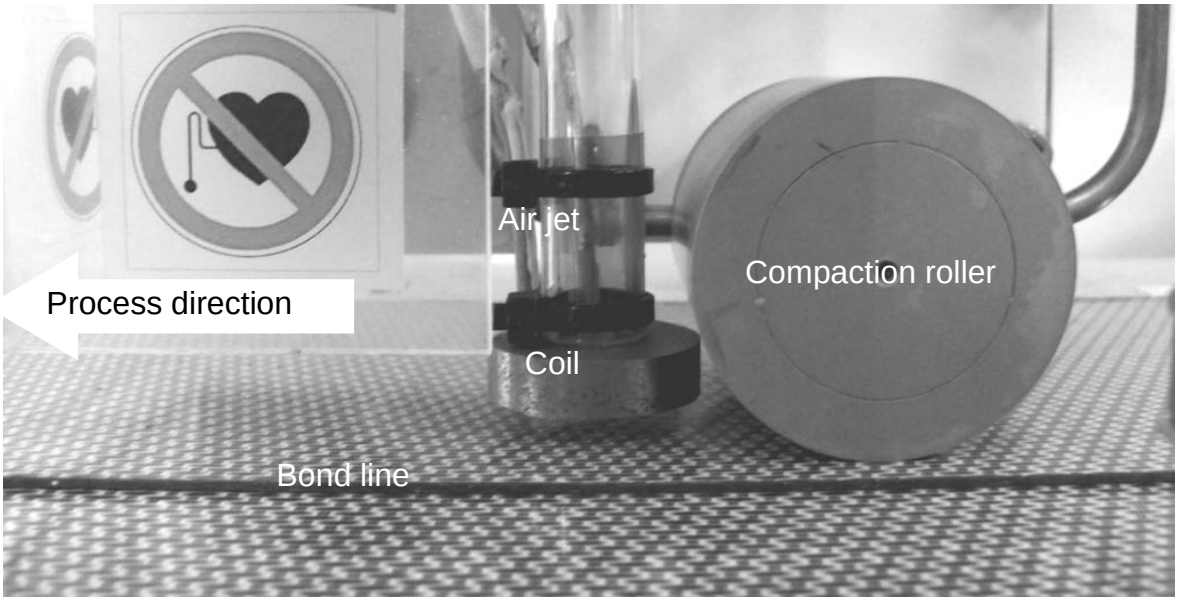

Figure 7.4: Picture of the induction welding set-up with surface cooling

In order to show the potential of the air jet cooling, the induction welding-time-temperature curve is measured at the top side and the bond line with and without air jet cooling. CF/PPS organo sheet was used supplied from TenCate nv with a laminate thickness of 2 mm. Mechanical and optical measurements for a similar

configuration are shown in [5] and [87]. A temperature in the bond line of 290 °C is set as target bonding temperature under the roller. The process parameters used are given in Table 7.2.

Table 7.2: Process parameters used for the induction welding process with and without air jet cooling

Roller diameter	50 mm	Coupling distance	5 mm
Roller temperature	20 °C	Air flow	167 nl/min
Consolidation force	100 N	Placement velocity	75 mm/min

The time-temperature curve with and without surface cooling is shown in Figure 7.5. There are different process steps: transport to coil (I), heating by induction (II), consolidation and cooling by roller (III), and cooling by atmosphere (IV).

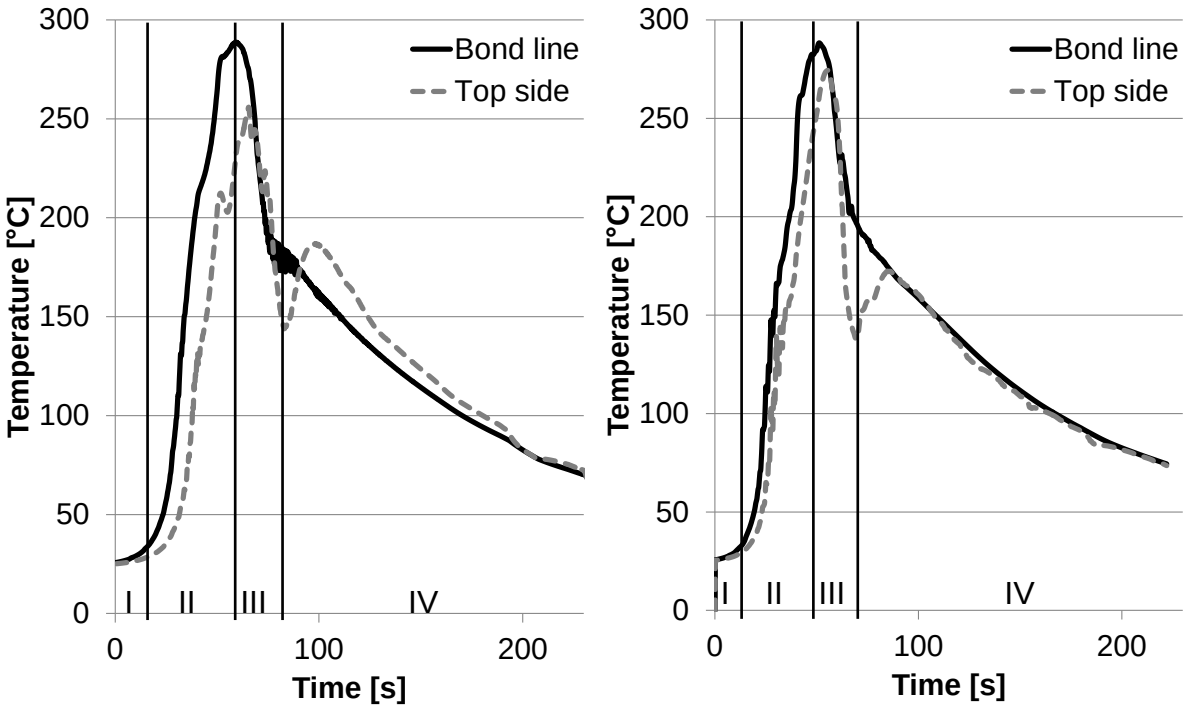

Figure 7.5: Time-temperature dependency of the induction welding process with surface cooling (left) and without surface cooling (right)

In both cases the target temperature in the bond line was achieved within 58 s (with cooling) and 51 s (without cooling). Because of the surface cooling, energy is drawn out of the specimen, which increases the time to achieve the target temperature. The temperature at the top side in case of cooling is below the melting temperature (282 °C) and in case of without cooling above the melting temperature. As soon as the part is in contact with the roller (III), the roller acts as a heat sink and decreases

the top temperature. In the last step (IV), the part cools to room temperature. It is interesting to note that in both cases the bond line behind the compaction roller is below the crystallization temperature of approximately 250 °C. The solid material leads to the assumption that no complete reconsolidation can be achieved by the compaction roller.

It is assumed, that no moisture can diffuse out of the specimen as a result of the rapid heating (~400 K/min). That means the moisture is vaporized at processing temperature resulting in an additional force enhancing deconsolidation. The restoring forces of crystallinity, thermal expansion, moisture, and the sum of all other deconsolidation forces are listed in Table 7.3. The calculated forces are independent from the air jet cooling due to minor differences in heating and cooling rate.

Table 7.3: Restoring forces during the heating by means of induction welding for PP SA 48, PC SA 50, and PPS TW 52

	PP SA 48	**PC SA 50**	**PPS TW 52**
Restoring force of crystallinity melt [N]	79,964	0	147,299
Restoring force of thermal expansion [N]	552,085	909,109	679,264
Restoring force of moisture [N]	81.8	356.8	335.9
Restoring force of all other deconsolidation mechanisms [N]	29.1	185.0	663.4

The restoring force of moisture is in the same range as the other deconsolidation forces. As investigated in chapter 5.8, moisture can significantly extend deconsolidation, which increases the thickness before consolidation of the roller. Therefore, it is recommended that the specimen is dried before welding to avoid an additional effort of reconsolidation. Because of the complex pressure and temperature distribution under the compaction roller, it is not possible to simulate the thickness evolution for induction welding. The reversible restoring forces of crystal melt and thermal expansion lead to a tremendous force of 79,964 N (32.0 MPa) to 147,299 N (58.9 MPa) for crystal melt and 552,085 N (220.8 MPa) to 909,109 N (363.6 MPa) for thermal expansion. These forces cannot be hindered by the

compaction roller. The corresponding transversal stresses were slightly higher than usual thermal shear stresses within the laminate of ~40 MPa [139; 140].

7.3 Tape Placement

Thermoplastic tape placement is a continuous process with a high temperature gradient through the thickness and a high local pressure. Deconsolidation and void formation were identified as the limiting factor of the process velocity. A possible matrix flow in fiber direction caused by a pressure gradient is neglected by many authors [9-10; 90–92]. The boundary conditions of the developed model are not fulfilled because of the temperature gradient through thickness, which suggest the occurrence of new effects. Nevertheless, the findings of the developed model are applied to the tape placement process. The resulting limits of the not fulfilled boundary conditions of the model are discussed, and possible new effects are proposed.

The material used was a UD carbon fiber reinforced polyetheretherketone from Suprem with a width of 12 mm, a height of 140 µm, and a fiber volume fraction of approximated 60 %. Material processing was carried out on a test rig developed at IVW GmbH with a diode laser system LDL40-500 manufactured by Laserline GmbH, Germany (Figure 7.6).

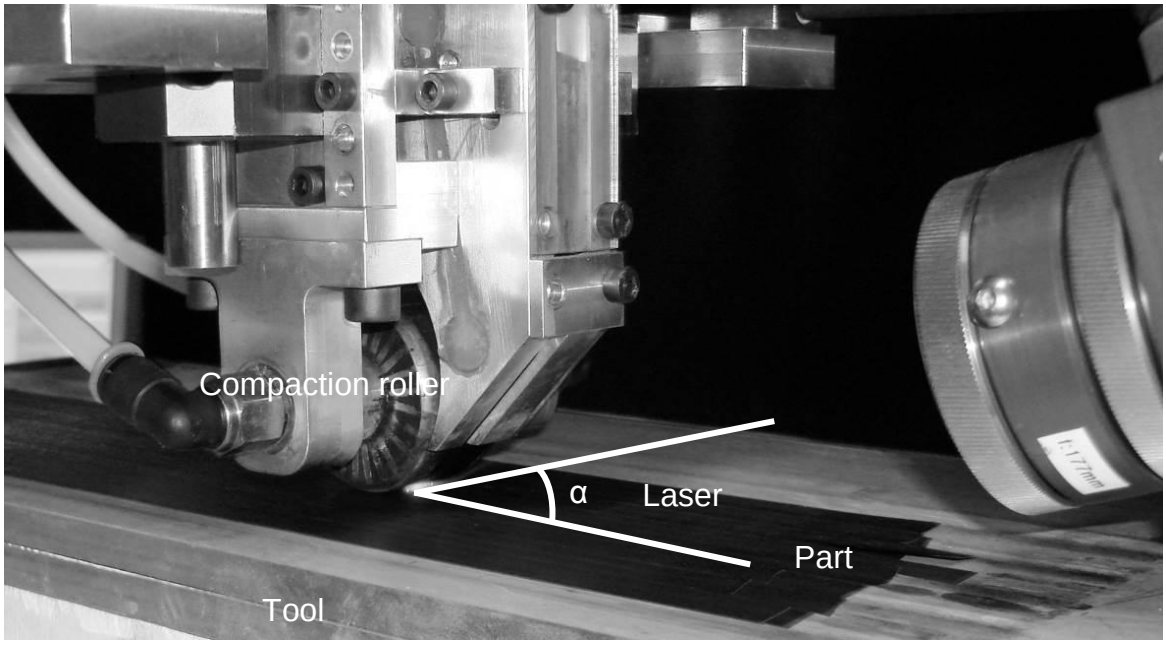

Figure 7.6: Picture of the laser assisted tape placement set-up

The laser had a maximum power of 600 W with a wavelength of 980 nm, and a rectangular spot of 12 mm by 2.08 mm at a working distance of 170 mm. Earlier studies showed that the parameters of Table 7.4 were optimal in terms of bonding strength and residual stresses [89; 93].

Table 7.4: Process parameters used for the tape placement process [93]

Roller diameter	50 mm	Tool temperature	240 °C
Roller temperature	90 °C	Laser power ratio	90/10
Consolidation force	220 N	Laser power	190 W
Angle of attack	14.5°	Placement velocity	6 m/min

For higher lay-up velocities, the laser power was changed, in order to achieve the same level of the degree of bonding by means of ProSimFRT [93]. The laser power was chosen for a velocity of 6 m/min to be 190 W, for 12 m/min to be 240 W, and for 18 m/min to be 300 W. 10 micrographs of each specimen were taken from embedded and polished samples. 3D computer tomography analyses were carried out for specimens with a geometry of 2.5x2.5x2 mm^3 by a nanotom manufactured by phoenix | x-ray. The x-ray photographs were taken from the specimens at different angles. From that data a 3D picture of the specimen was reconstructed with a resolution of 2.5 µm. Further analysis was conducted to show 3D void geometry and void content. Specimens were laid up according to a test plan and interlaminar shear strength was calculated from specimen size and fracture force.

The void content was similar for autoclave specimen (0.49 %) and the 6 m/min specimen (0.54 %), which was lower than in the tape as supplied (1.28 %). For higher placement velocities of 12 m/min and 18 m/min the void content increased to 3.49 % or 3.91 %. This was because the material was still in a molten state behind the roller and deconsolidated as it is shown in [93]. Further information can be conducted from the computer tomography pictures and the micrographs (Figure 7.8) to identify where the voids in the laminate occurred.

The autoclave specimens had a homogenous occurrence of small voids between the layers (interlaminar voids) and the plies were penetrated into each other. The 6 m/min placement velocity specimens showed small voids (Figure 7.7), which were located in groups inside the layers (intralaminar voids). Furthermore, the plies were

slightly penetrated into each other. The micrographs of the 18 m/min placement velocity specimens showed a high increase of void size and quantity. The plies are well visible as straight lines and there was a distinct occurrence of intralaminar voids. There were two reasons, where the significant increase of void content came from; either they were introduced by the process or by the supplied material.

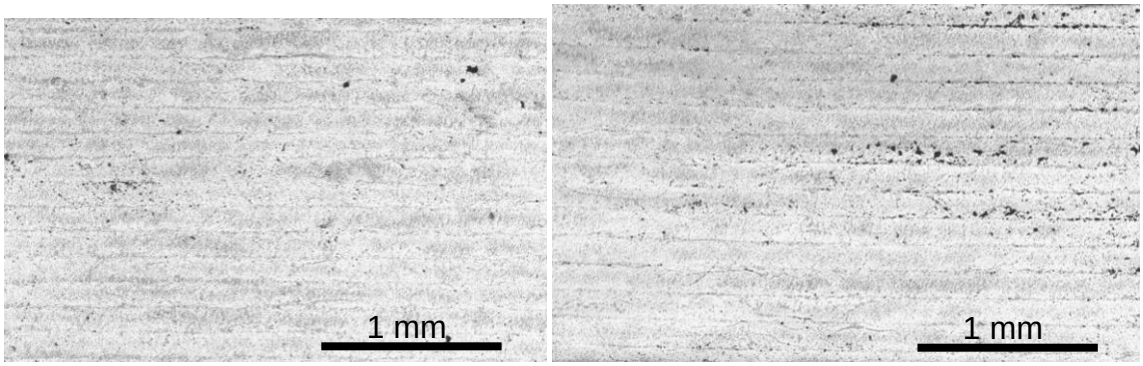

Figure 7.7: Micrographs of the tape placed laminate for a velocity of 6 m/min (left) and 18 m/min (right)

The total number of voids detected by computer tomography per 3 mm^3 increased from 1193 (tape as supplied) to 1339 (autoclaved). For the tape placed laminates, the void number further increased to 2014 (6 m/min), 3364 (12 m/min), and 3289 (18 m/min). It is assumed that the voids inside the tape did not relatively migrate to the resin because of the high viscosity of the resin and the fibers, which acted as barriers during placement. That means the intralaminar voids expanded or shrank during processing New voids came from the process and which must been interlaminar voids. There were areas, where no voids had been detected using computer tomography with a voxel size of 2.5 µm. Some of these areas were located between two plies, which can abated interlaminar fracture and decreased interlaminar shear strength. In Figure 7.8 images of the voids inside a slice of laminate (2.5x2.5x0.5 mm^3) are shown, where the matrix and the fibers were deleted by removal of the corresponding gray scale values.

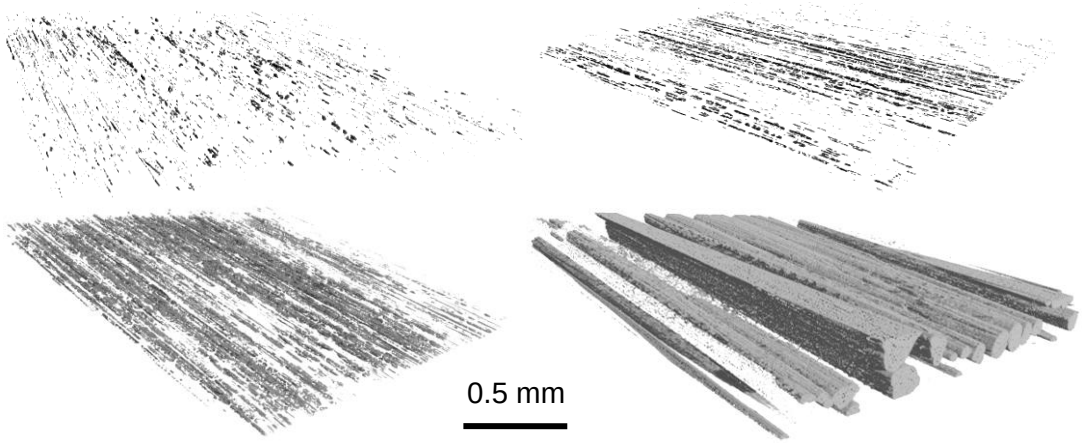

Figure 7.8: Computer tomography pictures of voids only of specimens with a placement velocity of 6 m/min (top left) 12 m/min (top right), 18 m/min (bottom left) and 6 m/min oven treated (bottom right)

After placement, specimens were deconsolidated in an oven at 380 °C for 30 min. These specimens showed a significant increase of void content. Figure 7.8 shows a void content increase from the 6 m/min placement velocity specimen to the oven deconsolidated specimen. The increase of void content corresponds to a tendency of the voids to accumulate to tubes with an increasing diameter. Several tubes are located close to each other. The results of the interlaminar shear strength analysis are shown in Figure 7.9.

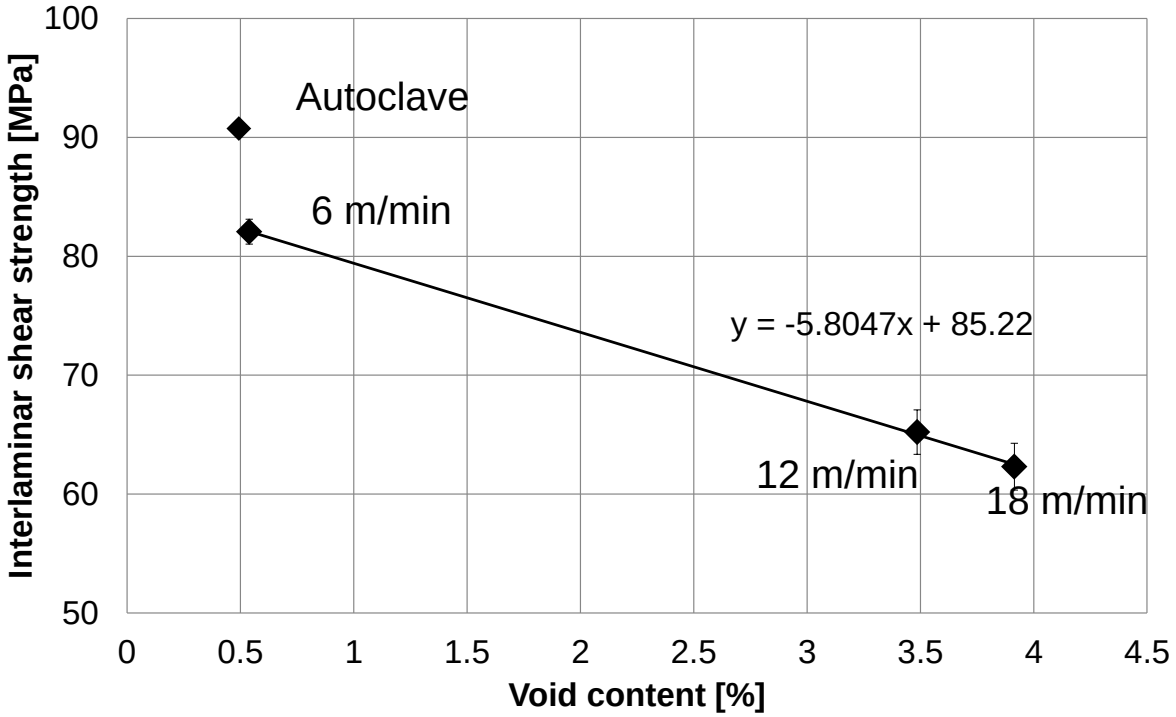

Figure 7.9: Interlaminar shear strength dependent on void content for specimen manufactured with an autoclave and with the tape placement process

It can be seen that the interlaminar shear strength of 6, 12, and 18 m/min placement velocity decrease from 82.06 MPa to 61.64 MPa, while the deviation of interlaminar shear strength between the placement velocity of 12 and 18 m/min is relatively small (3.58 MPa). According to the standard, the fracture type were analyzed, which revealed that the specimens with 12 m/min and 18 m/min showed interlaminar fracture. Only the autoclaved and 6 m/min specimens showed a mixed fracture type. It must be pointed out that the autoclaved specimens showed an increased fiber volume content. The interlaminar shear strength exhibited a decrease over the void content (factor: 5.8), which was higher than for the reinforced polypropylene, polycarbonate, and polyphenylensulfide (chapter 5.4). This result suggested that the voids of the tape placed specimen acted as a crack initiator and residual forces must occur. Therefore, it can be concluded that the consolidation of the tape placed specimens is lower than at the corresponding autoclave specimens.

It is interesting to note that the number of voids increased from the tape as supplied to the placement velocity of 6 m/min, but the void content decreased because of good compaction. The compaction of the bonding layers leads to an entrapment of air and therefore additional voids, which are locally compressed by the process pressure of 40 MPa to 60 MPa. Because of the lack of time, the pressure cannot be released. This leads to a tremendous pressure gradient between the void pressure and the atmosphere pressure after consolidation. Additional to the entrapped air, the fiber reinforcement network forces the specimen to deconsolidate. The corresponding temperature curves are published in [93] and showed an increase of the specimen after consolidation in a molten state of 2.1 s (6 m/min), 3.2 s (12 m/min), and 4.1 s (18 m/min). During this time some portion of the locked stresses can be released leading to a void content increase. The known effects would cause a circular void shape, which is in contrast to the computer tomography results.

In order to identify the cause of the tremendous interlaminar shear strength decrease, the temperature evolution of the specimen after compaction is qualitatively evaluated in Figure 7.10. The data are conducted from the temperature simulation of the ProSimFRT. Black is 450 °C and grey is 240 °C, which is the tool temperature.

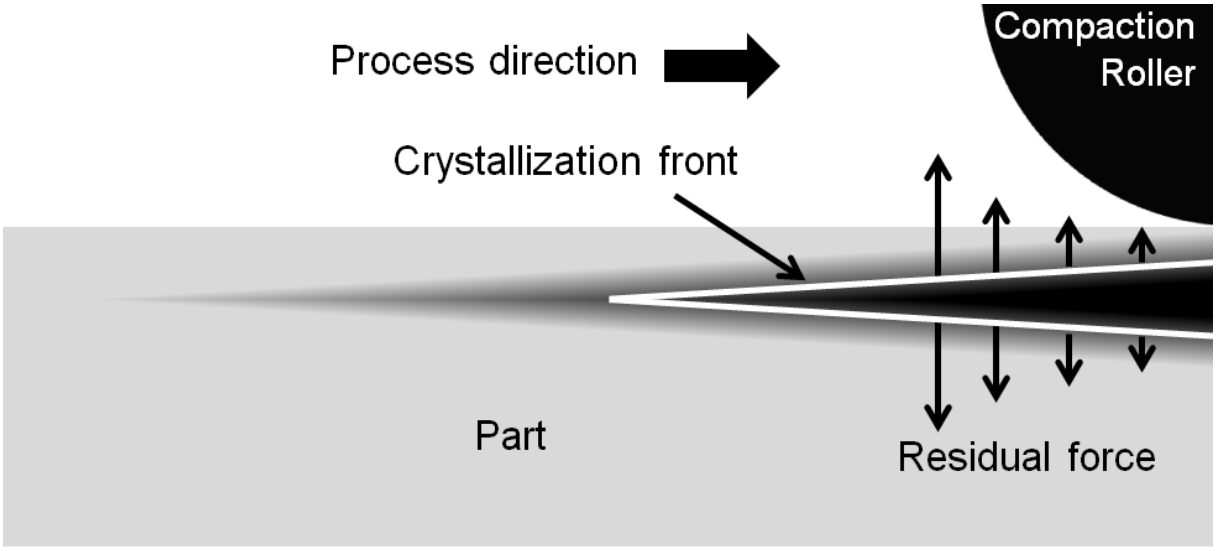

Figure 7.10: Qualitative temperature evolution after consolidation of the tape placement process for a semi-crystalline polymer

The white line indicates the crystallization front, which moves from the outside to the inside. As the temperature decreases below the crystallization temperature, crystals are build up and volume shrinkage occurs because of the higher density of the crystals compared with the amorphous phases. This leads to an increase of residual stresses in the remaining molten material, resulting in a pressure gradient in process direction. The pressure gradient could cause an elongation of the voids and is finished when the complete specimen is solid. As it was estimated in chapter 5.6 for different polymers, the crystallization pressure for polypropylene and polyphenylensulfide lays between 20 MPa and 70 MPa, which corresponds to the tape placement consolidation pressure determined by ProSimFRT. The high residual stress in the bond line decreases the interlaminar shear strength and explains the high decrease of interlaminar shear strength compared with the autoclaved specimen of 10 MPa.

Table 7.5 summarizes the influence of different parameters on deconsolidation and consolidation. The laser power can increase consolidation because of a higher temperature in the bond line, which enhances molecular diffusion and polymer flow. On the other hand, the laser power can increase the temperature after consolidation as well. If the temperature is above the crystallization temperature, deconsolidation occurs as stronger as higher the temperature is.

Table 7.5: Influence of different parameters on deconsolidation and consolidation for the thermoplastic tape placement process

Higher parameter	**Post deconsolidation**	**Consolidation**
Laser power	↗	↗ up to degradation
Roller temperature	↑	↗
Placement velocity	↑	↘
Consolidation pressure	↓	↗
Tool temperature	↗	→
Tape thickness	↗	→

More important for deconsolidation is the roller temperature because it acts as a heat sink by means of conduction. The influence on consolidation is negative for a lower temperature. In order to adjust the resultant crystallinity, the tool temperature determines whether the material is fully crystalline (high tool temperature) or partially crystalline or amorphous (low tool temperature). It also determines the cooling behavior caused by the heat sink of the tool. Therefore, a low tool temperature decreases deconsolidation, but the influence on the consolidation is rather low if the laser radiation is adjusted. Another effect is given by the tape and part thickness. The material thickness determines the heat flow length to the heat sink, which isolates the bond line and results in a lower cooling rate.

8 Conclusion

This study covers three polymers (polypropylene, polycarbonate, and polyphenylensulfide), three fabrics (twill, satin, and unidirectional), two processes (autoclave and hot press) and different fiber volume fractions.

The following mechanisms are identified to affect deconsolidation: void expansion, surface tension, fiber reinforcement network, polymer flow, crystallinity, thermal expansion of the composite, moisture, and external forces. Usually deconsolidation correlates to a void expansion. Voids expand because of thermal gas expansion and a forced thickness increase. Therefore, an underpressure is caused within the void, which hinders a further expansion. Surface tension hinders the void expansion, because new surface area must be created, which needs additional energy. The surface energy also causes a reduction of void number because of coalescence of neighboring voids resulting in a better volume to surface ratio. The fiber reinforcement network is the main driver of deconsolidation. The locked energy, built up during compaction, is released during deconsolidation. Decompaction pressures range from 0.02 MPa to 0.12 MPa for the investigated fabrics and fiber volume fractions. Another factor is the polymer flow, which decelerates the evolution of thickness increase because of the required energy of the viscous flow. No influence on the final deconsolidation level has the crystallinity and thermal expansion of the composite. Nevertheless, there is a reversible influence during the temperature cycle. Another factor is moisture. Moisture can have a tremendous influence on deconsolidation, if moisture is vaporized above melting temperature to steam. In this case the thickness of the composite expands several times until venting paths through the surface of the specimen are formed. It can be concluded that the developed model is capable to predict the thickness on equilibrium and the thickness evolution during deconsolidation.

In addition to this, the model can be used to predict reconsolidation under the defined boundary condition of pressure and specimen size. For high pressure matrix squeeze out occur, which falsifies the accuracy. Nevertheless, the model can be extended by the squeeze flow model of Rogers et al. [59].

In order to simplify the determination of the input parameters, universal applicable input parameters are presented with reasonable agreement to the measurement. This simplification reduces the effort to a minimum and enhances the usage in industry for a process optimization or a study with many different materials.

The effect of deconsolidation on the interlaminar shear strength was investigated. The slope for thermoplastic matrices was smaller than for thermoset matrices and laid in the range of 0.5 to 1.5 % per percentage of void content depending on the matrix polymer only. The interlaminar shear strength of the void free configuration is determined by the matrix polymer, the fiber volume fraction, the lay-up, and the reinforcement type.

In order to prove these statements and to show the industrial relevance, the model is applied to three processes, thermoforming, induction welding, and thermoplastic tape placement. For each process, a table with the effects of parameters on consolidation, reconsolidation, and deconsolidation is given, which helps to optimize the process. It is demonstrated that the load rate during thermoforming is a key factor of achieving a full reconsolidation. If the load rate is too slow, the specimen is already solid before a full reconsolidation is achieved even if the final pressure is high enough. Induction welding can be affected by deconsolidation, too. If the moisture inside the specimen is not released before exceeding the melting temperature, this leads to a tremendous thickness increase by a formation of steam. During tape placement deconsolidation is the key factor of limiting a further velocity increase. A full consolidation under the roller is could be achieved. Nevertheless the specimen can deconsolidate after the compaction, if the polymer is locally molten. This results in an increased void content and residual stresses by means of crystallization. Thermal stresses are introduced in the bond line over the same magnitude as the actual shear strength.

9 References

[1] Dr. Lässig, R.; Dr Eisenhut, M.; Mathias, A.; Dr. Schulte, R. T.; Peters, F.; Kühmann, T.; Waldmann, T.; Dr. Begeman, W.: Serienproduktion von hochfesten Faserverbundbauteilen. VDMA. 2012.

[2] Horejsi, K.; Schledjewski, R.; Noisternig, J.; Koch, O.: Cost-saving potentials for cfrp parts in early design stages. The 19th international conference on composite materials (ICCM). 28.07.2013 - 02.08.2014.Montreal.

[3] Hildebrandt, K.; Mack, J.; Becker, D.; Prof. Dr.-Ing. Mitschang, P.; Dr.-Ing. Medina, L.: Potenziale neuer Matrixpolymere für die FKV-Bauteilfertigung. Lightweight Design, Vol. 2 (2014).

[4] Grouve, W. J. B.; Warnet, L. L.; Rietman, B.; Visser, H. A.; Akkerman, R.: Optimization of the tape placement process parameters for carbon–PPS composites. Composites Part A: Applied Science and Manufacturing, Vol. 50. (2013), 44–53.

[5] Moser, L.: Experimental analysis and modeling of susceptorless induction welding of high performance thermoplastic polymer composites. IVW, Kaiserslautern. Diss. 2012.

[6] Bayerl, T.; Brzeski, M.; Martínez-Tafalla, M.; Schledjewski, R.; Mitschang, P.: Thermal degradation analysis of short-time heated polymers. Journal of Thermoplastic Composite Materials, Vol. 5 (2013), 1–25.

[7] Brzeski, M.: Comparison of methods to detect thermal degradation of short-time heated carbon reinforced thermo- plastic composites. Asia-Europe Symposium on Processing and Properties of Reinforced Polymers, 29.05.2011 - 01.06.2011. Dresden.

[8] Henniger, F.; Ye, L.; Friedrich, K.: Deconsolidation behaviour of glass fibre-polyamide 12 composite sheet material during post-processing. Plastics rubber and composites processing and applications, Vol. 27 (1998), 287–292.

[9] Maffezzoli, A.; Mascia, L.; Khan, M. A.; Mitschang, P.; Schledjewski, R.: Identification of some optimal parameters to achieve higher laminate quality through tape placement process. Advances in Polymer Technology, Vol. 29. 2 (2010), 98–111.

[10] Tierney, J. J.; Gillespie, J. W.: Crystallization kinetics behavior of PEEK based composites exposed to high heating and cooling rates. Composites: Part A, Vol. 35. (2004), 574-558.

[11] Ranganathan, S.; Advani, S. G.; Lamontia, M. A.: A Non-Isothermal Process Model for Consolidation and Void Reduction during In-Situ Tow Placement of Thermoplastic Composites. Journal of Composite Materials, Vol. 29. 8 (1995), 1040–1062.

[12] Pitchumani, R.; Ranganathan, S.; Don, R.; Gillespie, J.; Lamontia, M.: Analysis of transport phenomena governing interfacial bonding and void dynamics during thermoplastic tow-placement. International Journal of Heat and Mass Transfer, Vol. 39. 9 (1996), 1883–1897.

[13] Khan M A; Mitschang P; Schledjewski R: Tracing the void content development and identification of its effecting parameters during in situ consolidation of thermoplastic tape material. Polymers and Polymer Composites, Vol. 18. 1 (2010), 1–15.

[14] Ye, L.; Chen, Z.-R.; Lu, M.; Hou, M.: De-consolidation and re-consolidation in CF/PPS thermoplastic matrix composites. Composites: Part A, Vol. 36 (2005), 915–922.

[15] Wolfrath, J.; Michaud, V.; Månson, J.-A.: Deconsolidation in glass mat thermoplastic composites: Analysis of the mechanisms. Composites Part A: Applied Science and Manufacturing, Vol. 36. 12 (2005), 1608–1616.

[16] Baehr, H. D.; Kabelac, S.: Thermodynamik. Dreizehnte, neu bearbeitete und erweiterte Auflage, Berlin Heidelberg, Springer-Verlag 2006.

[17] Ye, L.; Lu, M.; Mai, Y.-W.: Thermal de-consolidation of thermoplastic matrix composites. Composites Science and Technology, Vol. 62. (2002), 2121–2130.

[18] Lu, M.; Ye, L.; Mai, Y.-W.: Thermal de-consolidation of thermoplastic matrix composites—II. “Migration” of voids and “re-consolidation”. Composites Science and Technology, Vol. 64. 2 (2004), 191–202.

[19] Cifra, P.; Nies, E.; Karasz, F. E.: Free Surface Profile and Surface Tension in a Polymer Melt: A Monte Carlo Study. Macromolecules, Vol. 27. 5 (1994), 1166–1171.

[20] Wei, H.; Thompson, R.; Park, C.; Chen, P.: Surface tension of high density polyethylene (HDPE) in supercritical nitrogen: Effect of polymer crystallization. Colloids and Surfaces A: Physicochemical and Engineering Aspects, Vol. 354. 1-3 (2010), 347–352.

[21] Menke, T. J.: Maßschneidern der Eigenschaften von Polypropen Mischungen und Olefincopolymeren. Halle (Saale). Diss. 2001.

[22] van Krevelen, D. W.; Nijenhuis, K. t.: Properties of polymers. 4th edition, Amsterdam, Boston. Elsevier. 2009.

[23] Brandrup, J.; Immergut, E. H.; Grulke, E. A.: Polymer handbook, 4th edition, New York, Chichester. Wiley. 2004.

[24]. Mittal, K. L.: Adhesion Aspects of Polymeric Coatings. BRILL; Brill USA, Inc., Leiden, Boston.

[25] Cai, Z.; Gutowski, T.: The 3-D Deformation Behavior of a Lubricated Fiber Bundle. Journal of Composite Materials, Vol. 26. 8 (1992), 1207–1237.

[26] Chen, Z.-R.; Ye, L.; Kruckenberg, T.: A micromechanical compaction model for woven fabric preforms. Part I: Single layer. Composites Science and Technology, Vol. 66. 16 (2006), 3254–3262.

[27] Chen, Z.-R.; Ye, L.: A micromechanical compaction model for woven fabric preforms. Part II: Multilayer. Composites Science and Technology, Vol. 66. 16 (2006), 3263–3272.

[28] Potluri, P.; Sagar, T.: Compaction modelling of textile preforms for composite structures. Composite Structures, Vol. 86. 1-3 (2008), 177–185.

[29] Chen, B.; Lang, E. J.; Chou, T.-W.: Experimental and theoretical studies of fabric compaction behavior in resin transfer molding. Materials Science and Engineering: A, Vol. 317. 1–2 (2001), 188–196.

[30] Somashekar, A.; Bickerton, S.; Bhattacharyya, D.: Modelling the viscoelastic stress relaxation of glass fibre reinforcements under constant compaction strain during composites manufacturing. Composites Part A: Applied Science and Manufacturing, Vol. 43. 7 (2012), 1044–1052.

[31] Kelly, P.; Umer, R.; Bickerton, S.: Viscoelastic response of dry and wet fibrous materials during infusion processes. Composites Part A: Applied Science and Manufacturing, Vol. 37. 6 (2006), 868–873.

[32] Kim, Y. R.; McCarthy, S. P.; Fanucci, J. P.: Compressibility and relaxation of fiber reinforcements during composite processing. Polymer Composites, Vol. 12. 1 (1991), 13–19.

[33] Govignon, Q.; Bickerton, S.; Kelly, P.: Simulation of the reinforcement compaction and resin flow during the complete resin infusion process. Composites Part A: Applied Science and Manufacturing, Vol. 41. 1 (2010), 45–57.

[34] Yenilmez, B.; Sozer, E. M.: Compaction of e-glass fabric preforms in the Vacuum Infusion Process, A: Characterization experiments. Composites Part A: Applied Science and Manufacturing, Vol. 40. 4 (2009), 499–510.

[35] Yenilmez, B.; Senan, M.; Murat Sozer, E.: Variation of part thickness and compaction pressure in vacuum infusion process. Composites Science and Technology, Vol. 69. 11-12 (2009), 1710–1719.

[36] Kruckenberg, T.; Ye, L.; Paton, R.: Static and vibration compaction and microstructure analysis on plain-woven textile fabrics. Composites Part A: Applied Science and Manufacturing, Vol. 39. 3 (2008), 488–502.

[37] Kelly, P. A.; Bickerton, S.: A comprehensive filling and tooling force analysis for rigid mould LCM processes. Composites Part A: Applied Science and Manufacturing, Vol. 40. 11 (2009), 1685–1697.

[38] Walbran, W. A.; Verleye, B.; Bickerton, S.; Kelly, P. A.: Prediction and experimental verification of normal stress distributions on mould tools during Liquid Composite Moulding. Composites Part A: Applied Science and Manufacturing, Vol. 43. 1 (2012), 138–149.

[39] Sonmez, F. O.; Hahn, H. T.; Akbulut, M.: Analysis of Process-Induced Residual Stresses in Tape Placement. Journal of Thermoplastic Composite Materials, Vol. 15. 6 (2002), 525–544.

[40] Barnes, J. A.; Simms, I. J.; Farrow, G. J.; Jackson, D.; Wostenholm, G.; Yates, B.: Thermal expansion characteristics of PEEK composites. Journal of Materials Science, Vol. 26. 8 (1991), 2259–2271.

[41] Barnes, J. A.: Thermal expansion behaviour of thermoplastic composites. Journal of Materials Science, Vol. 28. 18 (1993), 4974–4982.

[42] Wisnom, M. R.; Gigliotti, M.; Ersoy, N.; Campbell, M.; Potter, K. D.: Mechanisms generating residual stresses and distortion during manufacture of polymer–matrix composite structures. Internal Stresses in Polymer Composites, Vol. 37. 4 (2006), 522–529.

[43] Parlevliet, P. P.; Bersee, H. E. N.; Beukers, A.: Residual stresses in thermoplastic composites—A study of the literature—Part I: Formation of residual stresses. Composites Part A: Applied Science and Manufacturing, Vol. 37. 11 (2006), 1847–1857.

[44] Huo, P.; Cebe, P.: Effects of thermal history on the rigid amorphous phase in poly(phenylene sulfide). Colloid & Polymer Science, Vol. 270. 9 (1992), 840–852.

[45] Sorensen, L.; Gmür, T.; Botsis, J.: Residual strain development in an AS4/PPS thermoplastic composite measured using fibre Bragg grating sensors. CompTest 2004, Vol. 37. 2 (2006), 270–281.

[46] Parlevliet, P. P.; Bersee, H. E. N.; Beukers, A.: Residual stresses in thermoplastic composites – a study of the literature. Part III: Effects of thermal residual stresses. Composites Part A: Applied Science and Manufacturing, Vol. 38. 6 (2007), 1581–1596.

[47] Karami, G.; Garnich, M.: Micromechanical study of thermoelastic behavior of composites with periodic fiber waviness. Composites Part B: Engineering, Vol. 36. 3 (2005), 241–248.

[48] Lawrence, W. E.; Månson, J.-A. E.; Seferis, J. C.; J.W. Gillespie Jr.; Pipes, R. B.: Prediction of residual stress in continuous fiber semicrystalline thermoplastic composites: a kinetic-viscoelastic approach. ASC Annual Technical Conference, 1991, 401.

[49] Rayleigh, L.: VIII. On the pressure developed in a liquid during the collapse of a spherical cavity. Philosophical Magazine Series 6, Vol. 34. 200 (1917), 94–98.

[50] Joseph, D. D.; Funada, T.; Wang, J.: Potential flows of viscous and viscoelastic fluids. Cambridge University Press, Cambridge.2008.

[51] LIN, H. A.; STOREY, B. D.; SZERI, A. J.: Inertially driven inhomogeneities in violently collapsing bubbles: the validity of the Rayleigh–Plesset equation. Journal of Fluid Mechanics, Vol. 452 (2002).

[52] Brennen, C. E.: Fundamentals of multiphase flow. Cambridge University Press, Cambridge, New York. 2005.

[53] Plesset, M. S.; Prosperetti, A.: Bubble Dynamics and Cavitation. Annual Review of Fluid Mechanics, Vol. 9. 1 (1977), 145–185.

[54] Street, J. R.; Fricke, A. L.; Reiss, L. P.: Dynamics of Phase Growth in Viscous, Non-Newtonian Liquids. Initial Stages of Growth. Industrial & Engineering Chemistry Fundamentals, Vol. 10. 1 (1971), 54–64.

[55] Amon, M.; Denson, C. D.: A study of the dynamics of foam growth: Analysis of the growth of closely spaced spherical bubbles. Polymer Engineering and Science, Vol. 24. 13 (1984), 1026–1034.

[56] Wolfrath, J.; Michaud, V.; Månson, J.-A.: Deconsolidation in glass mat thermoplastics: Influence of the initial fibre/matrix configuration. Composites Science and Technology, Vol. 65. 10 (2005), 1601–1608.

[57] Gebart, B.R.: Permeability of unidirectional reinforcements for RTM. Journal of Composite Materials, Vol. 26. 8 (1992), 1100-1133 .

[58] Adams, K.L.; Rebenfeld, L.: In-plane flow of fluids in fabrics – structure/flow characterization. Textile Research Journal, Vol. 57. 11 (1987), 647-654.

[59] Rogers, T. G.: Squeezing flow of fibre-reinforced viscous fluids. Journal of Engineering Mathematics, Vol. 23. 1 (1989), 81–89.

[60] Lawal, A.; Kalyon, D. M.: Squeezing flow of viscoplastic fluids subject to wall slip. Polymer Engineering & Science, Vol. 38. 11 (1998), 1793–1804.

[61] Shuler, S. F.; Advani, S. G.: Transverse squeeze flow of concentrated aligned fibers in viscous fluids. Journal of Non-Newtonian Fluid Mechanics, Vol. 65. 1 (1996), 47–74.

[62] Saechtling, H.; Oberbach, K.: Kunststoff-Taschenbuch. 28, München Hanser, 2001.

[63] Domininghaus, H.: Die Kunststoffe und ihre eigenschaften. 6, Berlin, Heidelberg, Springer, 2005.

[64] Mantell, S. C.; Springer, G. S.: Manufacturing Process Models for Thermoplastic Composites. Journal of Composite Materials, Vol. 26. 16 (1992), 2348–2377.

[65] Schütz, A.; Schultz, W.: Feuchtigkeitsaufnahme und Einfluß der Feuchtigkeit auf die dielektrischen Eigenschaften glasfaserverstärkter Kunststoffe. Archiv für Elektrotechnik, Vol. 77. 6 (1994), 433–440.

[66] Deng, H.; Reynolds, C.; Cabrera, N.; Barkoula, N.-M.; Alcock, B.; Peijs, T.: The water absorption behaviour of all-polypropylene composites and its effect on mechanical properties. Composites Part B: Engineering, Vol. 41. 4 (2010), 268–275.

[67] Chevron Phillips LLC: Datasheet Ryton. 2013.

[68] Deng, S.; Ye, L.: Influence of Fiber-Matrix Adhesion on Mechanical Properties of Graphite/Epoxy Composites: II. Interlaminar Fracture and Inplane Shear Behavior. Journal of Reinforced Plastics and Composites, Vol. 18. (1999), 1041–1057.

[69] St John, N. A.; Brown, J. R.: Flexural and interlaminar shear properties of glass-reinforced phenolic composites. Composites Part A: Applied Science and Manufacturing, Vol. 29. 8 (1998), 939–946.

[70] Deng, S.; Ye, L.: Influence of Fiber-Matrix Adhesion on Mechanical Properties of Graphite/Epoxy Composites: I. Tensile, Flexure, and Fatigue Properties. Journal of Reinforced Plastics and Composites, Vol. 18. (1999), 1021–1040.

[71] Wisnom, M. R.; Reynolds, T.; Gwilliam, N.: Reduction in interlaminar shear strength by discrete and distributed voids. Composites Science and Technology, Vol. 56. 1 (1996), 93–101.

[72] Wisnom, M. R.: Modelling the effect of cracks on interlaminar shear strength. Composites Part A: Applied Science and Manufacturing, Vol. 27. 1 (1996), 17–24.

[73] Beehag, A.; Ye, L.: Role of cooling pressure on interlaminar fracture properties of commingled CF/PEEK composites. Composites Part A: Applied Science and Manufacturing, Vol. 27. 3 (1996), 175–182.

[74] Henninger, F. H.: Beitrag zur Entwicklung neuartiger Fertigungsverfahren zur Herstellung von Bauteilen aus kontinuierlich faserverstärkten Thermoplasten. Kaiserslautern. Diss. 2005.

[75] Hagstrand, P.-O.; Bonjour, F.; Månson, J.-A.: The influence of void content on the structural flexural performance of unidirectional glass fibre reinforced polypropylene composites. Composites Part A: Applied Science and Manufacturing, Vol. 36. 5 (2005), 705–714.

[76] Lauke, B.; Schneider, K.; Friedrich, K.: Interlaminar shear strength measruemtn of thin composite rings fabricated by filament winding. European conference on composite materials ECCM 5. 1992. Bordeaux.

[77] ZHU, H.-y.; LI, D.-h.; ZHANG, D.-x.; WU, B.-c.; CHEN, Y.-y.: Influence of voids on interlaminar shear strength of carbon/epoxy fabric laminates. Transactions of Nonferrous Metals Society of China, Vol. 19 (2009), s470.

[78] Yoshida, H.; Ogasa, T.; Hayashi, R.: Statistical approach to the relationship between ILSS and void content of CFRP. Composites Science and Technology, Vol. 25. 1 (1986), 3–18.

[79] Thomason, J. L.: The interface region in glass fibre-reinforced epoxy resin composites: 1. Sample preparation, void content and interfacial strength. Composites, Vol. 26. 7 (1995), 467–475.

[80] Casal, E.; Granda, M.; Bermejo, J.; Bonhomme, J.; Menéndez, R.: Influence of porosity on the apparent interlaminar shear strength of pitch-based unidirectional C–C composites. Carbon, Vol. 39. 1 (2001), 73–82.

[81] Beehag, A.; Ye, L.: Role of cooling pressure on interlaminar fracture properties of commingled CF/PEEK composites. Composites: Part A, Vol. 27. (1996), 175–182.

[82] Friedrich, K.; Hou, M.: On stamp forming of curved and flexible geometry components from continuous glass fiber/polypropylene composites. Composites Part A: Applied Science and Manufacturing, Vol. 29. 3 (1998), 217–226.

[83] Trudelboucher, D.; FISA, B.; Denault, J.; GAGNON, P.: Experimental investigation of stamp forming of unconsolidated commingled E-glass/polypropylene fabrics. Composites Science and Technology, Vol. 66. 3-4 (2006), 555–570.

[84] Hou, M.: Stamp forming of continuous glass fibre reinforced polypropylene. Composites Part A: Applied Science and Manufacturing, Vol. 28. 8 (1997), 695–702.

[85] Yousefpour, A.; Hojati, M.; Immarigeon, J.-P.: Fusion Bonding/Welding of Thermoplastic Composites. Journal of Thermoplastic Composite Materials, Vol. 17. (2004), 303.

[86] Yungwirth, C. J.; Wetzel, E. D.; Sands, J. M.: Induction Curing of a Phase - Toughened Adhesive. Army Research Laboratory, ARL-TR-299 (2003).

[87] Mitschang, P.; Hümbert, M.; Moser, L.: Susceptorless continuous induction welding of carbon fiber reinforced thermoplastics. ICCM. 28.07. - 02.08.2013.Montreal.

[88] Neitzel, M.; Mitschang, P.: Handbuch Verbundwerkstoffe. München, Wien. Hanser, 2004.

[89] Brzeski, M.; Schledjewski, R.: Effect of tool temperature on laminate properties during in situ consolidation placement process. SAMPE International Symposium. 17-20.05.2010. Seattle.

[90] Heider, D.; Piovoso, M. J.; Gillespie Jr, J. W.: A neural network model-based open-loop optimization for the automated thermoplastic composite tow-placement system. Composites Part A: Applied Science and Manufacturing, Vol. 34. 8 (2003), 791–799.

[91] Sonmez, F. O.; Hahn, H. T.: Analysis of the On-Line Consolidation Process in Thermoplastic Composite Tape Placement. Journal of Thermoplastic Composite Materials, Vol. 10. 6 (1997), 543–572.

[92] Sonmez, F. O.; Hahn, H. T.: Modeling of Heat Transfer and Crystallization in Thermoplastic Composite Tape Placement Process. Journal of Thermoplastic Composite Materials, Vol. 10. 3 (1997), 198–240.

[93] Brzeski, M.; Schledjewski, R.: Modeling and phenomena investigation of velocity depending laminate quality for thermoplastic tape placement by means of diode laser heating. ECCM 14. 07-10.06.2010. Budapest.

[94] Lynam, C.: Predicting thermal deformation during the roll forming of thermoplastic matrix composites, SAMPE International Symposium. 23-26.05.2011. Long Beach.

[95] van Krevelen, D.W; Nijenhuis, K. te: Properties of Polymers (Fourth Edition). Amsterdam. Elsevier, 2009.

[96] Hay, J. N.; Luck, D. A.: The conformation of crystalline poly(phenylene sulphide). Polymer, Vol. 42. 19 (2001), 8297–8301.

[97] Ageorges, C.: Experimental investigation of the resistance welding of thermoplastic-matrix composites. Part II: optimum processing window and mechanical performance. Composites Science and Technology, Vol. 60. 8 (2000), 1191–1202.

[98] Henninger, F. H.; Friedrich, K.: Production of textile reinforced thermoplastic profiles by roll forming. Composites: Part A, Vol. 35 (2004), 573–583.

[99] Standard: DIN ISO9278-1: Darstellung der Ergebnisse von Partikelgrößenanalysen - Teil 1: Grafische Darstellung. 2004-09-00.

[100] Standard: DIN ISO9278-2: Darstellung der Ergebnisse von Partikelgrößenanalysen - Teil 2: Darstellung der Ergebnisse von Partikelgrößenanalysen - Teil 2: Berechnung von mittleren. 2006-02-00.

[101] Schwister, K.: Taschenbuch der Verfahrenstechnik. 2, Fachbuchverl. Leipzig - München, Wien. Hanser, 2005.

[102] Standard: DIN EN ISO14130: Fibre-reinforced plastic composites - Determination of apparent interlaminar shear strength by short-beam method. 02.1998.

[103] Tierney, J.: Modeling of In Situ Strength Development for the Thermoplastic Composite Tow Placement Process. Journal of Composite Materials, Vol. 40. 16 (2006), 1487–1506.

[104] Standard: DIN55660-5: Beschichtungsstoffe - Benetzbarkeit - Teil 5: Bestimmung des polaren und dispersen Anteils der Oberflächenspannung von Flüssigkeiten aus Kontaktwinkelmessungen auf einem Festkörper mit rein dispersem Anteil der Oberflächenenergie. 2012-04-00.

[105] Garbassi, F.; Morra, M.; Occhiello, E.: Polymer surfaces. Chichester. Wiley,1998.

[106] Ma, K.-X.; Ho, C.-H.; Zhu, F.; Chung, T.-S.: Investigation of surface energy for organic light emitting polymers and indium tin oxide. Thin Solid Films, Vol. 371. 1-2 (2000), 140–147.

[107] Yang, D.; Xu, Z.; Liu, C.; Wang, L.: Experimental study on the surface characteristics of polymer melts. Colloids and Surfaces A: Physicochemical and Engineering Aspects, Vol. 367. 1-3 (2010), 174–180.

[108] Standard: DIN EN ISO11357-1: Kunststoffe – Dynamische Differenz-Thermoanalyse (DSC) – Teil 1: Allgemeine Grundlagen. 03.2010.

[109] Standard: DIN EN ISO11357-3: Kunststoffe – Dynamische Differenzkalorimetrie (DDK) – Teil 3: Bestimmung der Schmelz- und Kristallisationstemperatur und der Schmelz- und Kristallisationsenthalpie. Juli 2012.

[110] Standard: DIN EN ISO11357-3: Dynamische Differenzkalorimetrie (DDK) – Teil 3: Bestimmung der Schmelz- und Kristallisationstemperatur und der Schmelz- und Kristallisationsenthalpie. Juli 2013.

[111] Ehrenstein, G. W.; Riedel, G.; Trawiel, P.: Praxis der thermischen Analyse von Kunststoffen. 2, München. Hanser, 2003.

[112] Noll, A.: Effektive Multifunktionalität von monomodal, bimodal und multimodal mit Kohlenstoff-Nanoröhren, Graphit und kurzen Kohlenstofffasern gefülltem Polyphenylensulfid. Institut. für Verbundwerkstoffe, Kaiserslautern. Diss. 2012.

[113] Standard: DIN EN ISO3219: Polymere/Harze in flüssigem, emulgiertem oder dispergiertem Zustand. 1994-10.

[114] Standard: DIN EN ISO2884-2: Beschichtungsstoffe – Bestimmung der Viskosität mit Rotationsviskosimetern – Teil 2: Scheiben- oder Kugelviskosimeter bei festgelegter Geschwindigkeit. 2006-09.

[115] Standard: DIN54458: Strukturklebstoffe – Bestimmung des Fließ- und Applikationsverhaltens von viskoelastischen Klebstoffen mit Hilfe der Oszillationsrheometrie. 03.2013.

[116] Sunny Goh Eng Giap: The Hidden Property of Arrhenius-type Relationship: Viscosity as a Function of Temperature. Journal of Physical Science, Vol. 21. 1. (2010), 29–39.

[117] Thodesen, C.; Xiao, F.; Amirkhanian, S. N.: Modeling viscosity behavior of crumb rubber modified binders. Construction and Building Materials, Vol. 23. 9 (2009), 3053–3062.

[118] Tjong, S. C.: Structure, morphology, mechanical and thermal characteristics of the in situ composites based on liquid crystalline polymers and thermoplastics. Materials Science and Engineering: R: Reports, Vol. 41. 1–2 (2003), 1–60.

[119] Standard: DIN51045-1: Bestimmung der thermischen Längenänderung fester Körper - Teil 1: Grundlagen. 2005-08-00.

[120] Standard: ASTMD 570: Prüfung des Wasserabsorptionsvermögens von Kunststoffen. 1998-00-00.

[121] Kaiser, R.; Gottschalk, G.: Elementare Tests zur Beurteilung von Messdaten. Mannheim. Bibliographisches Institut, 1972.

[122] Karian, H. G.: Handbook of polypropylene and polypropylene composites. New York. Marcel Dekker, 2003.

[123] Gianferri, R.; Giampaoli, S.; Magini, V.; Sciubba, F.; Romano Spica, V.; Delfini, M.: Study of interaction of water with advanced materials for swimming pool sportswear by NMR spectroscopy. Microchemical Journal, Vol. 112. (2014), 132–136.

[124] Lucas, K.: Thermodynamik. 7, Berlin, Heidelberg. Springer-Verlag, 2008.

[125] Bayer MaterialScience AG: Datasheet Makrolon 2207. 2013.

[126] Varga, J.; Karger-Kocsis, J.: Interfacial morphologies in carbon fibre-reinforced polypropylene microcomposites. Polymer, Vol. 36. 25 (1995), 4877–4881.

[127] Arroyo, M.; Lopez-Manchado, M. A.; Avalos, F.: Crystallization kinetics of polypropylene: II. Effect of the addition of short glass fibres. Polymer, Vol. 38. 22 (1997), 5587–5593.

[128] Guillen, J.; Cantwell, W.: The Influence of Cooling Rate on the Fracture Properties of a Thermoplastic-Based Fibre-Metal Laminate. Journal of Reinforced Plastics and Composites, Vol. 21. 8 (2002), 749–772.

[129] Spruiell, J.; Janke, C. J.: A review of the measurement and development of crystallinity and its relation to properties in neat poly(phenylene sulfide) and its

fiber reinforced composites. Tennessee. Oak Ridge National Laboratory, 2004.

[130] Chung, J. S.; Bodziuch, J.; Cebe, P.: Effects of thermal history on crystal structure of poly(phenylene sulphide). Journal of Materials Science, Vol. 27. 20 (1992), 5609–5619.

[131] Wunderlich, B.: Thermal analysis of polymeric materials. Heidelberg, New York. Springer, 2005.

[132] Khan, M. A.: Experimental and simulative description of the thermoplastic tape placement process with online consolidation. Institut für Verbundwerkstoffe, Kaiserslautern. Diss. 2010.

[133] Thomason, J. L.; Groenewoud, W. M.: The influence of fibre length and concentration on the properties of glass fibre reinforced polypropylene: 2. Thermal properties. Composites Part A: Applied Science and Manufacturing, Vol. 27. 7 (1996), 555–565.

[134] Acha, B. A.; Reboredo, M. M.; Marcovich, N. E.: Creep and dynamic mechanical behavior of PP–jute composites: Effect of the interfacial adhesion. Composites Part A: Applied Science and Manufacturing, Vol. 38. 6 (2007), 1507–1516.

[135] Dai, Z.; Gao, Y.; Liu, L.; Pötschke, P.; Yang, J.; Zhang, Z.: Creep-resistant behavior of MWCNT-polycarbonate melt spun nanocomposite fibers at elevated temperature. Polymer, Vol. 54. 14 (2013), 3723–3729.

[136] Vieille, B.; Albouy, W.; Taleb, L.: About the creep-fatigue interaction on the fatigue behaviour of off-axis woven-ply thermoplastic laminates at temperatures higher than Tg. Composites Part B: Engineering, Vol. 58 (2014), 478–486.

[137] Lee, T. H.; Boey, F. Y. C.; Khor, K. A.: On the determination of polymer crystallinity for a thermoplastic pps composite by thermal analysis. Composites Science and Technology, 53 (1995), 259–274.

[138] Cabrera, N.; Reynolds, C.; Alcock, B.; Peijs, T.: Non-isothermal stamp forming of continuous tape reinforced all-polypropylene composite sheet. Composites Part A: Applied Science and Manufacturing, Vol. 39. 9 (2008), 1455–1466.

[139] Parlevliet, P. P.; Bersee, H. E. N.; Beukers, A.: Residual stresses in thermoplastic composites – a study of the literature. Composites: Part A, Vol. 38. (2007), 1581–1596.

[140] Sen, F.; Aldas, K.: Elastic–plastic thermal stress analysis in a thermoplastic composite disc applied linear temperature loads via FEM. Advances in Engineering Software, Vol. 40. 9 (2009), 813–819.

10 Appendix

List of Publications

1. Bayerl, T.; Brzeski, M.; Martínez-Tafalla, M.; Schledjewski, R.; Mitschang, P.: Thermal degradation analysis of short-time heated polymers. Journal of Thermoplastic Composite Materials. 5 (2013); 1-25.

2. Brzeski, M.; Bayerl, T.; Mitschang, P.: Comparison of methods to detect thermal degradation of short-time heated carbon reinforced thermo- plastic composites. 5th Asia-Europe Symposium on Processing and Properties of Reinforced Polymers. 29.05.2011 - 01.06.2011. Dresden.

3. Brzeski, M.; Schledjewski, R.: Effect of tool temperature on laminate properties during in situ consolidation placement process. SAMPE International Symposium. 17-20.05.2010. Seattle.

4. Brzeski, M.; Schledjewski, R.: Modeling and phenomena investigation of velocity depending laminate quality for thermoplastic tape placement by means of diode laser heating. ECCM 14. 07-10.06.2010. Budapest.

5. Becker, D.; Brzeski, M.; Linster, D.; Mitschang, P.: Preform compaction and deformation during through-the-thickness impregnation. ICCM19, 28.07 - 02.08 2013. Montreal.

6. Brzeski, M.; Mitschang, P.: The tendency of thermoplastic composite to lose consolidation during re-melting. ICCM19, 28.07- 02. 08.2013. Montreal.

7. Brogdon, S.; Brzeski, M.; Grebel, K.: Verfahren zur Herstellung eines Werkzeuges. DE102012105467A1. 2012

8. Bayerl, T.; Brzeski, M.; Grebel, K.; Mitschang, P.; Natter, E.: Verfahren zur Fertigung eines Bauteils. DE102012104316A1. 2012

9. Brzeski, M.: Verfahren zur Herstellung eines Faserverbundwerkstoffes, ein nach dem Verfahren hergestellter Faserverbundwerkstoff sowie eine Vorrichtung zur Durchführung des Verfahrens. DE102011056686A1. 2011

10. Brzeski, M.: Verfahren zur Fertigung eines Kunststoffbauteils. DE102011056637A1. 2011

11. Brzeski, M.: Verfahren zur Herstellung eines Faserverbundwerkstoffes, ein nach dem Verfahren hergestellter Faserverbundwerkstoff sowie eine Vorrichtung zur Durchführung des Verfahrens. WO002013092203A1. 2013

List of Supervised Student Research and Graduation Projects

Klein, T.: Konstruktion einer Apparatur zur Messung thermophysikalischer Eigenschaften thermoplastischer Faserverbundwerkstoffe, 2010

Wegner, J.: Aufbau und Inbetriebnahme einer Apparatur zur Messung thermophysikalischer Eigenschaften von thermoplastischer Faserverbundwerkstoffe, IVW-Bericht 11-013, 2011

Rieb, A.: Charakterisierung der interlaminaren Eigenschaften von Faser-Kunststoff-Verbunden hergestellt durchs Tapelegen, IVW-Bericht 11-026, 2011

Leithmann, A.: Untersuchung des De-Konsolidierungsverhaltens von thermoplastischen Faser-Kunststoff-Verbunden, 2012

Schmitt, F.: Korrelation der thermischen Zersetzung von thermoplastischen Bändchen während des Tapelegens mit mechanischen Kennwerten, IVW-Bericht 13-002, 2013

Wienen, B.: Kompaktierung und Dekompaktierung von Glasfasergeweben, IVW-Bericht 13-006, 2013

Ströer, M.: Untersuchung vom Temperatur- und Druckprofilen auf das Konsolidierungsverhalten von thermoplastischer . Faser-Kunststoff-Verbunden, IVW-Bericht 13-027, 2013

Bachmann, F.: Untersuchung der Prozessparameter auf das Konsolidierungsverhalten von thermoplastischen Faser-Kunststoff-Verbunden, IVW-Bericht 13-076, 2013

List of Supervised Student Internships

Kajtar, D.: Oberflächenspannungsbestimmung mittels Kontaktwinkelmessung, 2010

Martínez-Tafalla López, M.: Thermal degradation of thermoplastic composite materials in contactless heating processes, 2010

Aleksiev, K.: Simulation des Umformverhaltens während des Rollformens von thermoplastischem Faserverbundmaterial mit LS-Dyna, 2010

Gitsas, A.: Experimental and theoretical analysis of the consolidation of thermoplastic matrix composites, 2011

Ndjiognou, P.: Untersuchung des De-Konsolidierungsverhaltens von thermoplastischen Faser-Kunststoff-Verbunden, 2011